

292A0

SINTEF Report No.: STF22 F98685
DNV Report No.: 98-3097

Classification: Restricted

R
E
P
O
R
T

ULTIGUIDE Phase 2

Evaluation report on Dynamic Effects



DET NORSKE VERITAS



SINTEF

Civil and Environmental Engineering

292 c



SINTEF Civil and Environmental Engineering
Structural Engineering

Address: N-7034 Trondheim
NORWAY

Location: Otto Nielsens vei 10
Telephone: +47 73 59 56 11
Fax: +47 73 59 26 60
Enterprise No.: NO 948 007 029 MVA



DET NORSKE VERITAS AS
Division Nordic Countries
Offshore Classification & Technical Services

Veritasveien 1,
N-1322 HØVIK, Norway
Tel: +47 67 57 99 00
Fax: +47 67 57 74 74
Org. No: NO 945 748 931 MVA

TECHNICAL REPORT

TITLE

ULTIGUIDE Phase 2
Evaluation of Dynamic Effects

AUTHOR(S)

Øyvind Hellan, SINTEF
Arnfinn Reitan, DNV

CLIENT(S)

Ultigude JIP

CLIENTS REF.

Multiclient

PROJECT NO.

SINTEF 22L062
DNV 72010054

REPORT NO.

STF22 F98685
DNV 98-3097

CLASSIFICATION

Restricted

CLASS. THIS PAGE

Restricted

ELECTRONIC FILE CODE
s:\2270\pro\22L062\
dynamic-report-4.doc

NO. OF PAGES/APPENDICES

17 + 6

DATE

1998-09-09

PROJECT MANAGER (NAME, SIGN.)

Øyvind Hellan

CHECKED BY (NAME, SIGN.)

Jørgen Amdahl

APPROVED BY (NAME, POSITION, SIGN.)

Oddvar. I. Eide, Research Manager

ABSTRACT

Considerations on dynamic effects in non-linear analyses of jacket type structures are made.

The following issues are discussed:

- Current design practise for dynamic analysis of fixed offshore structures
- Dynamic effects in non-linear pushover analyses

Recommendations are given as to how dynamic effects should be taken into consideration in non-linear collapse analyses of jacket type structures.

KEYWORDS	ENGLISH	NORWEGIAN
GROUP 1	Marine Technology	Marinteknikk
GROUP 2	Structure	Konstruksjon
SELECTED BY AUTHOR	Non-linear analysis	Ikkelineær analyse
	Dynamic effects	Dynamiske effekter

<i>Table of Content</i>		<i>Page</i>
1	INTRODUCTION	2
2	CURRENT DESIGN PRACTISE FOR DYNAMIC EFFECTS ON OFFSHORE STRUCTURES	2
2.1	General	2
2.2	Quasi static single degree of freedom (SDOF) systems	3
2.3	Frequency domain linear dynamic analysis	5
2.4	Dynamic amplification factors obtained from time domain non-linear dynamic analysis	5
2.5	Time domain non-linear dynamic analysis	7
3	DYNAMIC EFFECTS IN NON-LINEAR PUSHOVER ANALYSES	8
3.1	Characterisation of structural behaviour	8
3.2	Dynamic collapse behaviour of fixed offshore structures	9
3.3	Single-degree of freedom analyses	13
3.4	Simplified formulae	14
4	RECOMMENDATIONS	16
5	REFERENCES	17
Appendix A	Stewart, G.: "Non-linear structural dynamics by the pseudo-force influence method. Part II: application to offshore platform collapse" Proc. Second International Offshore and polar Engineering Conference (ISOPE), San Francisco, USA, 1992	
Appendix B	Bea, R.G. and Young, C.: "Loading and capacity effects on platform performance in extreme condition storm waves and earthquakes" Proc. Offshore Technology Conference (OTC), Houston, USA, 1993, paper 7140	
Appendix C	Scmucker, D.G. and Cornell, C.A.: "Dynamic behaviour of semi-ductile jackets under extreme wave and wave-in-deck forces" Proc. seventh int. conf. on the Behaviour of Offshore Structures (BOSS), Boston, USA, 1994	
Appendix D	Emami Azadi, M.R., Moan, T. and Amdahl.: "Dynamic effects on the performance of steel offshore platforms in extreme waves" Proc. Eurosteel '95, Prague, Czechoslovakia, 1995.	
Appendix E	Emami Azadi, M.R. and Moan, T.: "Ductility demand of simplified pile-soil- jacket systems under extreme sea waves and earthquakes" Proc. EUROLYN '96, Trondheim, Norway, 1996.	
Appendix F	Moan, T., Hellan, Ø. and Emami Azadi, M.R.: "Non-linear dynamic versus static analysis of jacket systems for ultimate limits state check" Proc. Advances in Marine Structures (DERA), Dunfermline, Scotland, 1997.	

1 INTRODUCTION

The purpose of this report is to give some background for and guidance on how to take dynamic effects into consideration in non-linear analyses.

The report is prepared as part of the Ultiguide Phase 2 project and the recommendations are intended for inclusion in the Ultiguide document.

2 CURRENT DESIGN PRACTISE FOR DYNAMIC EFFECTS ON OFFSHORE STRUCTURES

2.1 General

In this Chapter the commonly used approaches for taking dynamic effects into account in the analysis of offshore structures, are reviewed.

According to API RP2A /1/ (Item 2.3.1c 7) time history methods of dynamic analysis are preferred for predicting the extreme wave response of template platforms, minimum structures and guyed towers because these structures are generally drag force dominated.

Also according to API RP2A (Item 2.3.1c 7) frequency domain methods may be used for extreme wave response analysis to calculate the dynamic amplification factor to combine with the static load, provided the linearisation of the drag force can be justified.

ISO /2/ (Item 6.9.12.2) states for platforms with natural periods larger than 3 seconds, structural dynamic response may influence collapse due to environmental overloading. Dynamic non-linear structural analysis may be performed in the following manner:

- Full structural dynamic non-linear analysis in which the dynamic structural collapse as result of environmental overloading is simulated in time;
- Pseudo-dynamic analysis, in which static non-linear analysis procedures are used in combination with the environmental load set augmented with an inertial component. The inertial component of the environmental load set may be derived consistent with defined procedures (ISO /2/ 6.9.7.6).

According to ISO /2/ (Item 6.9.7.6.4) time-history methods using random waves are preferred. Frequency domain methods may be used for the global dynamic analysis, provided the linearization of the force, inundation effects, and structure/foundation response can be justified.

2.2 Quasi static single degree of freedom (SDOF) systems

A commonly used simple approach for taking dynamic effects into account is to calculate a dynamic amplification factor (DAF) based on a single degree of freedom (SDOF) system.

This approach is as follows:

- A dynamic analysis computer model is prepared based on the same model a used for the static analysis, i.e. mass model, representative linear springs for the foundation.
- The natural periods are determined through an eigenvalue analysis.
- The dynamic amplification factors are calculated from equation: (2.1)

$$DAF = \frac{1}{\sqrt{(1 - \beta^2)^2 + (2 \cdot \beta \cdot \xi)^2}} \quad (2.1)$$

where β = frequency ratio = T_n / T_w

T_n = natural period

T_w = natural period

ξ = damping ratio, typically 2% of critical damping

- The calculated dynamic amplification factor is then applied as a global load factor in a quasi-static analysis.

This simple approach is normally used only if the dynamic sensitivity to the considered loading is of minor importance for the structural response, typically for structures with natural periods slightly above 3 seconds when considering wave loads in the ultimate limit state.

It should however be pointed out that the dynamic effects are not only governed by the wave period and eigenperiod. The magnitude of dynamic amplifications is also dependent on the structural arrangement/configuration. E.g. a complex or wide structure will experience different global wave loading than a narrow or column-type structure, as illustrated in Figure 2-1.

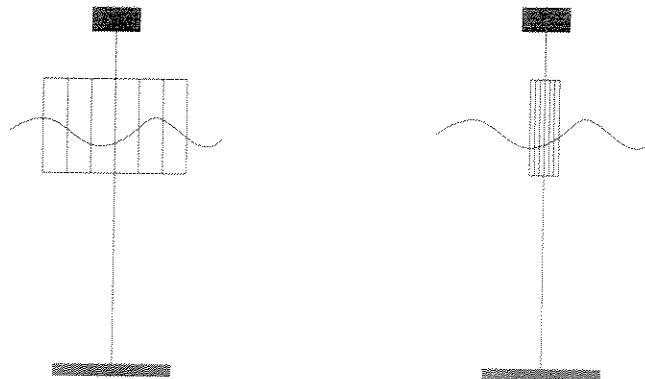


Figure 2-1 “Distributed” vs “lumped” structural configuration with respect to wave loading.

TECHNICAL REPORT

Also the global behaviour of the structure should be considered before using a simplified SDOF approach. For a structural configuration where a brittle type of failure mode may be anticipated, a precise assessment of the dynamic amplification is more important than for a system with a more ductile structural configuration, see Figure 2-2.

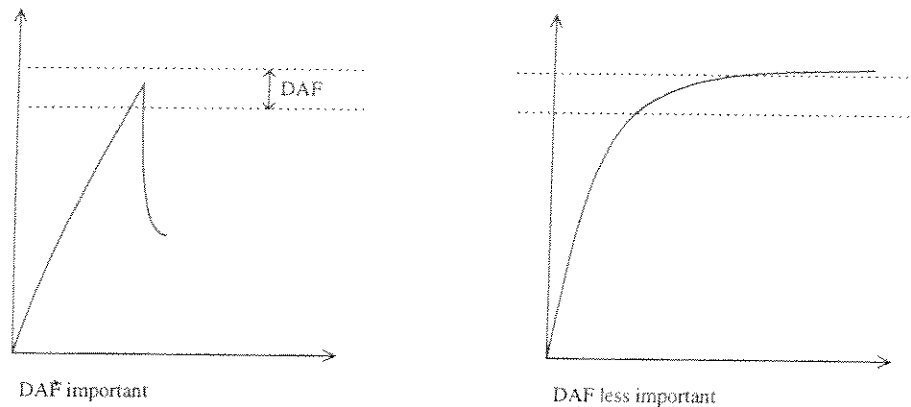


Figure 2-2 Global load-deformation curve: Brittle vs ductile structural behaviour

If the collapse behaviour is brittle, then system collapse will typically coincide with first component failure (first member failure/buckling). Non-linearities before first member buckling will be small (negligible on a global level) and the structure will for all practical purposes be linear until collapse.

For a system with a ductile behaviour the increased damping in the non-linear range will reduce the dynamic amplification. Hence, a DAF calculated on a linear system will then typically overestimate the real dynamic amplification.

The wave periods used in this approach are simply the periods of the regular design waves for the ultimate limit state for the different loading directions. It should be kept in mind that it is generally not known which single wave that gives max response. E.g. for system with little damping, say 2% of critical damping (i.e. typical jacket), the DAF at resonance is 25, see

Figure 2-3. Hence, even small waves may give significant structural response.

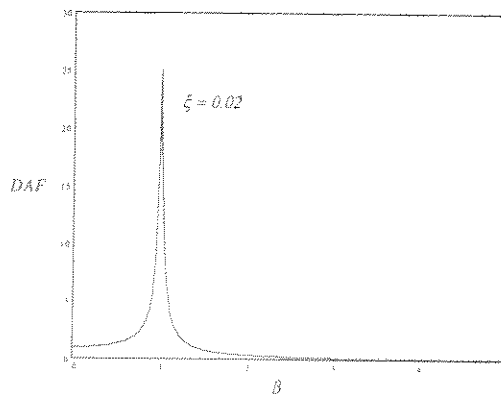


Figure 2-3 Dynamic amplification factor at damping $\xi = 2\%$ of critical damping.

2.3 Frequency domain linear dynamic analysis

Frequency domain methods may be used for the global dynamic analysis. The frequency domain approach is a linear approach. Using this approach requires that the linearisation of the drag force, inundation effects, and structure/foundation response can be justified.

Dynamic amplification factors may be established as the ratio between the response obtained from a dynamic and a quasi-static frequency domain linear analysis for selected response quantities.

Dynamic amplification factors may typically be established for the following response quantities:

- Base shear
- Over-turning moment
- Shear at each plan bracing level
- Deck displacement

The linear wave theory does not account for the fluctuation of the water surface due to the passage of the wave, and is strictly applicable only up to the still water level, since the members in the surface zone have varying degree of submergence during a wave cycle. To account for the surface zone effects the response may be obtained from a quasi-static analysis using regular waves and amplified with the DAF's obtained from the frequency domain linear dynamic analysis approach. Alternatively to using dynamic amplification factors, the dynamic effects may be accounted for by establishing an inertia load case. The inertial component of the environmental load may be derived consistent with procedures discussed in e.g. API RP-2A.

2.4 Dynamic amplification factors obtained from time domain non-linear dynamic analysis

A more advanced approach for estimating the dynamic amplification factors is by a non-linear time domain stochastic approach. This approach comprise the following steps executed sequentially:

1. A dynamic analysis computer model is prepared based on the same model a used for the static analysis (mass model).
2. Time series of irregular waves and corresponding water particle kinematics are simulated.
3. Hydrodynamic force time series are calculated on the basis of the simulated water particle kinematics.
4. Response time series are calculated by time-step integration of the equation of motion of the structural system.
5. The statistical properties of the simulated response sample are analysed.
6. The dynamic amplification factors to be applied in subsequent quasi-static analysis are evaluated.

Alternatively to using dynamic amplification factors, the dynamic effects may be accounted for by establishing an inertia load case. The inertial component of the environmental load may be derived consistent with procedures discussed in e.g. API RP-2A.

It should be noted that step 3 and 4 are linked, since the hydrodynamic loading depends on the structural response velocity and acceleration.

TECHNICAL REPORT

Both quasi-static and dynamic response analysis of the structure needs to be performed, in order to identify the dynamic amplifications of the structural responses. The same time series for the water particle kinematics is applied to both analyses.

The analysis is typically limited to one extreme sea state and one loading direction. The dynamic amplification factors derived for different response quantities of the structure are then used also for the other loading directions and extreme loading conditions in a standard quasi-static design wave analysis. It should be kept in mind that this may not necessarily be correct for other conditions.

Dynamic amplification factors may typically be established for the following response quantities:

- Base shear
- Over-turning moment
- Shear at each plane bracing level
- Deck displacement

For the ultimate limit state (ULS) condition the definition of the DAF may be given as:

$$DAF = \frac{\text{extreme dynamic response} - \text{mean dynamic response}}{\text{extreme quasistatic response} - \text{mean quasistatic response}} \quad (2.1)$$

or:

$$DAF = \frac{\hat{X}_{\text{dyn-max}}}{\hat{X}_{\text{quasi-max}}} \quad (2.2)$$

where $\hat{X}_{\text{dyn-max}}$ is the most probable dynamic maximum response and $\hat{X}_{\text{quasi-max}}$ is the most probable quasi-static maximum response.

In the cases where more than one simulation sample is applied for estimating the most probable maximum, then DAF is calculated as:

$$DAF = \frac{E[\hat{X}_{\text{dyn-max}}]}{E[\hat{X}_{\text{quasi-max}}]} \quad (2.3)$$

where $E[]$ denotes the expected or the mean values.

The extreme response is defined as the most probable largest response in a stationary extreme sea state of a given duration. Typically the extreme sea state is defined as sea state with 100-year return period for the significant wave height and the mean zero-crossing period. Formally the extreme response could be estimated directly from a set of simulated samples by applying standard extreme value statistics. However, this would require sets of samples with length corresponding to the storm duration. For large structural systems this is impractical, even with today's computers. An alternative procedure is therefore often applied. This is based on fitting an analytical probability distribution to the obtained sample distribution of local maxima after the mean response has been subtracted.

The three-parameter Weibull distribution is typically used:

$$F_X(x) = 1 - e^{-\left(\frac{x-\gamma}{\alpha}\right)^\beta} \quad (2.4)$$

The distribution parameters α (scale parameter), β (shape parameter) and γ (location parameter) are established by the method of moments to the observed data. The set of maxima is extracted from the time series by a level-crossing algorithm, which selects the largest maximum between each up-crossing and down-crossing through the mean response level.

The distribution for the largest maxima in a storm with a duration τ is derived from the distribution of the set of maxima as

$$F_{X_{\max}}(x) = (F_X(x))^{N_{\text{peak}}} \quad (2.5)$$

where $F_X(x)$ is given in the equation above, and N_{peak} is number of maxima in the storm,

estimated as
$$N_{\text{peak}} = \frac{\tau \cdot n_{\text{sim}}}{T_{\text{sim}}}$$

τ = storm duration

T_{sim} = sample length

n_{sim} = number of maxima in the simulated sample

The statistical properties for $F_{X_{\max}}(x)$ may be obtained by Monte Carlo simulation.

2.5 Time domain non-linear dynamic analysis

For a full time domain non-linear dynamic analysis, without the need of establishing dynamic amplification factors to be applied in separate quasi-static analyses, the approach described in Section 2.4 may be extended to include all loading directions and relevant extreme conditions.

3 DYNAMIC EFFECTS IN NON-LINEAR PUSHOVER ANALYSES

3.1 Characterisation of structural behaviour

The *residual strength ratio*, α is a measure of the structure's resilience once the deformations exceed those corresponding to the static ultimate strength. Ref. Figure 3-1. The *limiting ductility ratio*, μ_{\max} is a measure of the excess plastic deformation that the structure can withstand beyond that corresponding to its static ultimate strength.

The failure mechanism in the post-ultimate regime can now be categorised as either

1. ductile: $\alpha > 0.9$ AND $\mu_{\max} \gg 1$
2. brittle: $\alpha < 0.7$ OR $\mu_{\max} \approx 1$
3. semi-ductile: $0.7 < \alpha < 0.9$ AND $\mu_{\max} \gg 1$

In a static analysis, equilibrium cannot be achieved if the load factor is increased beyond λ_S^{ult} , and the deformations in the structure become unbounded. However, achieving a dynamic equilibrium is possible. The possibility of resisting peak environmental forces larger than the static ultimate capacity is improved if the mass is large (increased inertial resistance). However, the structure must have the ductility required to accelerate the mass and mobilise the inertia resistance. 'Failure' now becomes a question of how much deformation can be tolerated without detrimental effects on structural capacity or to ensure that the platform remains operable.

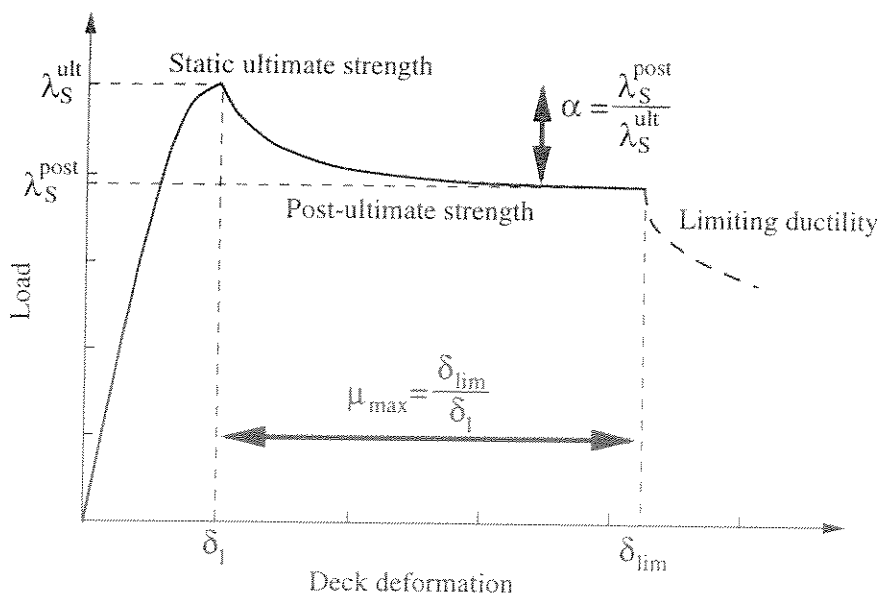


Figure 3-1 Typical static response characteristics

3.2 Dynamic collapse behaviour of fixed offshore structures

The dynamic equilibrium of a structure can be expressed as

$$F_i(t) + F_d(t) + F_r(t) = F_e(t) \quad (3.1)$$

where $F_r(t)$ is the vector of static structural and foundation restoring forces, $F_d(t)$ is the damping forces, $F_i(t)$ is the inertia forces and $F_e(t)$ is the external forces.

It is evident from equation (3.1) that the ultimate dynamic capacity of a system can be larger than the maximum static resistance due to the contributions from inertia $F_i(t)$ and damping $F_d(t)$. On the other hand, dynamic resonance effects can contribute to increase the loading on the structure (dynamic amplification).

Stewart (1992) have presented results from dynamic collapse analyses of full jacket models. Figure 3-2 shows the static response of the platform. It is noted that the platform has a near perfect plastic performance, with the ultimate capacity reached at a displacement of ≈ 0.7 m.

For the dynamic analyses, the load history was calculated for three wave periods and linearly ramped over the first two cycles to provide a start-up condition for the extreme wave. Figure 3-1. This force history was then normalised such that its peak value matched that corresponding to static collapse. Thereafter, the loading profile was scaled up and stepped through the structure at successively larger intensities. The platform was deemed to be inoperable if the permanent mudline rotation exceeded 1 degree, corresponding to a deck displacement of 3.5 m.

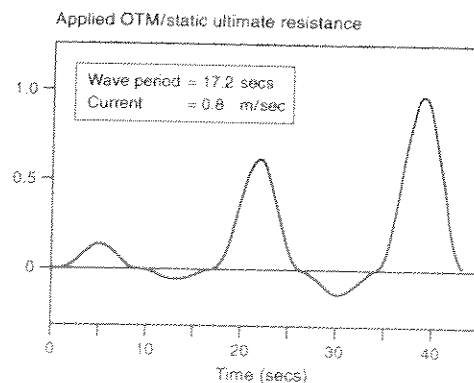
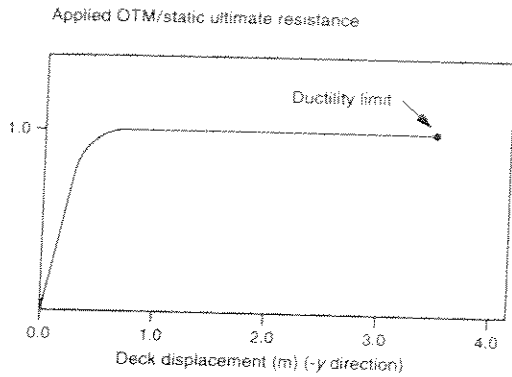
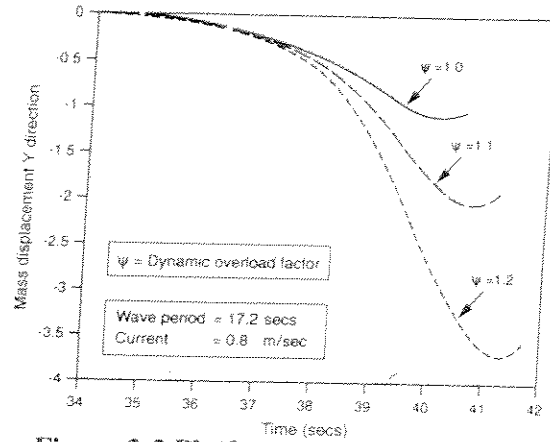
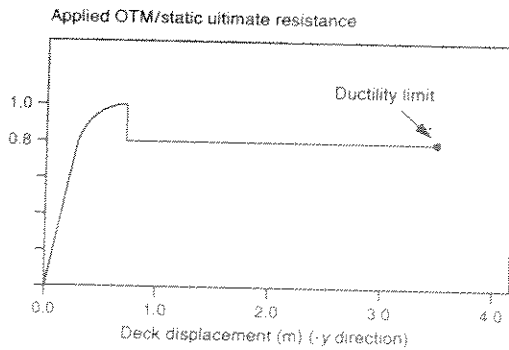
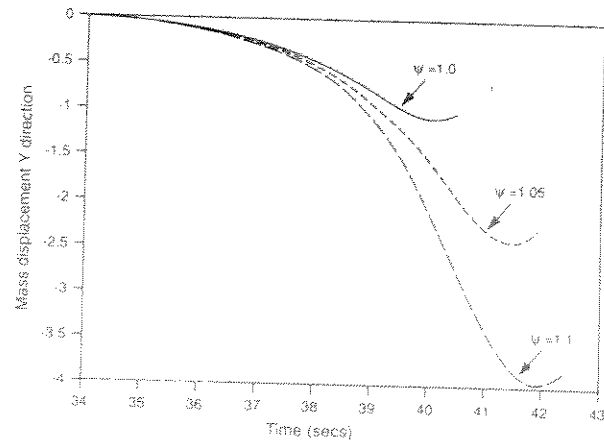


Figure 3-1 Normalised force history with linear ramping


Figure 3-2 Platform static response

Figure 3-3 Platform non-linear dynamic response

Selected results from the dynamic analyses, representing the passage of one extreme wave, are shown in Figure 3-3. It can be seen that the peak of the time dependent load history may be increased by about 20 % above that causing static collapse before the deformations exceed the available ductility.

By adjusting the foundation characteristics, the static response curve of the system was changed to that shown in Figure 3-4. This system was then used to investigate the dynamic collapse behaviour of semi-ductile systems. The system has a residual strength factor α equal to 0.8. The results of the dynamic analysis are presented in Figure 3-5 for the passage of one extreme wave. The dynamic overload required to reach a deck displacement of 3.5 m is now only 7 % instead of to the 20 % that could be accommodated if the system were ductile. This illustrates the detrimental effect on dynamic capacity if system strength deterioration occurs in the post-ultimate-strength regime.


Figure 3-4 Static response of semi-brittle system

Figure 3-5 Dynamic response of semi-brittle system

TECHNICAL REPORT

Schmucker (1994, 1996) has presented further results for both ductile and semi-brittle structural behaviour.

Figure 3-6 compares static and dynamic analyses of a Gulf of Mexico jacket. The static capacity is associated with a wave height of 50 ft. The figure illustrates that the structure is able to withstand larger waves when dynamic behaviour is included, but at the expense of increased global deformations.

Figure 3-7 compares static and dynamic results for another GoM jacket. The full line shows the static behaviour. The diamond marks indicate the peak-load/corresponding-deformation from dynamic analyses at different load intensities. The “+” signs show the results from simplified single-degree-of-freedom analyses. It is worth noting that the dynamic effects in this case leads to increased global deformations compared to the static case, even at load levels below the static ultimate capacity.

Figure 3-8 shows the dynamic “overload” as function of loading rate and structural ductility. The horizontal axis shows the ratio between wave period, t_d , and structures lowest eigen period, T . The vertical axis shows the ductility ratio, μ , defined as the ratio between the deformation at ultimate dynamic capacity, and the deformation at the ultimate capacity of a static analysis. For a system with a given ductility limit and a given loading rate, the diagram indicates the dynamic overload that can be sustained. Alternatively, the diagram indicates the increase in deformation (beyond that of a static analysis) for a structure exposed to a given dynamic overload, F_v , and a given loading rate.

It is again worth noting that dynamic effects lead to increased deformations even at load levels below the static ultimate capacity. For low t_d/T -ratios (<0.5), the static ultimate capacity ($F_v = 1$) is only reached after twice the deformations of the static system ($\mu \approx 2$). On the other hand, a structure with a ductility “capacity” of 4 will have a dynamic capacity of 1.15 times the static capacity (for t_d/T less than 4).

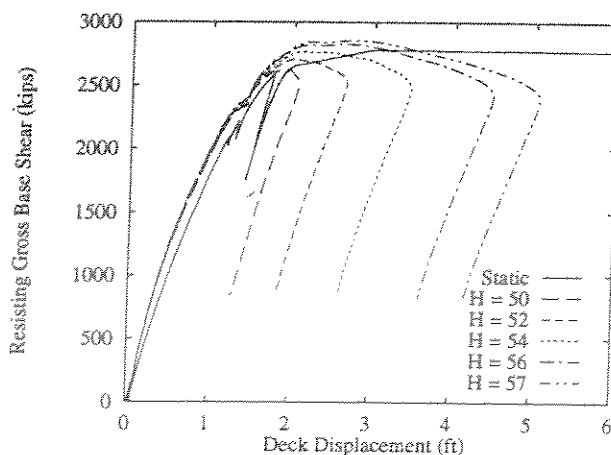


Figure 3-6 Static and dynamic analyses of example structure

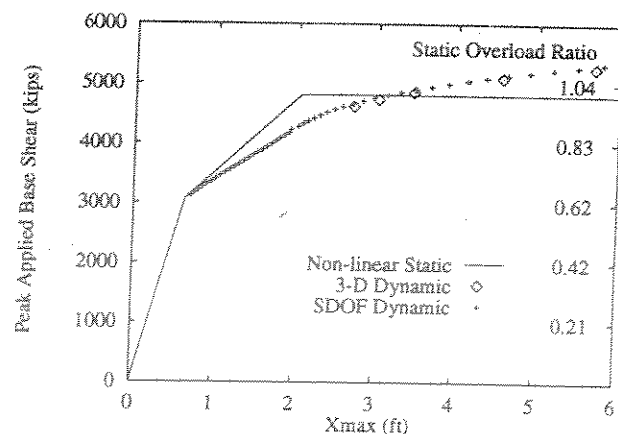


Figure 3-7 Static and dynamic analyses of example system

TECHNICAL REPORT

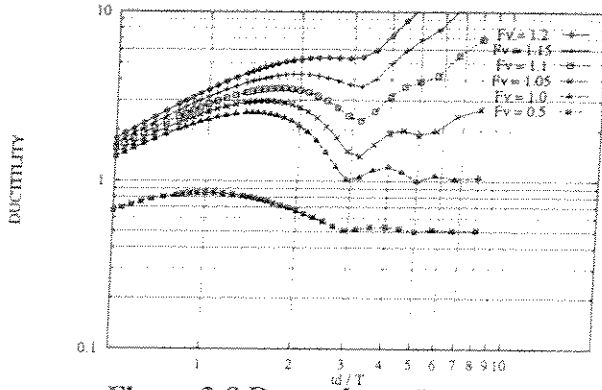


Figure 3-8 Dynamic performance of ductile systems

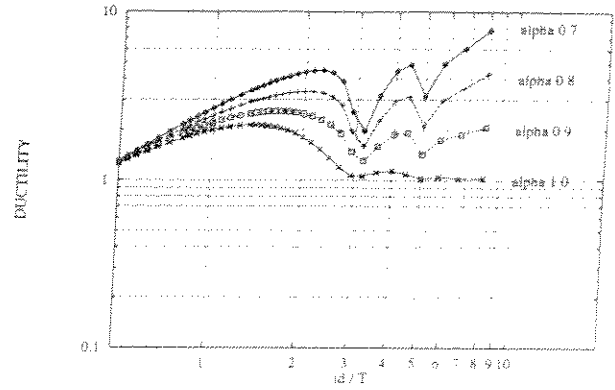


Figure 3-9 Dynamic performance of semi-ductile systems.

$$F_v = 1$$

Figure 3-8 indicates the ultimate dynamic performance of elastic-perfectly plastic systems.

Figure 3-9 gives the same information for semi-brittle systems, i.e. systems that have post-ultimate strength less than the ultimate capacity. Again, the loading rate is shown on the horizontal axis (t_d/T) and the ductility ratio μ is shown on the vertical axis.

Figure 3-9 illustrates the results for a single-degree-of-freedom system with varying amounts of residual capacity ($\alpha = 0.7, 0.8, 0.9, 1.0$). The static behaviour is shown in Figure 3-10. The system is subjected to a squared sinusoidal load profile with $F_v = 1.0$, shown in Figure 3-11. The yield plateau or "ultimate strength persistence" in Figure 3-10 is taken to be zero.

We observe from Figure 3-9 that the ductilities for semi-brittle systems are very sensitive to the residual capacity. For successively smaller α 's the ductility required to sustain the static ultimate load increases with successively larger amounts. The dynamic effects in this case are responsible for "kicking" the system into the post-ultimate region, where the system does not retain full ultimate capacity but drops off to a residual level.

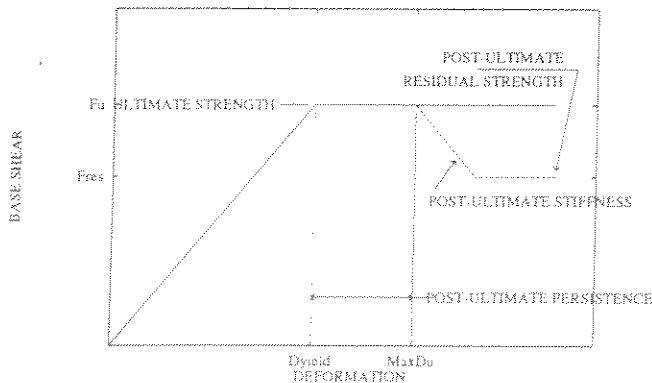


Figure 3-10 Semi-brittle P- δ characteristics

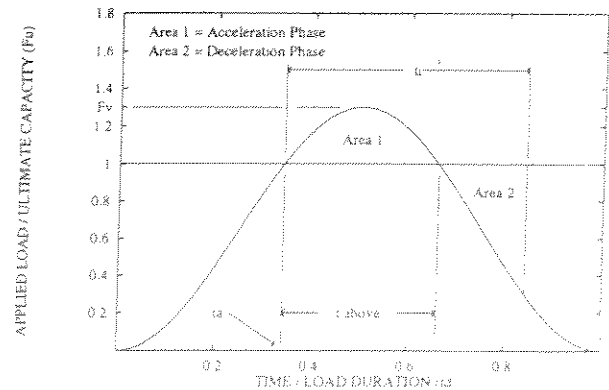


Figure 3-11 Squared sinusoidal loading profile.

3.3 Single-degree of freedom analyses

Schmucker (1994, 1996) has made extensive use of single-degree-of-freedom analyses to evaluate the dynamic effects on collapse behaviour.

The SDOF model is created from the 3D static pushover characteristics and a linear eigenvalue analysis of the 3D model. The force-deformation characteristics of the SDOF spring are obtained from the static pushover results, as an 'envelope' to any local peaks and valleys in the detailed P- δ behaviour.

The SDOF mass is estimated from the relationship between the natural period and the spring-mass combination: $T = 2\pi\sqrt{\frac{m}{k}}$. The fundamental period of free vibration is determined from a linear eigen-value analysis of the 3D model. The initial stiffness is estimated from the 3D P- δ

characteristics. The SDOF mass is then determined by $m = \frac{T^2}{4\pi^2} \cdot k$. This mass contrasts with the actual deck mass and the total mass of the structure above the mudline. However, using this mass the SDOF model is approximately preserving the ratio of "first mode of vibration mass" to the "first mode of vibration stiffness" (Schmucker, 1996).

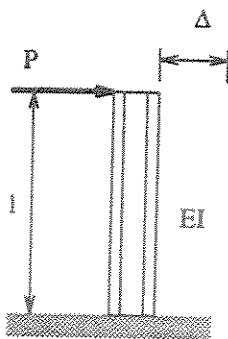


Figure 3-1 Single-degree-of-freedom system

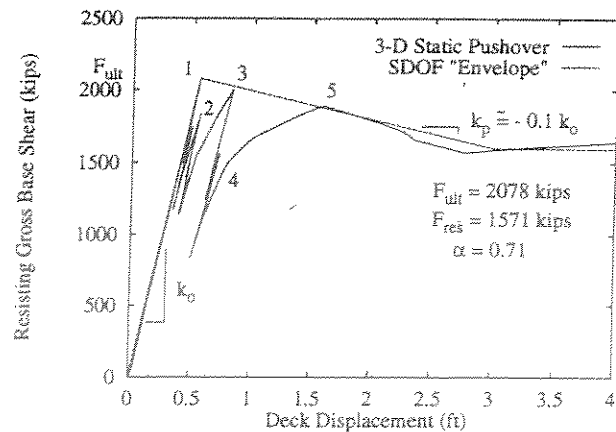


Figure 3-2 Envelope SDOF characteristic

3.4 Simplified formulae

Several authors have presented simplified formulae or simplified criteria to quantify the dynamic effects.

Stewart et al. (1988) has suggested the overload ratios in the range of

$$\begin{aligned} F_v &\approx 1.0 - 1.07 && \text{for semi-ductile structures} \\ F_v &\geq 1.2 && \text{for ductile structures} \end{aligned} \quad (3.1)$$

Bea and Young, (1993) have presented the following relationships for overload vs. ductility ratio for ductile systems with non-degrading post-peak behaviour:

$$F_v = \sqrt{2\mu - 1} \quad (3.2)$$

For ductile systems with post-peak strength degradation they suggest:

$$F_v = \alpha_{res} \cdot \mu \quad (3.3)$$

These relationships are derived from SDOF analyses of two systems with natural periods 1 sec. and 2.0 sec., and with damping ratio of about 5 %.

It should be noted that (3.2) and (3.3) have been suggested for seismic analysis results. Pushover analyses for extreme wave loading indicate ductility ratios in the order of 5-10 for typical jacket structures. According to (3.3) this would imply overload ratios (dynamic capacities) in the order of 3-4 times the static capacity. Obviously, (3.3) provides better results when applied to severe earthquake loading. However, for moderate ductility ratios ($1 < \mu < 2$), the two relations may provide rather reasonable estimates for F_v also for extreme wave loading.

Emami et al. (1995) have suggested the following relationship for semi-ductile structures with post-peak strength degradation:

$$F_v = \frac{1}{DAF} \cdot \sqrt{\mu} \quad (3.4)$$

This relation indicates that an ideally ductile system can achieve an infinitely large overload ratio. On the other hand, for a very brittle system no real positive inertia contribution can be mobilised and the system will be susceptible to detrimental dynamic effects even before reaching to its ultimate static capacity level.

Schmucker, (1996) obtained an overload-ductility ratio relationship based on analysis of idealised bi-linear elasto-plastic SDOF systems as follows:

$$F_v = \frac{1}{DAF} + a \left[\frac{1}{4\pi^2} \left(\frac{T_n}{t_d} \right)^2 (\mu - 1) \right]^b \quad (3.5)$$

in which T_n and t_d denote the fundamental natural period of the structure and the crest duration (~half cycle period) of the sea wave, respectively. The coefficients "a" and "b" in (3.5) depend on the load history "shape" and the structural natural period. Schmucker, (1996) has suggested that for squared-sinusoidal shape waves (similar to the shape of sea wave force) the coefficient "a" may be taken as 2.2 and the exponent term "b" as 0.5.

These suggested values are obtained for a bi-linear elasto-plastic SDOF system, and are basically derived based on linear dynamic assumption, i.e. that the restoring force is assumed to vary linearly with displacement response of the SDOF system. This implies that the natural period of the system is taken as constant throughout the elasto-plastic response of SDOF system.

However, this is not the case for a (gradually yielding) elasto-plastic system. Here, the effective natural period of system may increase when the system's tangent stiffness decreases towards collapse.

Based on these considerations, Emami (1998) proposed the following relationship, based dynamic analyses of SDOF systems and full 3D jacket models:

$$F_v = \frac{1}{DAF} \left\{ 1 + \alpha_{res} \frac{T_{ref} \cdot T_n}{T_w} \cdot \log \mu_{max} \left(\mu \left(16 \frac{T_n}{T_{ref} \cdot T_w} \right)^{\beta/2} \right) \right\} \cdot \mu^{\frac{1-\beta}{2}} \quad (3.6)$$

β is an indicator of the collapse behaviour of the jacket system which is defined as:

$$\beta = 1 - \frac{F_{r,res}}{F_{r,max}} \cdot \frac{T_n}{T_{eff}} = 1 - \alpha_{res} \cdot \frac{T_n}{T_{eff}} \quad (3.7)$$

where T_{eff} represents the effective natural period of the system:

$$T_{eff} = 2\pi \sqrt{\frac{m}{k_{eff}}} \quad (3.8)$$

(3.8) indicates that the effective natural period of a non-linear system will change as the system approaches collapse, and will approach infinity at the collapse when the effective (dynamic) stiffness value becomes nearly zero.

The ratio $\frac{T_n}{T_w T_{ref}}$ represents the variability of the μ with the natural period of system T_n and also

with the extreme wave period T_w . The base of the logarithmic function is set as μ_{max} , which is considered to be about 10 for practical purposes. A damage level of $\mu_{max} > 10$ is considered to represent an ultimate collapse of the structure in practice.

The associated function with the period variability is considered to be exponential which decays as seen on the spectra with increase of T_n towards values greater than 3 – 5.0 secs. T_{ref} may be defined as a reference period of e.g. .1 sec. The exponent term of $T_n/(T_{ref}T_w)$ function is

$$\frac{\beta}{2} = \frac{1}{2} \left(1 - \frac{F_{r,max}}{F_{r,res}} \frac{T_n}{T_{eff}} \right) \text{ which is a function of the residual strength ratio, the natural period and}$$

the effective period of the oscillatory system. The physical importance of this is that the effect of natural period is associated with the system's non-linear response and thus with its stiffness and strength degradation. Emami (1998).

4 RECOMMENDATIONS

While significant work has been done in the area of non-linear dynamic collapse analyses, and several simplified procedures and formulae have been put forward, it still seems a bit early to present recommendations for one formula over the other, or one procedure over the other.

Single-degree-of-freedom analyses

For a qualitative assessment of dynamic effects, SDOF analyses provide valuable insights. Such analyses are relatively simple, they are fast, and well suited for parametric studies etc.

Time-domain dynamic collapse analyses

For time domain analyses, the start-up condition prior to the extreme wave is important. It is recommended to define a load history comprising at least three wave periods, and linearly increase the load over the first two cycles to provide a start-up condition for the extreme wave.

The force history should be normalised such that the peak value corresponds to the static collapse load. In the subsequent dynamic analyses, the load history should be scaled up (or down) and stepped through the structure at successively larger (or smaller) intensities.

The failure criterion for the analyses should be defined by the amount of deformation that can be tolerated without degradation of structural capacity or to ensure that the platform remains operable.

Screening procedure for dynamic effects

As a simple screening procedure, the following points can be used as a simple rule-of-thumb:

- For brittle structures: use static pushover results, but add dynamic effects for environmental loads (divide the capacity by the DAF).
- For ductile structures: use the static pushover results without knock-down factor. The real dynamic capacity is probably some 10-20% higher.
- For semi-ductile structures: to be treated as brittle. The dynamic capacity may very well exceed this limit, but that has to be justified by separate studies in each case.

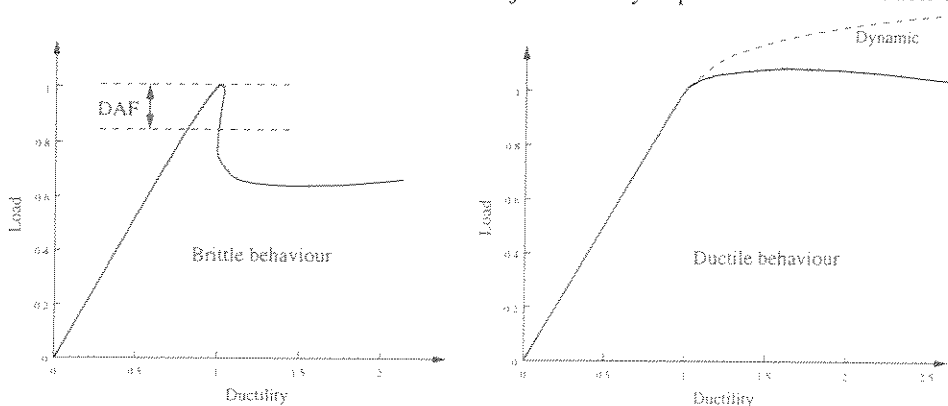


Figure 4-1 Dynamic loading effects

5 REFERENCES

- /1/ API RP2A: "Recommended Practice for Planning, Designing and Constructing Fixed Offshore Platforms, API recommended Practice 2A-WSD, 20. Edition, July 1, 1993.
- /2/ ISO 13819-2/Draft C: "Fixed steel structures", July 28, 1997
- /3/ Stewart, G.: "Non-linear structural dynamics by the pseudo-force influence method. Part II: application to offshore platform collapse" Proc. Second International Offshore and polar Engineering Conference (ISOPE), San Francisco, USA, 1992
- /4/ Bea, R.G. and Young, C.: "Loading and capacity effects on platform performance in extreme condition storm waves and earthquakes" Proc. Offshore Technology Conference (OTC), Houston, USA, 1993, paper 7140
- /5/ Schmucker, D.G. and Cornell, C.A.: "Dynamic behaviour of semi-ductile jackets under extreme wave and wave-in-deck forces" Proc. seventh int. conf. on the Behaviour of Offshore Structures (BOSS), Boston, USA, 1994
- /6/ Emami Azadi, M.R., Moan, T. and Amdahl.: "Dynamic effects on the performance of steel offshore platforms in extreme waves" Proc. Eurosteel '95, Prague, Czechoslovakia, 1995.
- /7/ Emami Azadi, M.R. and Moan, T.: "Ductility demand of simplified pile-soil-jacket systems under extreme sea waves and earthquakes" Proc. EUROLYN '96, Trondheim, Norway, 1996.
- /8/ Moan, T., Hellan, Ø. and Emami Azadi, M.R.: "Non-linear dynamic versus static analysis of jacket systems for ultimate limits state check" Proc. Advances in Marine Structures (DERA), Dunfermline, Scotland, 1997.
- /9/ Schmucker, D.G: "Near-failure behaviour of jacket-type offshore platforms in the extreme wave environment" Ph.D thesis, Reliability of Marine Structures Program, report RMS-21, Dept. of Civil Engineering, Stanford University, California, USA 1996
- /10/ Emami Azadi, M.R.: "Analysis of static and dynamic pile-soil-jacket behaviour" Ph.D thesis 1998:52, MTA-report 1998:121, Dept. of Marine Structures, Norwegian University of Science and Technology, Trondheim, Norway, 1998

- o0o -

APPENDIX

A

**STEWART, G.: "NON-LINEAR STRUCTURAL DYNAMICS BY THE
PSEUDO-FORCE INFLUENCE METHOD. PART II: APPLICATION TO
OFFSHORE PLATFORM COLLAPSE" PROC. SECOND
INTERNATIONAL OFFSHORE AND POLAR ENGINEERING
CONFERENCE (ISOPE), SAN FRANCISCO, USA, 1992**

- o0o -

NON-LINEAR STRUCTURAL DYNAMICS BY THE PSEUDO-FORCE INFLUENCE METHOD PART II: APPLICATION TO OFFSHORE PLATFORM COLLAPSE

G. Stewart
Shell Research B.V.
Rijswijk, The Netherlands

ABSTRACT

A novel feature of the pseudo-force influence method's formulation (presented in Part I) enables a non-linear dynamic simulation system to be developed around an unmodified, linear finite-element program. Such a simulation system is used to investigate the dynamic collapse resistance of an offshore platform subjected to extreme storm overload. From this study it is concluded that, for structures possessing ductile (post-ultimate-strength) failure modes, the peak dynamic load that can be resisted may exceed the static ultimate capacity by a considerable margin. This conclusion provides a major incentive for designing ductile behaviour into all new offshore platforms and not only for those operating in seismically active regions. For certain existing platforms that are required to meet operational demands outside their original design intent, expensive remedial work may be avoided owing to the increased resistance rating.

Keywords

Dynamic collapse, non-linear, pseudo-force, influence matrix, PFI-method, structures, ductility.

1. INTRODUCTION

With the recent advent/availability of non-linear analysis techniques (e.g. USFOS, FENRIS, INTRA, and the method developed by Stewart & van de Graaf, 1990), structural integrity assessments may now be based on the static collapse strength of the entire system rather than on the strength of each component. Therefore, the reserve capacity beyond first component failure may be evaluated and utilised, and a more realistic indication of the structure's performance may be obtained. Assessments based on these more advanced methods can compliment traditional linear analysis procedures (e.g. API-RP2A). They have been used, for example, to:

- (a) verify the fitness for purpose of existing platform sub-structures whose present or envisaged operational demands are outside the original design intent (Stewart et al., 1988; Bea et al., 1988). (Thus, unnecessary and expensive in-situ strengthening can be avoided and/or it may be possible to tie in a satellite field without the need for a costly new platform.)
- (b) select bracing configurations/dimensions for platforms to provide adequate system reserve capacity (Lloyd & Clawson, 1984; Moan et al., 1985; Titus & Banon, 1988; Nordal, 1990; Piermattei et al., 1990); and

(c) estimate the reliability of existing structures (Anderson et al., 1982; Tromans & van de Graaf, 1992).

In this paper the possibility of achieving a resistance rating higher than the static ultimate capacity for extreme storm loading is considered by taking account of the time-varying nature of the wave force and the platform's post-ultimate-strength and inertial resistance. Investigating this 'non-linear dynamic collapse' problem using a standard non-linear finite-element (f.e.) program with time-dependent capabilities (e.g. FENRIS, INTRA) would be computationally intensive and laborious, especially if sensitivity studies are done. More efficient methods are therefore required (in particular for preliminary analyses) to enable the influence of these dynamic effects to be evaluated.

Using the *pseudo-force influence method* (PFI-method) described in Part I of this publication, one can obtain the dynamic collapse behaviour of even the most complex structures by solving a reduced system of non-linear dynamic equations. A unique feature of the PFI-method's formulation makes it possible to build a non-linear simulation system using any standard linear f.e. program together with stand-alone modules that generate the non-linear member/pile resistance data and solve the reduced system.

Here, in Part II of this publication, the development of this simulation system is described, and its practical application demonstrated for an existing structure. The factors influencing dynamic collapse resistance of structures exposed to extreme storms are discussed. In particular, the importance of ductile (post-ultimate-strength) behaviour for enhancing the performance of new structures designed for these conditions is emphasised. Hitherto, post-ultimate-strength ductility has been considered applicable only to structures installed in regions with seismic activity.

2. THE DYNAMIC COLLAPSE PROBLEM

The problem of interest is to determine whether, by accounting for inertial resistance and time-dependent loading, a structure can be shown to resist peak environmental loads greater than its static capacity. Investigating this problem requires an understanding of the structural response in the post-ultimate-strength regime and some knowledge about the loading conditions experienced during a severe storm.

2.1 Structural resistance - static pushover analyses

The response characteristics of a structure to extreme environmental loading can be obtained from a static pushover analysis

(Fig. 1). From this curve (which is idealised but fairly representative of actual behaviour) the following can be identified:

- (a) the load factor λ_1 at which the first component (member, joint, etc.) fails;
- (b) the static ultimate strength, λ_S^{ult} and the corresponding deformation, δ_u ;
- (c) the post-ultimate-strength, λ_0 ; and
- (d) the maximum permissible deformation δ_0 .

The following parameters are useful for characterising the structural response.

$$RF = \frac{\lambda_S^{ult}}{\lambda_1} \quad \alpha = \frac{\lambda_0}{\lambda_S^{ult}} \quad \mu_{max} = \frac{\delta_0}{\delta_u}$$

The *redundancy factor*, RF , was introduced by Stewart et al. (1988). It provides a measure of the static reserve capacity of the structure. The other two parameters relate to the post-ultimate-strength behaviour and are of interest for dynamic response. The *robustness factor*, α is a measure of the structure's resilience once the deformations exceed those corresponding to the static ultimate strength, while the *limiting (post-ultimate-strength) ductility*, μ_{max} , is a measure of the excess plastic deformation that the structure can withstand beyond that corresponding to its static ultimate strength. (This limitation may be imposed to prevent member fracture or to ensure that the platform remains operable, for example.) The product of the redundancy factor and the robustness factor immediately indicates whether the post-ultimate-strength is below the first component failure load.

Making use of the latter two parameters, failure mechanisms in the post-ultimate-strength regime can be categorised as either:

- (1) ductile: $\alpha \approx 1$ and $\mu_{max} \gg 1$;
- (2) brittle: $\alpha \ll 1$ or $\mu_{max} \approx 1$; or
- (3) semi-brittle: somewhere between ductile and brittle.

In a static analysis, equilibrium cannot be achieved if the load factor is increased beyond λ_S^{ult} and the deformations in the structure become unbounded. However, dynamic equilibrium is always possible. Owing to the time-dependent nature of wave forces and the inertial resistance offered by the platform's mass, it is quite conceivable for the peak dynamic loading to exceed the static ultimate capacity by a considerable margin before the deformations become unacceptable. 'Failure' now becomes a question of how much deformation can be tolerated. The possibility of resisting peak environmental forces larger than the static ultimate capacity is improved if the mass is large (increased inertial resistance) and the failure mechanism (in the post-ultimate-strength regime) is ductile. In Section 4 the dynamic response of an actual platform that possesses these properties is considered.

2.2 Extreme storm loading

A storm generating a wave force in excess of the static ultimate strength of the structure is a rare event. However, within such a storm there will be a number of large waves, several of which may result in peak loads beyond the static capacity. To assess whether the dynamic resistance rating of a platform can be increased beyond its static ultimate strength, the cumulative deformation resulting from these large waves in the storm needs to be estimated.

Number of large waves

A simple but useful model to estimate the cumulative deformation (assuming that the strength of the structure does not degrade upon repeated loading) is developed as follows. Using *order statistics*, one can obtain the probability distributions of the m largest waves in a storm (Gumbel, 1958). Taking the most probable value of each of these distributions as representative of the heights of the largest waves, and assuming the underlying wave generating process to be Rayleigh, gives

$$\frac{h_m}{h_1} = \sqrt{1 - \frac{\log(m)}{\log(N)}} \quad (1)$$

where h_1 is the height of the most probable largest wave and h_m that of the m th largest. N is the sample size from which the largest values are generated; $N = 2000$ has been found to be appropriate for severe storms in the North Sea. The corresponding peak force ratios are

$$\frac{f_m}{f_1} = \left(\frac{h_m}{h_1}\right)^\beta \quad (2)$$

where β lies between 1.5 and 2.0 for typical platforms and depends on the magnitude of the current and the ratio of drag to inertia loading. Letting

$$f_1 = \psi \lambda_S^{ult} \quad (3)$$

where ψ is the *dynamic overload ratio*, the number of waves to be taken into account is

$$m = N^{(1 - \psi^{-2/\beta})} \quad (4)$$

Time history

For a dynamic analysis the time history of the environmental loading associated with the passage of each large wave needs to be prescribed. The ocean surface may be considered to comprise a number of individual wavelets of differing height and frequency. A large (extreme) wave is produced when the peaks of these wavelets coincide. Since each wavelet travels at a different speed, the waves immediately preceding the large wave are much smaller because the wavelet peaks no longer coincide. Thus, the arrival of large waves may be treated as independent events that are preceded by smaller waves producing 'background noise'. A suitably representative time history is judged to be obtained by running the large wave through the structure for three periods, ramping the force linearly over the first two cycles to provide a gradual 'start up' of the system response.

3. A NON-LINEAR DYNAMIC SIMULATION SYSTEM

Having defined the problem and how to analyse it, a computational method is required to solve it. The development of an efficient computational method is described in this section.

Past experience has shown that buckling/tensile-yielding of bracing members and pull-out/punch-through of the piles dominate the failure modes of most offshore steel jacket structures. The materially non-linear bar element (Fig. 2) offers the possibility of modelling these non-linearities (see discussion in Part I), and the simulation system developed in Section 3.2 below centres around structures whose non-linear member behaviour can be modelled with elements of this type. (The complexity of the linear elements used in the structural model are of no consequence.) First, however, a summary is given of the new method upon which the simulation system is based.

3.1. Summary of the pseudo-force influence method

In Part I it was shown how the non-linear dynamic response of a complex structure could be obtained by solving a reduced system of equations involving only the deformations of inelastic elements and the displacements of nodes at which mass/damping properties are lumped. This reduction technique was called the pseudo-force influence method (PFI-method).

Since the collapse behaviour of offshore jackets is generally controlled by only a few (around 10) non-linear bar elements, and since their mass/damping characteristics can be adequately represented by lumping these properties at a few nodes, the dimension of the reduced system of equations can be many times smaller than that of the original structural model. For example, a fairly typical structure with 2000 degrees of freedom (d.o.f.) can normally be

reduced to around 20 or so non-linear dynamic equations using the PFI-method. (Section 3.2 describes how to identify the non-linear elements that control collapse.)

The reduced system was achieved by identifying material non-linearity and inertia/damping resistance as unknown, deformation-dependent *pseudo-forces* acting on an equivalent linear-elastic model (Fig. 3). For the dynamic analysis of a structure with *NE* materially non-linear bars and *NM* mass/dampers, the reduced system equations are:

$$\underline{U} = \underline{U}^L + H1 \{^0(\underline{\eta})\} + H2 \underline{z}(\underline{U}) \quad (NM \text{ equations}) \quad (5)$$

$$\underline{\eta} = \underline{\eta}^L + D1 \{^0(\underline{\eta})\} + D2 \underline{z}(\underline{U}) \quad (NE \text{ equations}). \quad (6)$$

In these equations $\underline{U}^L(t)$ and $\underline{\eta}^L(t)$ are obtained from the static solution to the linear-elastic problem with applied external loading only; $\{^0$ and \underline{z} are the pseudo-force multipliers; and *H1*, *H2*, *D1*, *D2* are the (time-independent) *reduced system elastic influence matrices*. These matrices are obtained from the linear-elastic model by applying unit loads in turn to each mass/damper d.o.f. and pairs of unit loads in turn to the ends of each non-linear element. (For further details, refer to Part I.)

Solving Eqs. (5) and (6) using a suitable algorithm (see Part I) yields the pseudo-forces and applying these to the linear-elastic structure in addition to the external loading furnishes the non-linear dynamic response. This procedure gives results identical to more conventional non-linear dynamic f.e. formulations of the problem.

3.2. Building a non-linear dynamic simulation system

Of course, the PFI-method can be implemented directly in a finite-element code. However, this could be time consuming and requires a detailed knowledge of the f.e. program's architecture. Furthermore, if the f.e. program is provided by a third party, this option may not be feasible.

A powerful and unique feature of the PFI-method is the possibility of developing a portable and efficient non-linear dynamic simulation system without having access to the f.e. source code. The concept is to use an f.e. program to provide the static linear-elastic response and the influence coefficients. This information is then read by a separate program module that generates (or reads from a file) the non-linear member resistances and solves the reduced-system equations for the pseudo-forces. Feeding these pseudo-forces back into the linear f.e. program provides the non-linear dynamic response of the complete structure. The trick here is to calculate from the reduced model the pseudo-forces for the complete time history and later use a post-processor to obtain the response of the entire structural model.

With this approach, post-processing/graphics facilities associated with the f.e. package can be directly employed, and the learning time for new users is minimal. For many situations, the linear structural model will already be available and, since this can be used directly without modification, the dynamic collapse behaviour of even the most complex structures can be obtained very rapidly.

The additional stand-alone program may be viewed as an 'add on convertor module' that provides any 'off-the-shelf' static linear f.e. program with certain non-linear (dynamic) capabilities. Therefore, a user-friendly system can be developed for design engineers who are not familiar with or do not have access to non-linear f.e. programs. By setting the inertia/damping forces to zero, this system reduces to the static analysis simulator described previously by Stewart & van de Graaf (1990), which is used operationally within Shell.

The basic steps in the development of the dynamic simulation system are shown schematically in Fig. 4. They are:

1. Perform a static push-over analysis using the procedure described previously by Stewart & van de Graaf (1990) and identify the critical members (see Note 1 below) in the failure mode. The influence matrix *D1* is obtained as part of this procedure.
2. For the critical members and mass/dampers, generate the additional influence matrices *D2* and *H2* using unit load cases

applied to the linear-elastic model. Obtain *H1* by transposing *D2*. Store either the decomposed stiffness matrix or the response in all elements for each unit load case for later post-processing.

3. Obtain the static linear response time history for the critical members and mass/dampers by applying the external load to the linear-elastic model for all time steps.
4. Pass this information into the separate non-linear dynamic solver and calculate the pseudo-forces for each time step. The non-linear element resistances are also calculated (or read from a file) within this algorithm.
5. Use a post-processing facility to combine the pseudo-force response and the linear-elastic static response for all elements at each time step.
6. Check, for selected time steps, whether any other members should have been considered non-linear. If so, include these in the non-linear group, update *D1* and go to Step 2.

Notes

1. With some experience in collapse studies, one can usually identify the controlling elements on the basis of the stress ratios obtained from a linear analysis. If any are initially omitted, they will be picked up in due course and can be included with little additional effort.
2. In practice, it is easier and more accurate to retrieve the axial force in the member rather than its deformation. The deformation is obtained by dividing the axial force by the axial stiffness.
3. Step 6 covers the possibility that the dynamic failure mode differs from the static failure mode.

This simulation system is ideally suited to parametric/optimisation studies: once the base data have been derived, subsequent analyses with changes, say, to the mass/damper or critical member properties can be performed within a few minutes. This demonstrates a further advantage of the PFI-method over a direct finite-element approach.

The application of this simulation system is discussed in the next section.

4. DYNAMIC COLLAPSE ANALYSIS OF A PLATFORM HAVING A DUCTILE FAILURE MODE

To demonstrate the usefulness of the PFI-method for quickly quantifying the benefits that can be derived from inertial resistance and ductility during extreme storm loading, a preliminary assessment of the North Sea platform (or more specifically its foundation system) shown in Fig. 5 was undertaken using the non-linear dynamic collapse simulator.

4.1 The structural model

Previous work based on a static version of the simulation system (Stewart and van de Graaf, 1990) had indicated that global overturning of the platform caused by axial pull-out/punch-through of the piles was the failure mode. The critical wave attack direction was identified as 30 degrees east of platform North (Fig. 5b). The overturning-moment/static-displacement response for the *y*-direction is shown in Fig. 6, indicating a ductile failure mode.

On this basis, a suitable representation for a preliminary dynamic analysis was taken to be a linear-elastic jacket supported by a rigid base resting on the eight pile groups, each modelled as a non-linear axial spring (i.e. bar element), as shown in Fig. 5. The primary assumption in this model is that the vertical loading and overturning moment on the foundation are resisted by pile-head axial forces alone. As discussed in the publication referred to above, a detailed static analysis of the structure/foundation system indicated that this assumption was valid.

An effective mass of 24,000 tonnes was placed at the deck level (with *x* and *y* d.o.f.) to represent topside, jacket and added mass. The jacket broadside and end-on lateral stiffnesses were selected such that the first two natural periods (obtained from measured response

data) were well approximated and damping was set at 3% of critical as suggested by API-RP2A (1989). For completeness, large-displacement effects of the gravity loads were included in the pseudo-forces at the deck level. The influence of these effects was insignificant, however.

The advantage of this particular (10 d.o.f.) model was that all of the elastic response data for the non-linear dynamic simulator could be calculated analytically. This was realised as follows.

- (1) The piles were initially taken to be linear-elastic with equal stiffnesses $k_0 = 2800 \text{ MN/m}$. This defined a reference model to which the pseudo-forces and external loads were later applied to obtain the true non-linear dynamic response.
- (2) As the base was rigid, beam bending theory could be employed to calculate the response of the elastic pile springs to both vertical loading and overturning moment. For example, the influence matrix **D1** was derived by applying a unit tensile load to each pile j and calculating the extension of all piles i , giving

$$D1(i,j) = \left(\frac{1}{n} + x_i x_j / \sum_{k=1}^n x_k^2 + y_i y_j / \sum_{m=1}^n y_m^2 \right) / k_0, \quad (7)$$

where x_i, y_i are the co-ordinates of the i 'th of the n piles with respect to the centroid of the pile system.

- (3) Taking the jacket to have a constant stiffness EI^j over its entire height (but different stiffnesses in the x and y directions), elementary structural mechanics principles were used to determine the response of the deck to the environmental loading. For example, the deck deflection in the y -direction is given (Fig. 7) as

$$\delta_y = \frac{F_y L^2}{EI^j} \left(\frac{L}{3} + \frac{h-L}{2} \right) + \frac{F_y L h}{k_0 I_{xx}} \quad (8)$$

where $I_{xx} = \sum_{m=1}^n y_m^2$ is the moment of inertia of the foundation

system about the x - x axis; $L(t)$ is the height above the mudline to the centre of action of the applied load $F_y(t)$; and h is the height of the deck. The first term in Eq. (8) arises from bending of the jacket, while the second term comes from the rotation of the foundation. The deflection in the x -direction is obtained similarly.

The development of this model should provide some additional insight into influence matrices and their generation. For more complex structural models, the procedure is only a little more involved in that the elastic response and influence matrices are now calculated using a linear elastic f.e. program. All other aspects of the simulation system, however, remain unchanged.

4.2 Wave and current loading

A wave-load program was written to generate the applied shear-force and overturning-moment time history. The structure was represented as a set of parallel vertical cylinders with appropriate hydrodynamic coefficients. Airy wave theory with delta stretching (Rodenbusch, 1986) was used to generate the wave particle velocities. A uniform current profile was used, and the forces on the cylinders integrated using Simpson's rule. The base-case data were: wave height = 29.2m; wave period = 17.2 secs; current = 0.8m/sec.

4.3 Analysis procedure and results

Several non-linear dynamic analyses were undertaken for the 30° wave attack direction, with the current and wave period varied to determine the sensitivity of the results to the input data. In all cases the force time history was calculated for three wave periods and linearly ramped over the first two cycles to provide a start-up condition.

This force history was then normalised such that its peak value matched that corresponding to static collapse (see Fig. 8 for a typical trace of the overturning moment). Thereafter, the loading profile was scaled up by the dynamic overload factor ψ and time marched through the structure. The platform was deemed to be inoperable if the permanent mudline rotation exceeded 1 degree, corresponding to a deck displacement of 3.5 m (Fig. 6).

Selected results from these analyses, representing the passage of one extreme wave, are shown in Fig. 9. It can be seen that the peak of the time dependent load history may be increased by about 20% above that causing static collapse before the deformations exceed the available ductility. From Fig. 9b it is noted that increasing either the current or the wave period results in an increased deformation; since the time during which the applied load exceeds the structural resistance is extended.

Taking account of the other large waves in the extreme storm (see Section 2.2) reduced the acceptable overload to 15% (for the base-case data). The β value used in this calculation (cf. Eq. (2)) was 1.7.

5. PERFORMANCE OF SEMI-DUCTILE SYSTEMS

The model described above can be used to gain some insight into the dynamic collapse behaviour of semi-ductile systems. By adjusting the characteristics of pile A3, the static response curve shown in Fig. 10a was obtained. This (hypothetical) system has a robustness factor α equal to 0.8. The results of the dynamic analysis for the base-case data are presented in Fig. 10b for the passage of one extreme wave. The dynamic overload required to reach a deck displacement of 3.5m is now only 7% instead of the 20% that could be accommodated if the system were ductile. Accounting for multiple wave encounters in the storm would reduce this to unity. This illustrates the detrimental effect on dynamic capacity if system strength deterioration occurs in the post-ultimate-strength regime.

Additional work is required in this complex area of dynamic response of semi-ductile systems, taking account of strength degradation upon repeated loading in a severe storm. The dynamic simulation system presented is ideally suited for this investigation.

6. DISCUSSION

The need to provide structures with adequate ductility in offshore regions affected by earthquakes is well appreciated (Gates et. al., 1977; API-RP2A, 1989). However, most offshore structures in non-seismic zones are designed only with strength in mind. Thus, structural configurations that are not permitted in seismic zones (e.g. K-bracing in primary vertical frames) are commonly found in areas such as the North Sea, where earthquake loading is not a design event.

The lack of industry interest in designing ductile performance into offshore structures exposed to extreme storms can perhaps be attributed to the fact that the benefits of doing so were not visible. From the above study, however, it is apparent that ductile performance is a highly desirable feature for these structures. Additionally, ductile structures usually have good damage tolerance and high reserve capacities.

7. CONCLUSIONS

1. By taking advantage of the pseudo-force influence method, a portable and efficient non-linear dynamic simulation system can be constructed around an unmodified, linear, finite-element program.
2. A simulation system of this type was developed and then used to perform a preliminary extreme storm dynamic overload analysis of a large North Sea platform having a ductile foundation failure mechanism. This analysis revealed a 15% increase in capacity over the static ultimate strength. Accumulated permanent deformations resulting from several large waves in the extreme storm were taken into account.

3. A semi-ductile system was considered in which the post-ultimate-strength was 80% of the ultimate static strength. For this case the dynamic resistance was limited to the static capacity.
4. This work confirms that ductile platform behaviour (in the post-ultimate-strength regime) is highly desirable for all offshore structures and not only for those that are subjected to earthquake loading.

REFERENCES

Anderson, W.D., Silbert, M.N. & Lloyd, J.R. (1982). 'Reliability procedure for fixed offshore platforms', *J. of the Structural Div., ASCE*, Vol. 108, No. ST11.

Bea, R.G., Puskar, F.J., Smith, C., & Spencer, J.S. (1988). 'Development of AIM programs for fixed and mobile platforms', *Offshore Technology Conference*, OTC 5703.

API-RP2A (1989). *Recommended practice for planning, designing and constructing fixed offshore platforms*, Eighteenth Ed., American Petroleum Institute.

FENRIS. *Finite Element Non-linear Integrated System*, computer program, Veritec, Norway.

Gumbel, E.J. (1958). *Statistics of extremes*, Columbia University Press.

Gates, E.W., Marshall, P.W. & Mahin, A. (1977). 'Analytical methods for determining the ultimate earthquake resistance of fixed offshore structures', *Offshore Technology Conference*, OTC 2751.

INTRIA. *Inelastic Tower Response Analysis*, computer program, ISEC, USA.

Lloyd, J.R. and Clawson, W.C. (1984). 'Reserve and residual strength of pile founded offshore platforms', *Int. Symposium on The role of Design Inspection and Redundancy in Marine Structural Reliability*, (Eds. Faulkner, Shinozuka, Fiebrant & Franck), National Academy Press.

Moan, T., Amdahl, J., Engseth, A.G. & Granli, T. (1985). 'Collapse behaviour of trusswork steel platforms', *Behaviour Of Offshore Structures conference*, BOSS '85.

Nordal, H. (1990). 'Application of ultimate strength analysis in design of offshore structural systems', *Integrity of Offshore Structures - 4*, Elsevier Applied Science.

Piermattei, J., Ronalds, B.F. & Stock, D.J. (1990). 'Jacket ductility design', , OTC 6383.

Rodenbusch, G. (1986). 'An empirical model for random directional wave kinematics near the free surface', *Offshore Technology Conference*, OTC 5097.

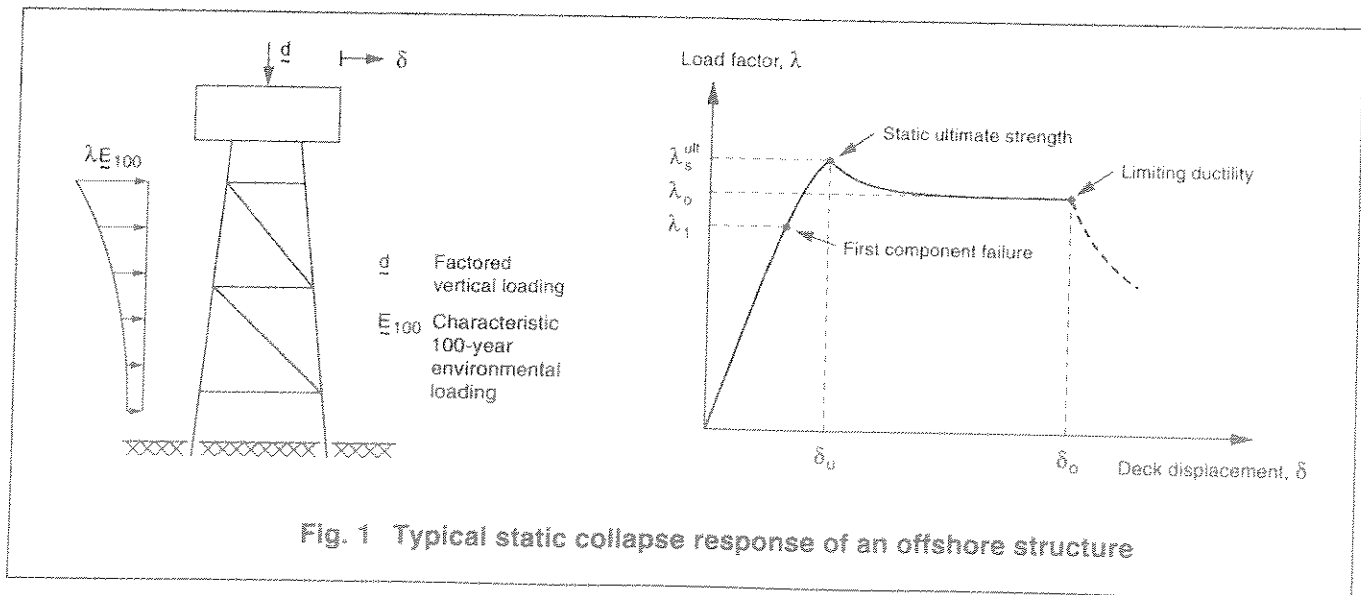
Stewart, G., Efthymiou, M. & Vugts, J.H. (1988). 'Ultimate strength and integrity assessment of fixed offshore platforms', *Behaviour Of Offshore Structures conference*, BOSS '88.

Stewart, G., and van de Graaf, J.W. (1990). 'A methodology for platform collapse based on linear superposition', *Offshore Technology Conference*, OTC 6311.

Tromans, P. and van de Graaf, J.W. (1992). 'A substantiated risk assessment of a jacket structure', *Offshore Technology Conference*, OTC 7075.

Titus, P.G. and Banon, H. (1988). 'Reserve strength analyses of offshore platforms', *7 th Offshore South East Asia conference*, OSEA 88179.

USFOS. *A Computer Program for Progressive Collapse Analysis of Steel Offshore Structures*, SINTEF, Norway.



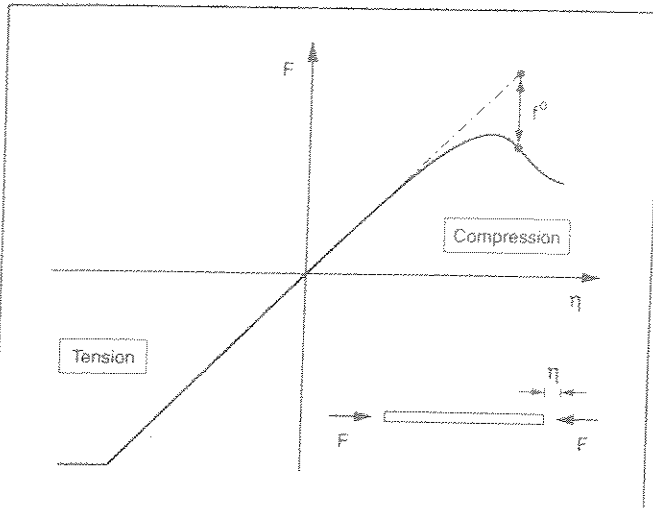


Fig. 2 Non-linear bar element

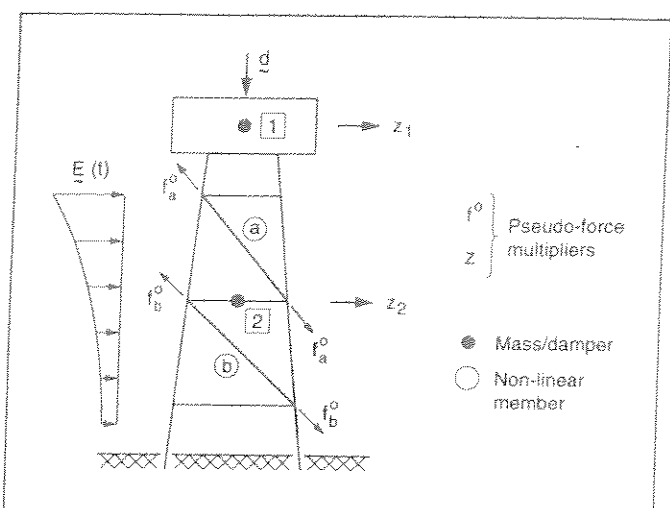


Fig. 3 Non-linear dynamic simulation principle

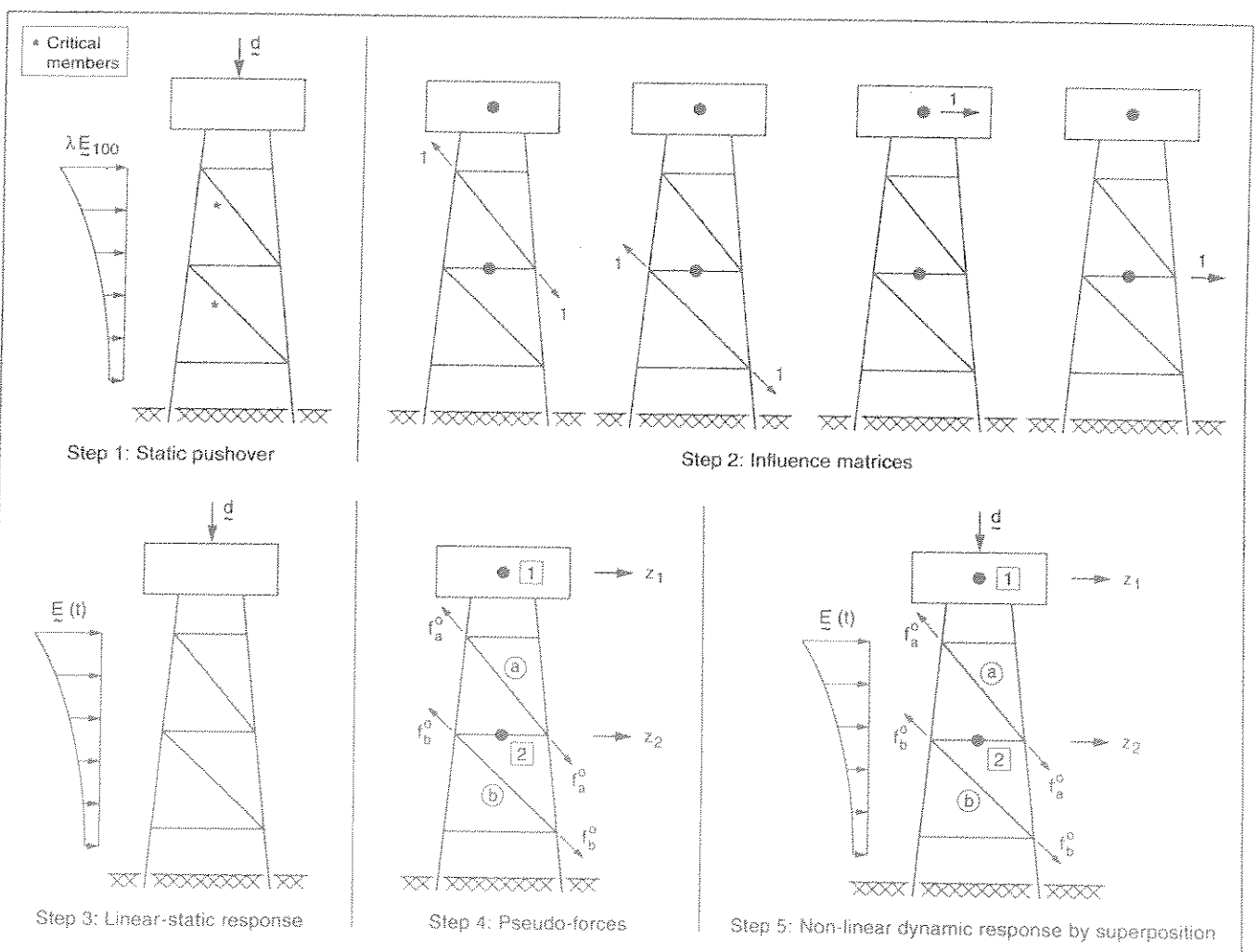


Fig. 4 A step-by-step guide to developing a non-linear dynamic simulation system

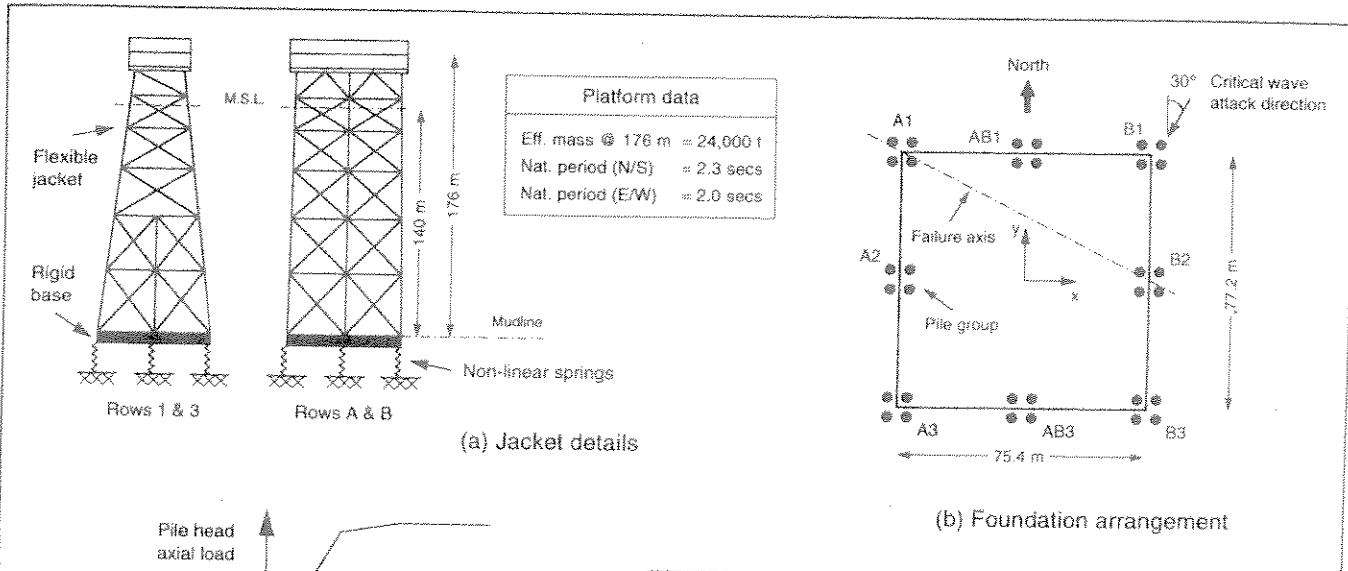


Fig. 5 Structural model data

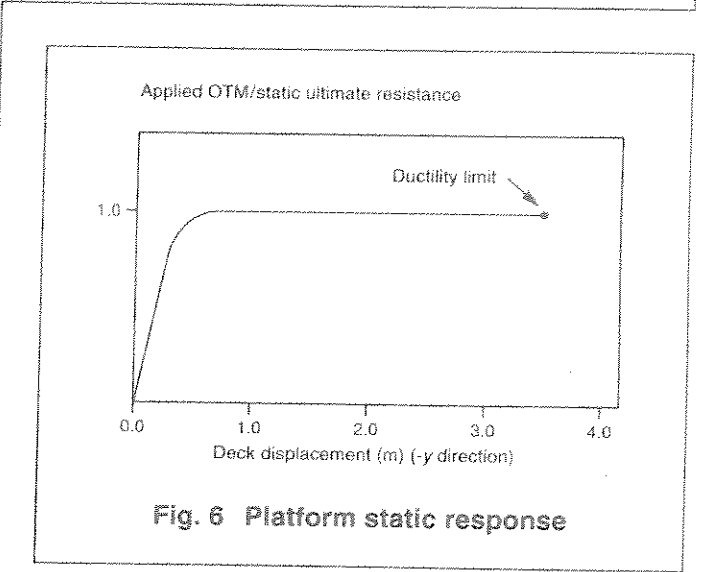


Fig. 6 Platform static response

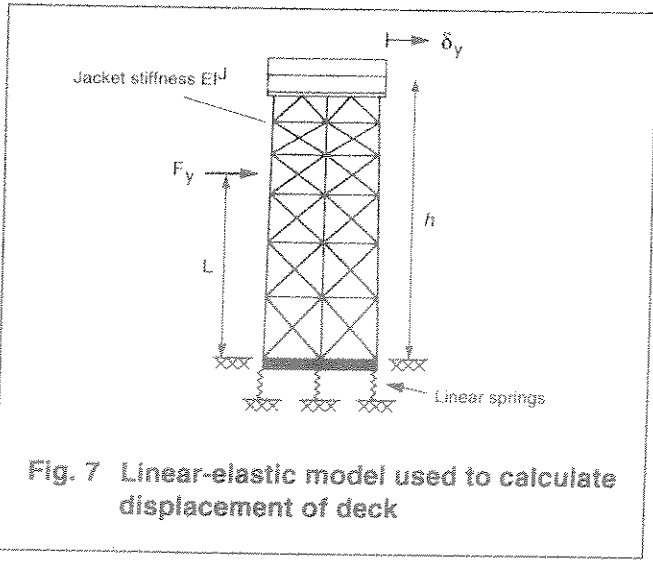


Fig. 7 Linear-elastic model used to calculate displacement of deck

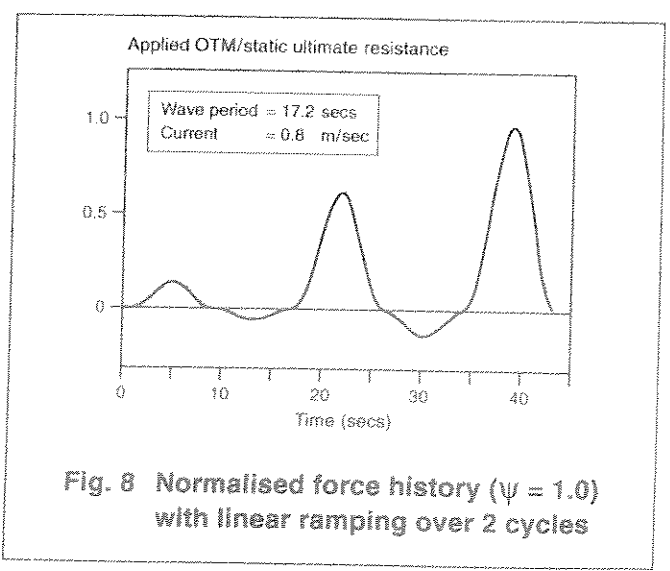
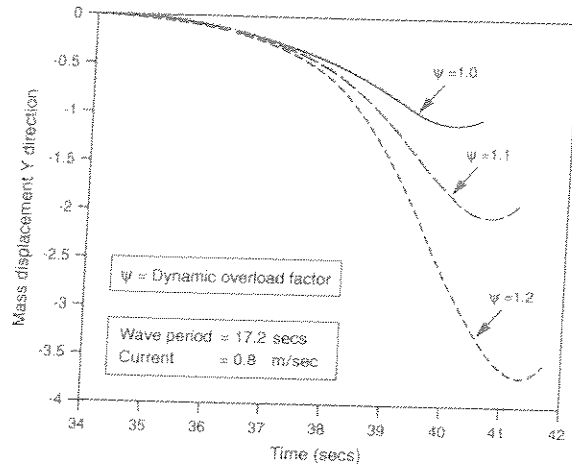


Fig. 8 Normalised force history ($\psi = 1.0$) with linear ramping over 2 cycles

(a) Base-case data



(b) Sensitivity at $\psi = 1.2$

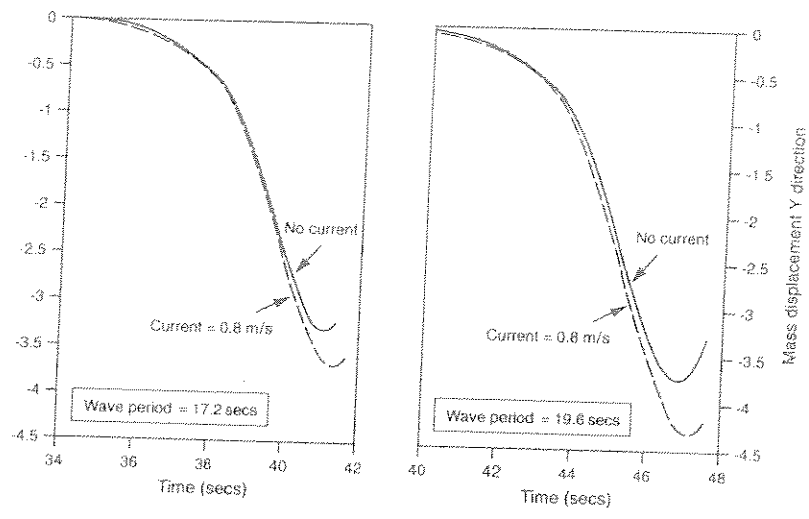
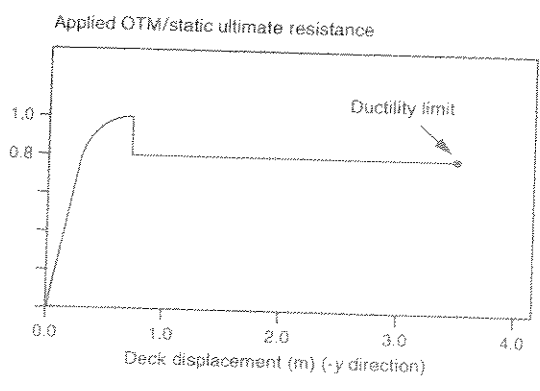


Fig. 9 Platform non-linear dynamic response

(a) Static response



(b) Non-linear dynamic response

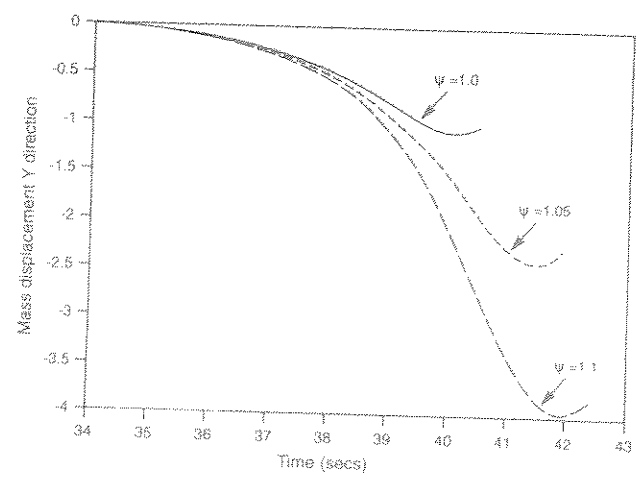


Fig. 10 Response of Semi-Ductile system

APPENDIX

B

BEA, R.G. AND YOUNG, C.: "LOADING AND CAPACITY EFFECTS ON PLATFORM PERFORMANCE IN EXTREME CONDITION STORM WAVES AND EARTHQUAKES" PROC. OFFSHORE TECHNOLOGY CONFERENCE (OTC), HOUSTON, USA, 1993, PAPER 7140

- o0o -



OTC 7140

Loading and Capacity Effects on Platform Performance in Extreme Condition Storm Waves and Earthquakes

R.G. Bea and Carlton Young, U. of California

Copyright 1993, Offshore Technology Conference

This paper was presented at the 25th Annual OTC in Houston, Texas, U.S.A., 3-6 May 1993.

This paper was selected for presentation by the OTC Program Committee following review of information contained in an abstract submitted by the author(s). Contents of the paper, as presented, have not been reviewed by the Offshore Technology Conference and are subject to correction by the author(s). The material, as presented, does not necessarily reflect any position of the Offshore Technology Conference or its officers. Permission to copy is restricted to an abstract of not more than 300 words. Illustrations may not be copied. The abstract should contain conspicuous acknowledgment of where and by whom the paper is presented.

ABSTRACT

Dynamic - transient loading effects from extreme storm waves and earthquakes can have important influences on the nonlinear ultimate limit state performance of fixed offshore platforms. Recorded and synthetic storm wave and earthquake time histories have been used to develop loading time histories acting on template-type platforms having natural periods in the range of 1 to 5 sec. The interactions of these loading histories with the dynamic, nonlinear, hysteretic performance characteristics of idealized systems have been analyzed. A static push-over capacity modification factor has been developed to recognize transient loading - structure performance characteristics. The results from the idealized systems have been correlated with results from time domain nonlinear analyses of platform structure systems subjected to intense wave and earthquake loadings. For the global behavior of the platforms studied, the results based on the simplified systems are in good agreement with those from the complex analyses.

References at end of paper.

INTRODUCTION

Due to the transient and dynamic aspects of most environmental loadings imposed on and induced in offshore platforms, it can be important to recognize the differences between loadings and loading effects.^{1,2,3} The term "loadings" is taken to represent the forces that are imposed on an offshore structure that are fundamentally independent of how the structure responds to the imposed forces. Such forces frequently are referred to as being static even though they vary with time.

The term "loading effects" is taken to represent the internal forces that are generated within an offshore structure that are dependent on how the structure responds to the imposed forces.

Loading effects induced in an offshore structure are determined by: (a) the characteristics of the loadings, and (b) the performance characteristics of the structure, Table 1 summarizes the primary loading and structure performance characteristics (Fig. 1).

Table 1: Loading and Capacity Factors

Loading Factors	
t_d / T_n	ratio of duration of the force pulse imposed on the structure (t_d) to the natural period of the structure (T_n)
N_c	numbers of cycles of the force pulses (N_c); the degree of periodicity of the imposed loads
$F-t$	specific forms of the force (F) - time (t) pulses
Ψ	resultant load factor
Structure Performance Factors	
T_n	elastic stiffness and mass reflected in the natural period of the structure (T_n)
D	damping (structural, foundation, and hydrodynamic) expressed through a viscous damping ratio (D)
F_m / R_{us}	ratio of the maximum static loading (F_m) to the structure maximum static load capacity (R_{us}); the overload ratio
α	residual load capacity (R_r) expressed as a residual strength ratio (α); $\alpha = R_r / R_{us}$
μ	ultimate deformation capacity (Δ_p) expressed as ductility (μ); $\mu = \Delta_p / \Delta_e$; Δ_e is the deformation at which the first significant nonlinear behavior occurs
H_c	hysteretic behavior as influenced by cyclic degradation and rate of loading characteristics (H_c)
H_m	multi-mode response characteristics (H_m)
Ω	resultant capacity factor

The platform global factor-of-safety for lateral loadings can be expressed by the Reserve Strength Ratio (RSR):

$$RSR = \frac{R_{us}}{S_D} (F_v) = RSR_s (F_v) \dots \dots \dots (1)$$

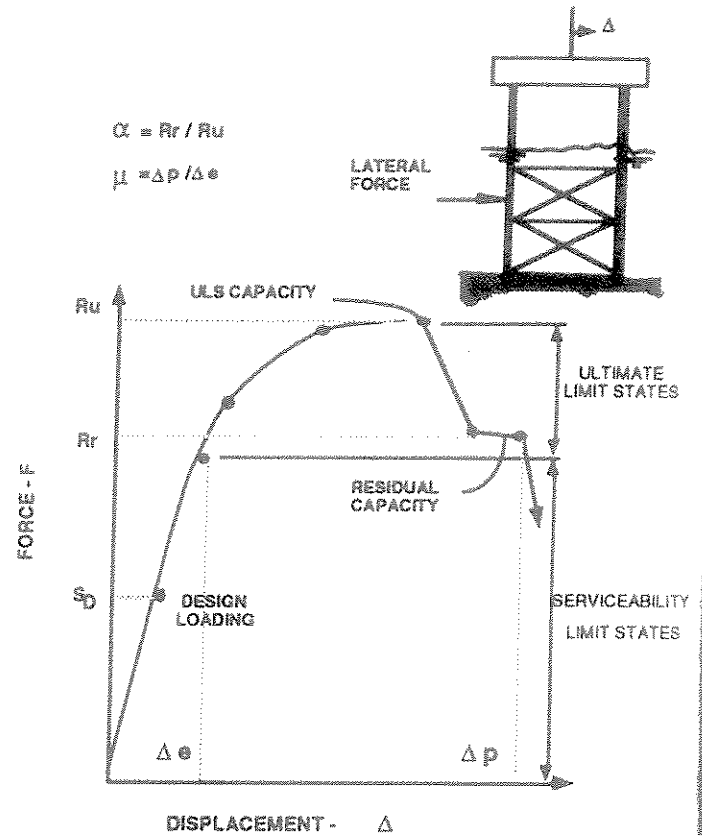


Fig. 1. Structure performance factors

S_D is the maximum static lateral loading (Fig. 1) determined by the design environmental condition parameters and force determination procedures in design guidelines. R_{us} is the ultimate limit state maximum lateral loading capacity determined by static push-over analyses. The static Reserve Strength Ratio (RSRs) is based on S_D and R_{us} . F_v is the ratio of the resultant capacity factor (Ω) to the resulting loading factor (Ψ) (Table 1):

$$F_v = \frac{\Omega}{\Psi} \dots \dots \dots (2)$$

The "capacity modifier", F_v , combines the loading and ultimate limit state performance characteristics of the platform structure - foundation system.

This paper addresses F_v for extreme condition wave and earthquake lateral forces developed on conventional steel, template-type platforms having natural periods (T_n) in the range of $T_n = 1$ to 5 sec.

Ductility (μ) is used as a primary reflector of the damage producing potential of the transient loadings. The ductility capacity of a platform (Fig. 1) is determined by the lateral displacement at which the structure can no longer support its gravity loadings (Δp) divided by the lateral displacement at which the overall system demonstrates its first significant nonlinear behavior (Δe):

$$\mu = \frac{\Delta p}{\Delta e} \dots\dots\dots (3)$$

The study summarized in this paper has been focused on the performance characteristics of elastic and nonlinear, hysteretic, single-degree-of-freedom (SDOF) systems. This has been done for three reasons. The first is for simplicity in analysis and interpretation. The analyses of SDOF systems are relatively easy to perform and understand. A large number of different parameters and characteristics can be studied efficiently.

The second reason is related to the performance characteristics of the type of platforms that were of concern in this study. Generally the first two lateral orthogonal modes control the primary response characteristics of the platforms. Nonlinear behavior is often concentrated in one of the three major components that comprise the platform: the deck supporting system, the jacket, and the pile foundation. The nonlinear performance characteristics of each of these components can be different and SDOF systems can be utilized to study the importance of these differences to the loading effects induced in the platform system.

A third reason is related to the objectives of this study. The objective is not to understand

the details of how nonlinear and dynamic-transient loadings affect individual elements within a platform. Very detailed and complex multi-degree of freedom (MDOF) analytical models must be used for such purposes. The objective of this study is to understand how dynamic-transient loadings and the overall nonlinear behavior of the platform interact to influence the effective capacity of the platform to resist intense environmental loading events.^{1,2,3}

WAVE FORCE EFFECTS

Wave Records

Results based on three recorded wave amplitude time histories are discussed in this paper. These are wave amplitude time histories recorded in deep water during intense hurricanes in the Gulf of Mexico. They are identified as "Camille", "Juan", and "Elena". These recorded time histories were chosen from the most intense parts of the storms. Recorded wave time histories were chosen for the initial studies because they contain realistic combinations of wave amplitudes, frequencies, and phases. Fig. 2 is an example of one of the recorded wave amplitude time histories used in this study (Elena).

Synthetic wave amplitude time histories also were studied. The component amplitudes, frequencies, and phases in the recorded time histories were determined from Fourier decomposition analyses. The component amplitudes and frequencies were retained and using random phases the amplitude and frequencies were linearly superimposed to develop other realizations of wave amplitude time histories. Two such synthetic time histories were generated from each of the recorded histories.

Short-term time histories having durations of 140 sec were used for the majority of the analyses. This strategy was adopted after analyses of longer term time histories having lengths up to 1,200 sec indicated that the extreme responses (largest ductilities) of the sys-

tems were associated with a few waves that preceded and followed the peak wave amplitude in the time history.

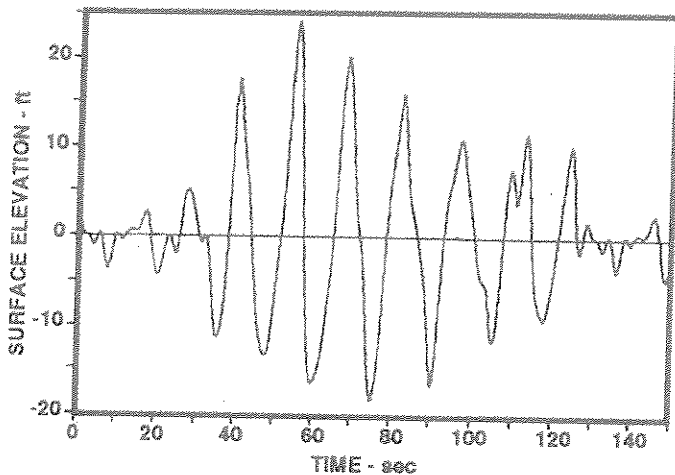


Fig 2. Recorded wave amplitude time history from intense portion of hurricane Elena

Wave Forces

The characteristics of the wave force amplitude time histories are determined by the characteristics of the platform that the waves act on. In this study, the structural characteristics of an 8-leg template-type self-contained drilling and production platform (Fig. 3) in a water depth of 322 ft were utilized to generate the global horizontal force-time histories.⁴⁻⁶ The irregular wave amplitude time histories were imposed broadside to the platform. Steady currents also were imposed broadside to the platform. The magnitude and depth profile of these currents were based on results from hindcast studies of the three hurricanes. The surface currents ranged from 1.5 fps to 3.5 fps and decreased to 0.2 fps to 0.5 fps at the sea floor.

The Morison equation was used together with the revised API wave force guidelines to generate the hydrodynamic forces.⁷ Water depth stretched linear wave theory was used to determine the kinematics of the irregular waves. Drag and inertia coefficients were used that recognized the effects of flow conditions

(Reynolds Numbers and Keulegan-Carpenter Numbers), currents, marine fouling, directional spreading, shielding, and blockage.

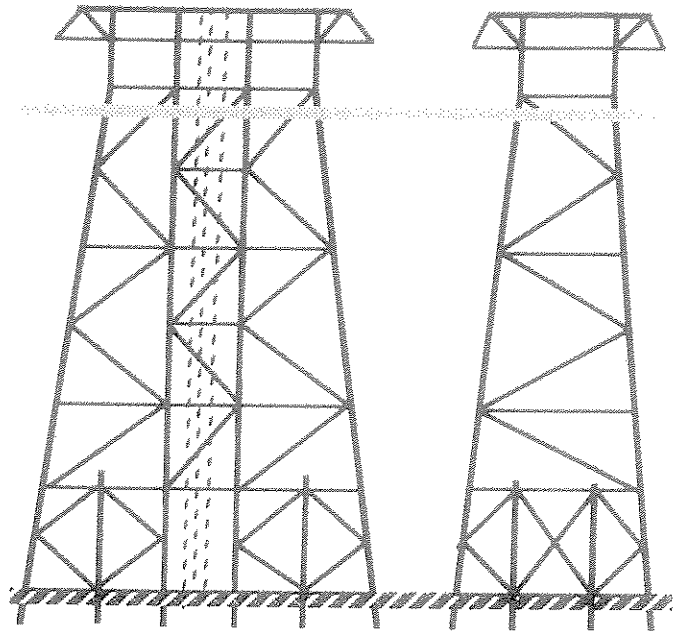


Fig. 3. Elevations of platform used to generate wave force time histories

An adaptation of the Morison equation was used to describe the wave forces that were developed when the crests of the waves reached the lower decks of the platform.⁸ To generate the wave force time histories that included wave forces developed on the lower deck of the platform, the mean water depth was artificially raised to bring the highest crests in the wave record 10 ft into the lower deck of the platform. In this manner, global horizontal force-time histories were generated with and without the effects of wave crest loadings acting on the platform lower decks.

Fig. 4 and Fig. 5 are examples of wave force time histories without and with deck forces, respectively, for the recorded Elena wave amplitude time history. The records that incorporate deck wave forces have much sharper loading peaks. These "force spikes" can be expected to have important effects on the dynamic response of a platform.

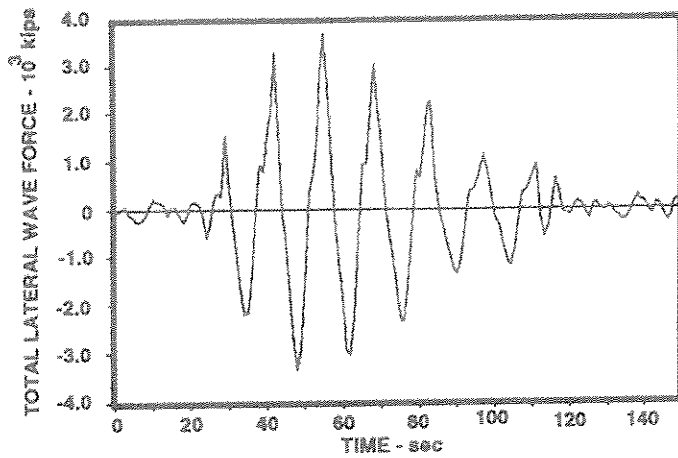


Fig. 4. Wave force time history without deck forces (recorded Elena)

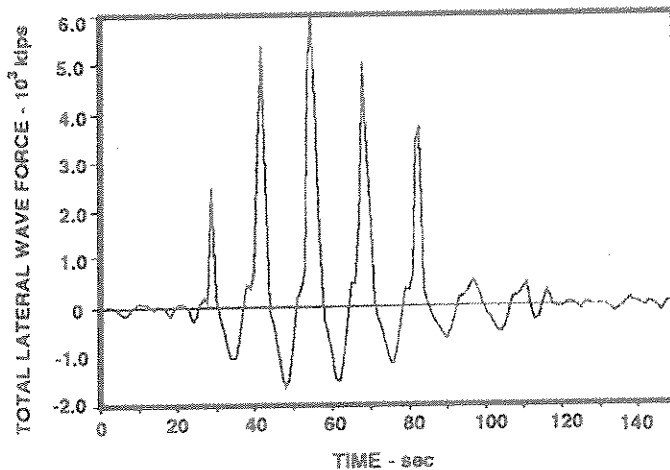


Fig. 5. Wave force time history with deck forces (recorded Elena)

Idealized Systems

As a first step, the performance characteristics of elastic-perfectly plastic (EP), non-cyclic degrading (ND), SDOF systems that had periods in the range of $T_n = 1$ to 5 sec were studied. As a base case condition, the viscous damping ratio (D) was assumed to be $D = 5\%$. Damping in the range of 1% to 10% was studied. This amount of damping is attributed to structural, foundation, and hydrodynamic sources.^{9,10}

Ductility spectra (plots of μ versus T_n) are presented in Fig. 6 as a function of the overload ratio (ratio of peak static force to maximum static load resistance) for EP ND SDOF systems subjected to the recorded Elena force history without deck wave forces (Fig 4).

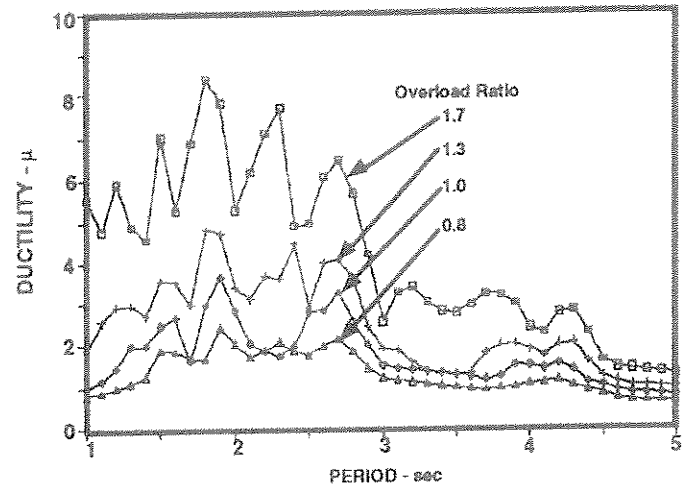


Fig. 6. Elena ductility spectra (recorded without deck wave forces)

There is a general increase in the ductility demand with decreasing period and with increases in the overload ratio. There are significant "peaks and valleys" in the ductility spectra, particularly for $T_n \leq 3$ sec. Slight differences in T_n can result in substantial differences in the ductility demands.

The quadratic drag forces due to the wave and current velocities can be expected to produce force harmonics at even and odd multiples of the primary force frequencies.¹¹⁻¹³ The primary force frequencies for the records studied were in the range of 10 to 12 sec. The major peaks in the ductility spectra appear to be associated with these harmonics.

Note that the ductility demand can be greater than one ($\mu > 1$) even though the overload ratio is less than one. This is due to the dynamic forces induced in the system by the loadings.

These ductility demand major peaks and valleys could help explain why adjacent platforms in hurricanes such as "Andrew" could be expected to perform very differently. For the same overload ratio, differences in the mass and stiffness characteristics that could result in differences in the periods of the structures could result in dramatic differences in ductility demands. As will be discussed, differences in damping and cyclic - strain degradation characteristics of the structures could result in additional dramatic differences in ductility demands.

Ductility spectra for the Elena record that incorporated deck wave forces are summarized in Fig. 7. For a given period and the same overload ratio, the ductility demands generally are much larger. This is due to additional dynamic forces imparted to the systems by the wave crest in the deck force spikes. Platforms that have decks that are inundated not only experience a significant increase in the maximum wave forces, but as well there can be an impulsive dynamic loading effect (Fig. 5) that will dramatically increase the ductility demands in the structure.

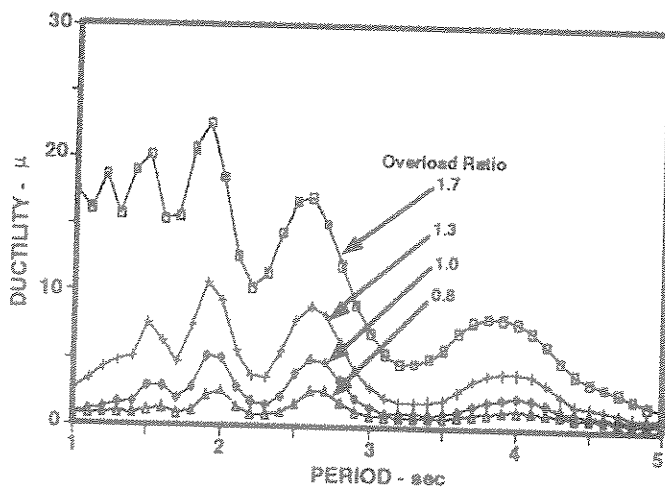


Fig. 7. Elena ductility spectra (recorded with deck wave forces)

The ductility spectra for one of the synthetic time histories based on the recorded Elena amplitude time history (with deck wave

forces) are presented in Fig. 8. Even though the random phase record has the same amplitude and frequency components, it generally produces higher ductility demands than the record that preserved the recorded phases (Fig. 7). The ductility demands depend on the degree of periodicity of the forces that are developed in a particular time history in the sector of the time history that produces the maximum responses. The synthetic time histories generally produced higher ductility demands because of a greater degree of periodicity in the random phase wave amplitude time histories.

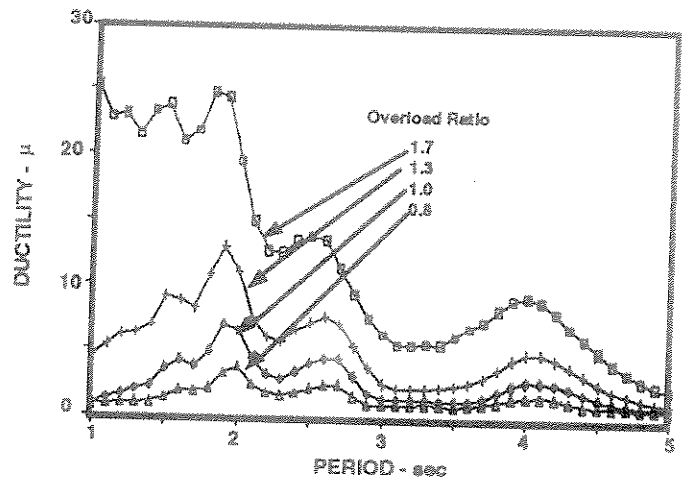


Fig. 8. Elena ductility spectra (random phases with deck wave forces)

Fig. 9 summarizes the ductility spectra for recorded Camille amplitude time history (with deck wave forces). Compared with Fig. 7 there are generally larger ductility demands for given overload ratios associated with the peaks in the spectra and about the same ductility demands for the valleys. Note that the peaks in the ductility spectra at $T_n \approx 4$ sec and $T_n \approx 2.6$ sec occur at about the same periods in all of the spectra.

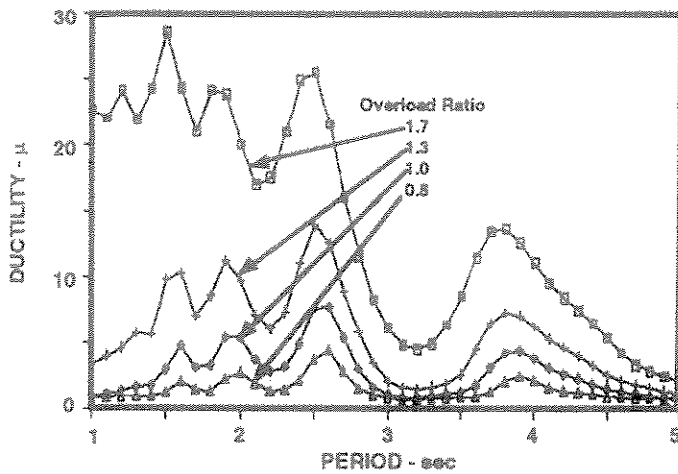


Fig. 9. Camille ductility spectra (recorded with deck forces)

The effects of damping on the ductility spectra are illustrated in Fig. 10. For a given overload ratio, damping in the range of $D = 1\%$ to 10% generally is not important in determining the ductility demands. The major exception is associated with the primary peaks in the ductility spectra. In the vicinity of these peaks, the lightly damped systems develop significantly greater ductility demands. The high degree of periodicity associated with the primary force harmonics results in a resonance effect that is significantly influenced by damping.

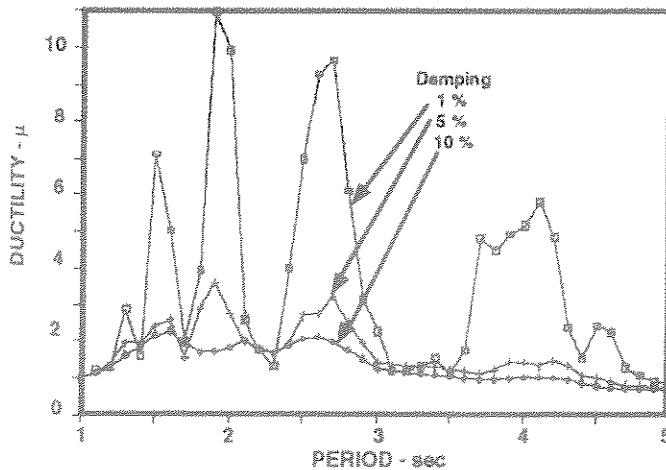


Fig. 10. Elena ductility spectra for various damping ratios (recorded, without deck forces, $F_v = 1.0$)

SDOF degrading systems also have been studied. The degradation characteristics model those determined from cyclic compression - tension axial loading tests on a tubular braced frame.^{14,15} The braces degrade in capacity after the peak buckling strength is reached and also degrade in capacity as a function of the intensity and numbers of cycles (Fig. 11). The brace characteristics that have been studied are based on braces that have effective length to radius of gyration (KL/r) ratios in the range of 50 to 85, diameter to thickness ratios (D/t) in the range of 30 to 40, and are fabricated with A36 steel. These are characteristics typical of braces found in many template-type platforms.

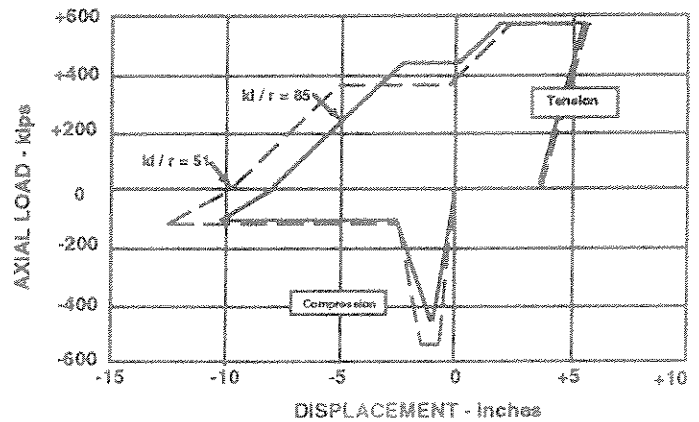


Fig. 11. Analytical model of brace tensile - compressive behavior

The effects of the simulated brace behavior on the recorded Elena (without deck forces) ductility spectra are illustrated in Fig. 12 for an overload ratio of 1.0. The simulated brace does not differ appreciably from that of a comparable EP ND system except in the vicinity of the peaks in the ductility spectra. The lowered energy dissipation capacity in the simulated brace system has an effect on the ductility demand that is similar to that of an EP system with lowered damping. This is an aspect that warrants further study and additional analyses of strain and cyclic degrading SDOF systems are presently being performed.

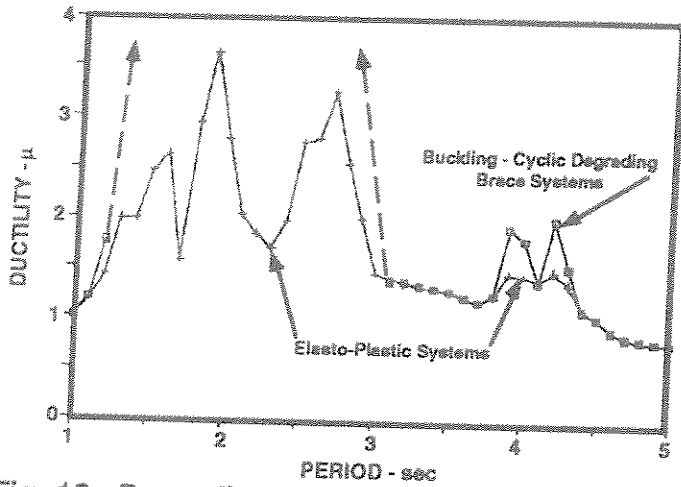


Fig. 12. Degrading brace ductility spectra (Elena, recorded, no deck loading, $F_v = 1$)

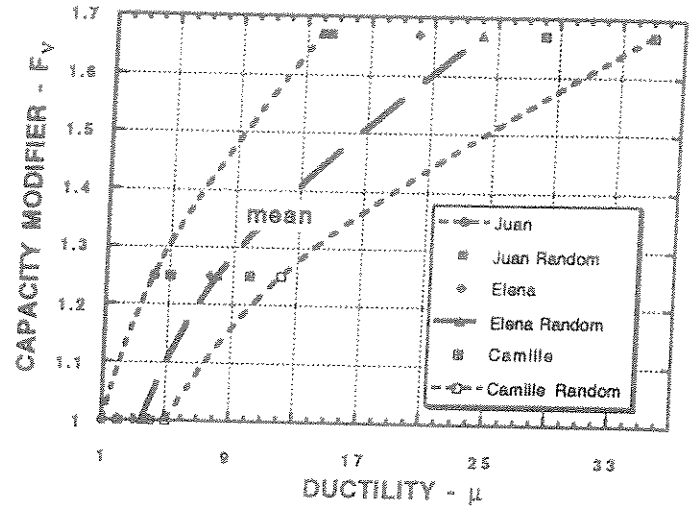


Fig. 14. Capacity factors for given ductility capacities ($T_n = 1.5$ sec, with deck loadings)

Fig. 13 and Fig. 14 summarizes the results from the analyses of the EP ND systems in terms of the capacity modifier, F_v , and the ductility capacity, μ , for $T_n = 1.5$ sec, $D = 5\%$, with and without deck wave loadings for six of the force time histories. The mean F_v - μ trend together with an outline of the upper and lower bounds are shown.

In the case of no deck wave forces, the Elena recorded and synthetic time histories bracket all of the other results. In the case of the time histories that have deck wave forces, the Juan recorded and Camille synthetic records bracket all of the other results.

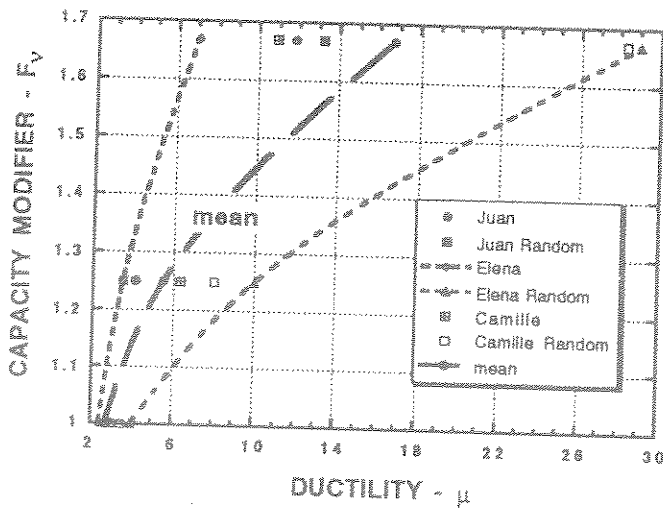


Fig. 13. Capacity factors for given ductility capacities ($T_n = 1.5$ sec, without deck loadings)

For a platform that could develop a ductility capacity in the range of $\mu = 3$ to 4 and for the case of no deck wave forces, the mean capacity modifier would be $F_v \approx 1.2$. This modifier would have a coefficient of variation (V_{F_v}) of $V_{F_v} = 39\%$. For the case with deck forces, $F_v \approx 0.9$.

Platform Response Characteristics

Nonlinear time-history wave force analyses were performed on the platform shown in Fig. 3. The platform was loaded broadside with the recorded Camille and Elena wave amplitude time histories without deck wave forces. The drag coefficients were increased to produce a maximum static lateral storm force overload of $F_v = 1.2$.

The cyclic nonlinear behavior characteristics of the platform braces and pile supporting

soils were based on algorithms that have been developed to describe the behavior of these elements.¹⁴⁻¹⁷ The degradation in strength due to plastic cycling and the increase in strength due to strain rate effects were taken into account. The platform legs, piles, and deck legs were modeled as elastic elements.^{6,18} Based on results from ambient vibration measurements that have been performed on this platform⁹, damping was assumed as $D = 5\%$. The measurements indicated that the natural period of the platform was $T_n = 1.5$ sec.

Fig. 15 summarizes the results from the recorded Camille nonlinear time history analyses as the time history of the broadside horizontal displacements of the upper platform deck. The first significant yielding of the platform structural system occurred at a displacement of approximately $\Delta e = 1.0$ ft (the soils yielded at much smaller displacements). The nonlinear behavior was concentrated in the platform's diagonal braces above the bottom bay that contained the skirt pile bracing. The maximum ductility demand was approximately $\mu = 3.5$. This result is in good agreement with the ductility results from the SDOF EP ND idealized system results summarized in Fig. 10.

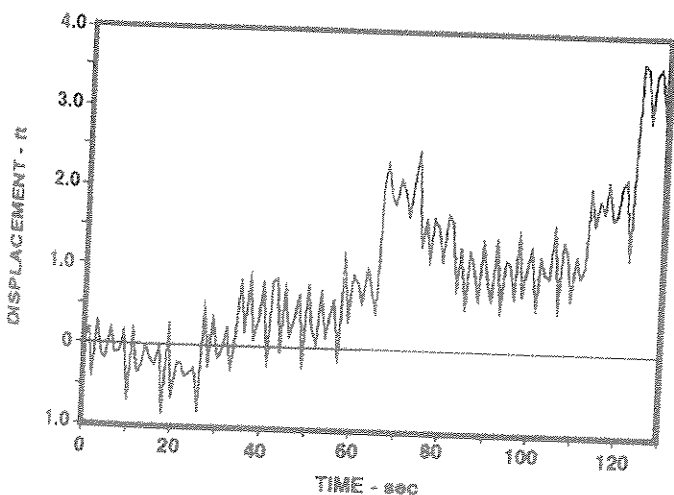


Fig. 15. Platform displacement - time history for overload factor of $F_v = 1.2$ (recorded Camille)

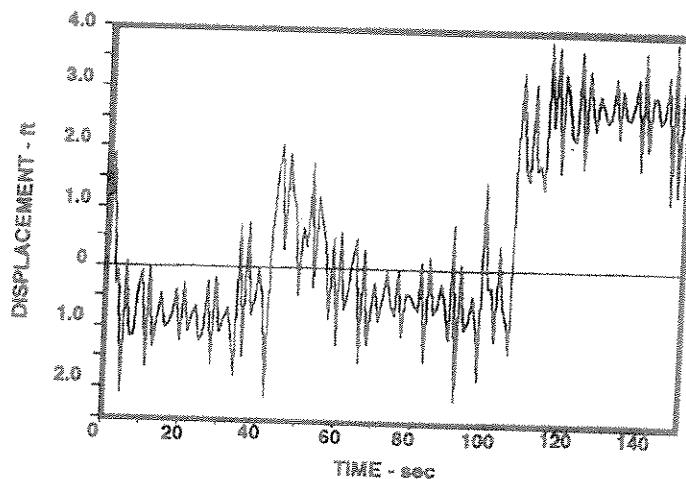


Fig. 16. Platform displacement - time history for overload factor of $F_v = 1.2$ (recorded Elena)

Fig. 16 summarizes the comparable results from the recorded Elena time history. The peak ductility developed during the force time history was $\mu = 4.0$. This result is in good agreement with the ductility results from the SDOF EP ND idealized system results summarized in Fig. 10.

While these comparisons of results from complete platform systems with those from idealized systems are limited, they are encouraging. For the class of platform which has been studied, the analyses indicate that the results from idealized systems can be used to infer the global capacity and ductility behavior of the complete platform system. The load - deformation performance characteristics of the idealized system must be able to mimic the behavior of the complete platform system.

Stewart has performed a study of the ultimate limit state performance characteristics of an 8 - leg platform in a water depth of 459 ft ($T_n = 2.0$ to 2.3 sec) subject to dynamic wave forcing.¹⁹ Stewart's study results are comparable with those from this study. His results indicate $F_v = 1.2$. Consideration of semi-ductile member behavior and cyclic loading effects resulted in $F_v = 1.07$ to 1.0 .

EARTHQUAKE FORCES

The ultimate limit state dynamic response of simplified and complex structural systems subjected to earthquake excitations has been an area of intense research for more than 25 years.²⁰⁻²⁷ The concepts of elastic and nonlinear response spectra, ductility based modifications to earthquake induced forces and similar modifications to evaluations of structural capacities are products of these developments.^{28,29}

The analyses summarized in this section repeat some of these earlier studies and extend their applications to offshore platforms.

Ground Motion Time Histories

The response of SDOF and MDOF systems subjected to twelve recorded earthquake horizontal acceleration time histories have been evaluated. The recorded time histories were chosen to represent nearby and distant large magnitude earthquakes recorded on sites that could be characterized as firm alluvium. In addition, six synthetic earthquake acceleration time histories were studied. The earthquake acceleration components frequency content, phasing, and energy development characteristics were defined analytically to model the characteristics of large magnitude earthquakes shaking firm alluvium sites.

Idealized Systems

The earthquake loading effects were studied for SDOF, EP ND systems having $T_n = 1$ to 5 sec and $D = 5\%$.

Ductility spectra for two of the recorded earthquake time histories are shown in Fig. 17 (1940 El Centro SE) and Fig. 18 (1971 San Fernando NW). The earthquake acceleration magnitudes were scaled so that the records would contain a peak imposed earthquake force that equaled the yield capacity of the SDOF EP systems ($F_v = 1$), and then each of the records was progressively scaled up to

produce increasing overload factors and ductility demands. The F_v factor represents the factor by which the record must be scaled up (accelerations multiplier) to produce a given ductility demand in the SDOF systems.

In many respects, the earthquake ductility spectra are similar to the wave ductility spectra. For SDOF system periods greater than about $T_n = 3$ sec, there is not much variation in the ductilities produced by a given earthquake excitation. For these long period systems large overload ratios are required to produce ductility demands greater than unity. Due to the very small duration of the induced earthquake forces relative to the natural periods of the systems, there is a significant "deamplification" of the induced forces. The peak ductility demands of these long period systems are determined by the peak ground displacements developed during the earthquake time histories.

As for the wave ductility spectra, the ductility demands progressively increase as the periods become smaller. At the small periods, the ductility demands are determined by the peak ground accelerations.

The variability in ductility for a given earthquake record and for the different records decreases as the structure period increases. Even though the records have been scaled to produce equal peak forces on the SDOF EP systems, the systems respond very differently. This is a natural variability that is caused by the differences in the earthquake horizontal acceleration time histories.

Fig. 19 shows the ductility spectra for the same San Fernando time history for SDOF systems that have $D = 10\%$. As for the wave ductility spectra, increased damping decreases the peak magnitudes of the ductility demands and smooths the ductility spectra. However, for this range of periods, the effect of damping is relatively small when compared with the variability introduced by different earthquake time histories.

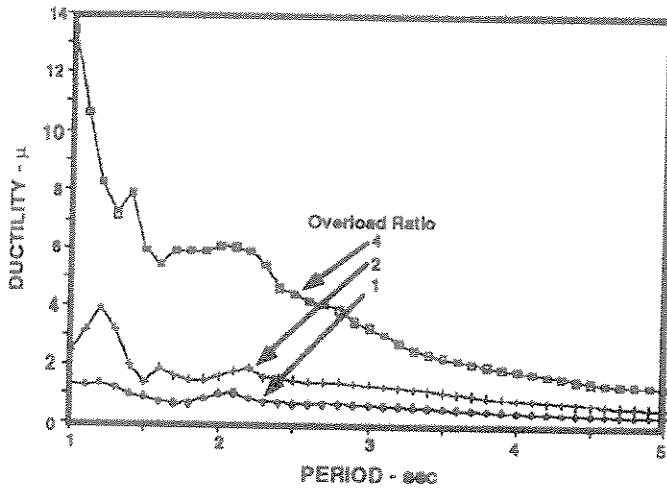


Fig. 17. Ductility response spectra (1979 Imperial Valley, D = 5 %)

the average, for a given F_v , the synthetic records indicated lower ductility demands.

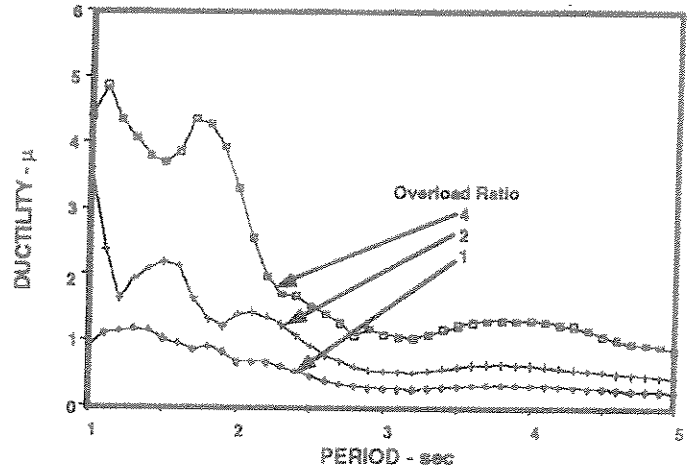


Fig. 19. Ductility response spectra (1971 San Fernando, D = 10 %)

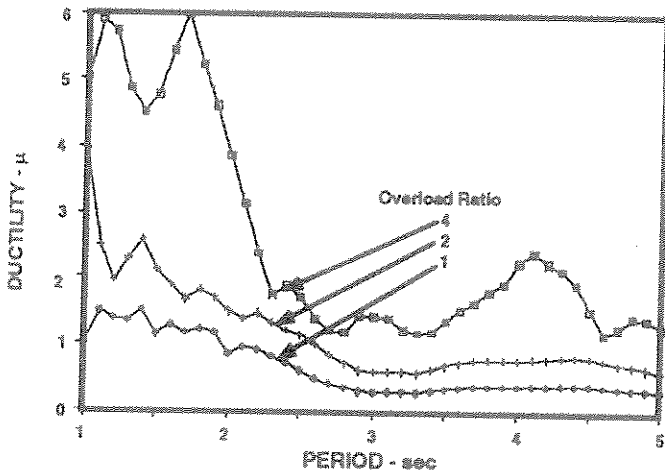


Fig. 18. Ductility response spectra (1971 San Fernando, D = 5 %)

Fig. 20 presents capacity modifiers and ductility capacities for EP ND systems that have $T_n = 1$ sec and $D = 5\%$ for eight of the recorded earthquake time histories studied. The mean F_v is 50 to 60 % of μ . The coefficient of variation of F_v is in the range of 20 to 40 %. For the synthetic time histories studied, the mean F_v is 60 to 70 % of μ . The coefficient of variation of F_v is in the range of 10 % to 30 %. On

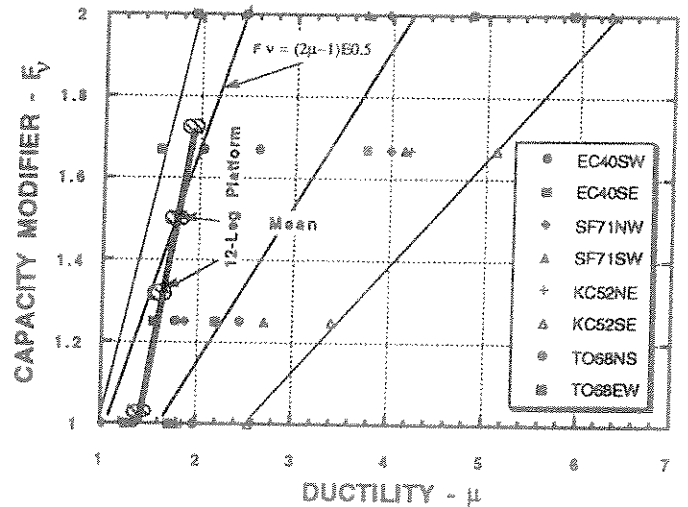


Fig. 20. Capacity modifiers and ductility demands for recorded earthquakes ($T_n = 1.0$ sec, $D = 5\%$)

These results are in good agreement with the results from previous studies of EP ND systems.²⁰⁻²⁵ These studies have shown that for this range of T_n and D , that the capacity modifier can be estimated as:

$$F_v = \sqrt{2\mu - 1} \dots \dots \dots (4)$$

Comparisons of this relationship with the results summarized in Fig. 20 indicate that Eqn. 4 results in a conservative estimate of the mean F_v .

Braced Frame Systems

The response of SDOF and MDOF systems subjected to earthquake excitations have been studied. The response of single and multiple axially loaded brace systems whose nonlinear response characteristics are typical of compressive buckling and tensile yielding tubular braces were analyzed (Fig. 11).

The first set of results were developed for SDOF systems that had nonlinear hysteretic performance characteristics of an axially loaded single brace. The second set of results were developed for MDOF systems that had nonlinear hysteretic performance characteristics of a multi-brace system characteristic of the vertical bracing system of a horizontally K-braced platform (transverse truss of jacket, Fig. 21).

The platform is an unbattered 12-leg drilling and production platform located in a water depth of 58 ft.^{6,30} The platform has a natural period of $T_n \approx 1.0$ sec (broadside and end-on) and low amplitude damping of $D = 5\%$. These characteristics have been confirmed with ambient vibration measurements.⁶

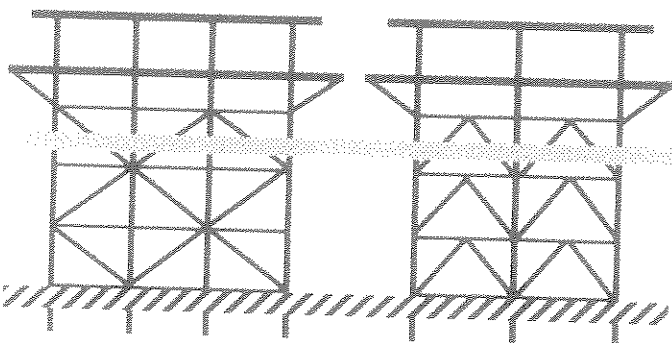


Fig. 21. Example platform analyzed to determine earthquake response characteristics

Results also were developed for the complete platform subjected to the three-dimensional El Centro earthquake acceleration time history. The platform braces and pile soils were modeled using nonlinear, hysteretic characterizations appropriate for these elements.¹⁴⁻¹⁷ The deck and leg elements were characterized as being elastic. The intensity of the El Centro record was progressively increased and the global ductility of the platform determined. Results from the analyses of the single and multiple brace systems, from the idealized EP systems, and from the example platform all subjected to the 1940 El Centro time history are summarized in Fig. 22.

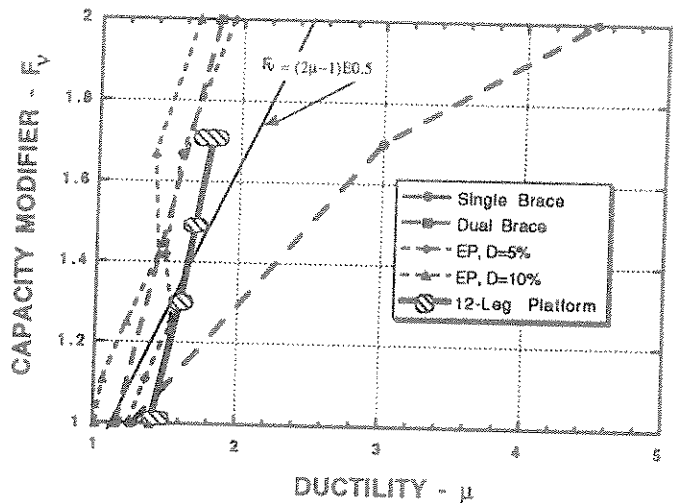


Fig. 22. Performance characteristics of idealized, brace, and platform systems ($T_n = 1$ sec, $D = 5\%$) subjected to the 1940 El Centro time history

For a given F_v , the EP systems indicate somewhat lower ductility demands than the single brace system and the platform system. The ductility demands for the EP systems having $D = 5\%$ and $D = 10\%$ differ very slightly. The EP systems bracket the behavior of the multiple brace system. The single brace performance indicates much higher ductility demands due to its much lower hysteretic energy dissipation. The interactions of the tensile and compression loaded multiple braces

result in a system that has high hysteretic energy dissipation. The platform system indicates ductility demands that are reasonably well characterized by the EP system that has $D = 5\%$.

Fig. 23 summarizes the results from this study for SDOF EP ND systems having a period of $T_n = 2$ sec. and damping $D = 5\%$ for the recorded earthquake time histories. The mean results and upper and lower bounds from the time history analyses are indicated.

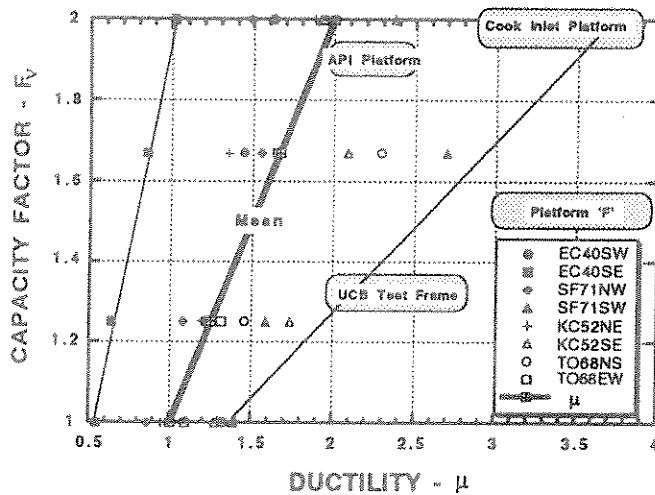


Fig. 23. Capacity factors and ductility demands for synthetic earthquakes ($T_n = 2.0$ sec, $D = 5\%$)

For this range of SDOF system periods and damping, previous studies have indicated that the mean capacity modifier can be evaluated as:²⁰⁻²⁵

$$F_v = \mu \dots \dots \dots (5)$$

This estimate provides an excellent fit to the mean results from this study.

The performance characteristics of strain and cyclic degrading SDOF systems also have been studied.³⁵ For systems having periods $T_n \geq 2$ sec. the mean results can be evaluated as:

$$F_v = \mu \alpha \dots \dots \dots (6)$$

where α is the residual strength ratio (Table 1, Fig. 1).

Presented in Fig. 23 are results from nonlinear time history analyses of complete platform systems having natural periods of $T_n = 2$ sec to 3 sec.^{6,31-33} The API platform³¹ and Platform 'F'⁶ are conventional 8-leg and 12-leg platforms, respectively. The Cook Inlet platform is a steel X-braced tower-type platform.^{32,33}

Results from a scale model of a vertical frame that was extensively tested to determine its performance characteristics when subjected to earthquake induced force time histories also are shown (indicated as "UCB test frame").^{14,15} This test frame also has been studied extensively by Bazzurro and Cornell.³⁴ The results developed by Bazzurro and Cornell are very similar to those summarized here.

For a given F_v , the complete platform systems generally indicate greater ductility demands than indicated by the SDOF EP ND systems. The platform performance characteristics are described much better by the SDOF strain-cyclic degrading system results for residual strength ratios of $\alpha = 0.75$ to $\alpha = 0.50$.

CONCLUSIONS

Capacity modifiers for platforms subjected to extreme condition wave and earthquake forces have been developed to adjust the ultimate limit state lateral load resistance determined from static push-over analyses. These capacity modifiers are functions of the transient loadings and the performance characteristics of the platform systems (Table 1).

Based on the verification analyses that have been performed on complete platform systems and for the class of structures and perfor-

mance characteristics studied, results from idealized systems can be used to develop reasonable evaluations of global capacity modifiers if appropriate nonlinear hysteretic characteristics are chosen for the idealized systems. Additional analyses of platform structures subjected to ultimate limit state intensity loadings and analyses of idealized nonlinear hysteretic systems are needed to further develop these results.

ACKNOWLEDGMENTS

This paper is the result of a research project conducted at the University of California at Berkeley. Funding for the project have been provided by the National and California Sea Grant College Program, the Minerals Management Service, the California State Lands Commission, Phillips Petroleum Co., Chevron Corp., and UNOCAL Corp.

Special appreciation is expressed to Chevron Corp. and UNOCAL corp. for their continued support of the graduate students that have performed the analytical work summarized in this paper. In addition to Mr. Carlton Young, Mr. Don Kingery, Dr. Dagang Zhang, Dr. Sajid Abbas, and Mr. David McDonald performed the wave and earthquake analyses that are summarized in this paper.

This paper is funded in part by a grant from the National Sea Grant College Program, National Oceanic and Atmospheric Administration, U. S. Department of Commerce, under grant number NA89AA-D-SG138, project numbers R/OE-11 and R/OE-19 through the California Sea Grant College, and in part by the California State Resources Agency. The views expressed herein are those of the authors and do not necessarily reflect the views of NOAA or any of its sub-agencies. The U. S. Government is authorized to reproduce and distribute for governmental purposes.

REFERENCES

1. Bea, R. G. (1991). *Loading and Load Effects Uncertainties*. Report to Canadian Standards Assoc., Verification Program for CSA Code for the Design, Construction and Installation of Fixed Offshore Structures Project No. D-3, October.
2. Bea, R. G., (1992). "Structural Reliability: Design and Re-Qualification of Offshore Platforms." *Proc. Int. Workshop on Reliability of Offshore Operations*, Nat. Inst. of Standards and Tech., NIST Special Pub. 833, E. Simiu (Ed.), Gaithersburg, Va.
3. Bea, R. G. (1992). "Evaluation of Uncertainties in Loadings on Offshore structures Due to Extreme Environmental Conditions." *Proc. of the 11th Int. Conf. on Offshore Mechanics and Arctic Engineering*, ASME Paper No. OMAE-92-1218, Calgary, Canada, June.
4. Marshall, P. W. and Bea, R. G. "Failure Modes of Offshore Platforms," *Proceedings, Behaviour of Offshore Structures, BOSS '76*, Trondheim, Norway, 1976.
5. Tromans, P. S., and van de Graaf, J. W. (1992). "A Substantiated Risk Assessment of A Jacket Structure." *Proc. of Offshore Tech. Conf.*, OTC No. 7075, Houston, Tx.
6. Bea, R. G. and Craig, M. J. K. (1993). "Developments in the Assessment and Requalification of Offshore Platforms." *Proc. of the Offshore Tech. Conf.*, OTC No. 7138, Houston, Tx.
7. Heideman, J. C., and Weaver, T. O. (1992). "Static Wave Force Procedure for Platform Design," *Proc. of Civil Eng. in the Oceans V*, American Society of Civil Engineers, College Station, Texas, Nov., 496-517.
8. McDonald, D. T., Bando, K., Bea, R. G., Sobey, R. J. (1990). *Near Surface Wave Forces on Horizontal Members and Decks of Offshore Platforms, Final Report*. Coastal

- and Hydraulic Eng., Dept. of Civil Eng., Univ. of California at Berkeley.
9. Ruhl, J. A. (1976). "Offshore Platforms: Observed Behavior and Comparisons with Theory," *Proc. Offshore Tech. Conf.*, OTC 2553, Houston, Tx.
 10. Spidsøe, N. and Langen, I. (1985). "Damping of Fixed Offshore Platforms." *Proc. of the Behaviour of Offshore Structures BOSS'85 Conference*, Elsevier Science Publishers, Amsterdam.
 11. Dello Stritto, F. J., and Horton, T. E. (1984). "Harmonics of Wave Forces Predicted by the Morison Equation," *Proc. 3rd Conf. on Offshore Mechanics and Arctic Eng.*, New Orleans, La, Vol. 1.
 12. Veletsos, A. S., Dodson, K. W., and Ventura, C. E. (1987). "Dynamic Response of Simple Systems to Periodic Forces." *Jl. of Struct. Eng.*, American Society of Civil Engineers, Vol. 113, No. 10, Oct.
 13. Morison, D. G. (1992). "Dynamic Design of Deep Water Bottom-Founded Towers." *Proc. of Civil Eng. in the Oceans V*, R. T. Hudspeth (Ed), American Society of Civil Engineers, College Station, Tx.
 14. Popov, E. P., Mahin, S. A., and Zayas, V. A. (1980). "Inelastic Cyclic Behavior of Tubular Braced Frames." *J. Struct. Div.*, American Society of Civil Engineers, Vol. 106, No. ST12, Dec.
 15. Zayas, V. A., Shing, P-S, B., Mahin, S. A., and Popov, E. P. (1981). *Inelastic Structural Modeling of Braced Offshore Platforms for Seismic Loading*, Earthquake Eng. Research Center, Univ. of Cal., Rpt. No. UCB/EERC-81/04, Jan.
 16. Bea, R. G., Litton, R. W., Nour-Omid, S., Chang, J. Y., and Vaish, A. K. (1984). "A Specialized Design and Research Tool for the Modeling of Near-Field Pile-Soil Interactions." *Proc. of the Offshore Tech. Conf.*, OTC 4858, Houston, Tx.
 17. Bea, R. G. (1992). "Pile Capacity for Axial Cyclic Loading." *J. of Geotechnical Eng.*, American Society of Civil Engineers, Vol. 118, No. 1, Jan.
 18. Bea, R. G. and DesRoches, R. (1993). "Development and Verification of a Simplified Procedure to Estimate the Capacity of Template-Type Platforms." *Proc. of 5th Int. Symp. on Integrity of Offshore Structures IOS '93*, Glasgow.
 19. Stewart, G. (1992). "Non-Linear Structural Dynamics by the Pseudo-Force Influence Method, Part II: Application to Offshore Platform Collapse." *Proc. Int. Offshore and Polar Engineering (ISOPE) Conf.*, San Francisco, Ca.
 20. Veletsos, A. S. (1969). "Maximum Deformations of Certain Nonlinear Systems." *Proc. of the Fourth World Conf. on Earthquake Eng.*, Santiago, Chile, Jan.
 21. Veletsos, A. S., and Vann, W. P. (1971). "Response of Ground Excited Elastoplastic Systems." *Journal of the Structural Division*, American Society of Civil Engineers, Vol. 97, No. ST4, April.
 22. Riddell, R. and Newmark, N. M. (1979). *Statistical Analysis of the Response of Nonlinear Systems Subjected to Earthquakes*. Dept. of Civil Eng., Univ. of Illinois at Urbana-Champaign, Rpt. No UILU 79-2016, August.
 23. Iwan, W. D. (1980). "Estimating Inelastic Response Spectra from Elastic Spectra," *Earthquake Engineering and Structural Dynamics*, Vol. 8, No. 4.
 24. Al-Sulaimani, G. J. and Roessett, J. M. (1984). "Design Spectra for Degrading Systems," *Jl. of Struct. Eng.*, American Society of Civil Engineers, Vol. 111, No. 12, Dec.

25. Lin, J. and Mahin, S. A. (1985). *Effect of Inelastic Behavior on the Analysis and Design of Earthquake Resistant Structures*. Earthquake Engineering Research Center, Report No. UCB/EERC-85/08, Univ. of Cal., Berkeley, Ca, June.
26. Sewell, R. T. (1988). *Damage Effectiveness of Earthquake Ground Motions*. Ph.D. Dissertation, Dept. of Civil Eng., Stanford Univ., Palo Alto, Ca, Dec.
27. Inoue, T. (1990). *Seismic Hazard Analysis of Multi-Degree-of-Freedom Structures*. Report to Reliability of Marine Structures Program, Dept. of Civil Engineering, Stanford Univ., Report No. RMS-8, July.
28. Newmark, N. M. and Rosenbleuth, E. (1976). *Fundamentals of Earthquake Engineering*. Prentice-Hall, Inc., Englewood Cliffs, New Jersey.
29. Kennedy, R. P., Short, S. A., Merz, K. L., Tokaraz, F. J., Idriss, I. M., Power, M. S., and Sadigh, K. (1984). *Engineering Characterization of Ground Motion - Task I: Effects of Characteristics of Free-field Motion on Structural Response*. NUREG/CR-3805, Vol. 1. U. S. Nuclear Regulatory Commission, Wash. D. C., Feb.
30. Miller, T. M., Dolan, D. K., Eskijian, M. L., and Craig, M. J., K. (1991). "Requalification of an Older California Platform: API and Risk-Based Approaches," *Proc. Offshore Technology Conf.*, OTC 6648, Houston, Tx.
31. Wilson, B. M. (1981). Final Report, Stage II - Time History Analyses, Earthquake Analytical Studies for Offshore Structures. Report to the American Petroleum Institute, API PRAC 26 Project, PMB Systems Engineering Inc., San Francisco, Ca, Oct.
32. Bea, R. G. (1991). "Earthquake Geotechnology in Offshore Structures." *Proc. Second Int. Conf. on Recent Advances in Geotechnical Earthquake Engineering and Soil Dynamics*, St. Louis, Missouri.
33. Bea, R. G., Landeis, B., and Craig, M. J. K. (1992). "Re-qualification of a Platform in Cook Inlet, Alaska," *Proc. Offshore Technology Conf.*, OTC 6935, Houston, Tx.
34. Bazzurro, P., and Cornell, C. A. (1992). "Seismic Risk: Non-linear MDOF Structures," *Proc. World Conference on Earthquake Engineering*, Barcelona, Spain.
35. Bea, R. G. (1992). "Seismic Design and Requalification Methodologies for Offshore Platforms," *Proc. of the Int. Workshop on Seismic Design and Requalification of Offshore Structures*, Pasadena, Ca.

APPENDIX

C

SCMUCKER, D.G. AND CORNELL, C.A.: "DYNAMIC BEHAVIOUR OF SEMI-DUCTILE JACKETS UNDER EXTREME WAVE AND WAVE-IN-DECK FORCES" PROC. SEVENTH INT. CONF. ON THE BEHAVIOUR OF OFFSHORE STRUCTURES (BOSS), BOSTON, USA, 1994

- 000 -

DYNAMIC BEHAVIOR OF SEMI-DUCTILE JACKETS UNDER EXTREME WAVE AND WAVE-IN-DECK FORCES

D. G. Schmucker and C. A. Cornell

Civil Engineering Dept.,
Stanford University, Stanford, CA 94305 USA

ABSTRACT

During extreme storms, peak wave loads may exceed a platform's ultimate static base shear capacity. A ductile structure may be able to resist such static overloads by taking advantage of the inertial resistance and the limited duration of the peak load. Another related problem occurs when the wave crest exceeds the lowest deck level. A basic understanding of the dynamic and post-elastic behavior of jacket-type offshore platforms in these loading environments is the principal objective of this study. Insight into these problems is facilitated by the use of single-degree-of-freedom models (SDOF) that represent the global (pushover) force-deformation properties of structural systems such as K- and X-braced frames. The wave-in-deck problem is considered by uncoupling the (SDOF) deck portal from the jacket. While the global jacket problem is quasi-static in the linear region, the deck problem is dynamically sensitive in this region; both systems effectively behave as sliding masses in the non-linear region.

KEYWORDS

Dynamic; semi-ductile; extreme wave; wave-in-deck

INTRODUCTION

New design and reassessment of existing facilities attempt to ensure that a structure has sufficient strength reserve and damage capacity to fulfill requirements of serviceability and safety. Recent work (e.g., Billington *et al.* (1994); Bea and Young (1993); Eberg *et al.* (1993); Hellan *et al.* (1993); Stewart (1992);) has focused on understanding performance of platforms in extreme wave and seismic environments. Component limit states such as ultimate strength, fatigue, deformation, ductility, and damage tolerance are one set of performance measures. State-of-the-art finite element methods allow full non-linear dynamic modeling of components and assist in determining component utilization values. However, component measures should be used with caution since alone they may not clearly predict complex system performance (Stewart *et al.* (1993a), Bazzurro (1993)). System measures such as global reserve strength, post-ultimate residual strength, and global inelastic deformation (ductility) capacity provide better indicators of

system performance. These measures assist us in the principal objective of this study: developing and communicating an understanding of and predicting extreme-wave near-failure behavior of jacket-type offshore platforms.

The loading environment of interest consists of peak wave loads which may exceed the platform's static ultimate capacity. A static analysis would predict collapse for overload conditions; however, recognizing the transitory nature of the peak load allows the structure to resist static overloads if sufficient post-ultimate strength and ductility are available. The disbenefit of resisting static overloads, of course, is the subsequent inelastic damage.

For the bulk of jacket structures and water depths under consideration here, the structure's first natural period of vibration is less than 2 seconds while the peak period, T_p , of the large or "damaging" wave is 12 or more seconds. These wave and structure combinations typically induce small linear oscillatory effects relative to the static nature of the response. In practice, these effects are ignored or dealt with by simple dynamic amplification factor (DAF) estimates (e.g., API 20th Ed (1993)). These DAF's are typically 1.1 or less. In contrast, when wave periods are closer to the structural period or when exposed to seismic loading, the DAF's may be quite large (on the order of 1.6). The initial analysis perspective therefore for the extreme wave, i.e., low DAF environment, is more naturally from a static point of view.

We anticipate that the load history and non-linear force deformation characteristics of the structural system are the dominant factors determining system response. The study performed by Stewart *et al.* (1993a) concluded that system strength as found from a non-linear static pushover analysis provided an acceptable basis for evaluating system performance in the extreme wave environment. These authors also concluded that the critical loading effect is derived from a single large wave rather than from multiple or cumulative, non-linear wave effects.

To develop physical understanding, to guide focus on factors that deserve the most attention, and to provide gross, but simple, predictions, our procedure will be to study single-degree-of-freedom systems (SDOF) under the action of single-wave-crest load pulses. The SDOF model will represent the gross global force-deformation properties of various jacket systems as found from a non-linear, static-pushover analysis. We begin with a basic elasto-plastic system and gradually increase the complexity of the system model to include ultimate strength persistence, post-ultimate residual capacity, and pre-ultimate, post-elastic strength reserves. Quasi-static and full-dynamic analysis techniques are utilized to draw out the effects of different wave load histories and the role of linear oscillator dynamics and mechanics on the prediction of damage (as represented by the maximum ductility factor).

LOAD, SYSTEM, AND ANALYSIS DESCRIPTION

Simplified Load Model

A squared sinusoidal history is chosen to represent the time varying character of the total base shear. The duration of loading t_d is one-half of the underlying sinusoidal wave surface-elevation period. For predominant wave periods T_p of 12 seconds, this implies $t_d = 6$ sec. The wave loading studied represents the crest portion of the wave cycle (see Fig. 1). The peak amplitude of the load is characterized by a static overload ratio F_v defined to be the ratio of the peak amplitude to the ultimate force capacity of the system.

Simplified System: Elastic Perfectly Plastic

The simplest SDOF global force-deformation model that includes capacity limitations is the elastic-perfectly-plastic model (EPP). This "standard" model is well known and widely studied; it provides a good starting point for developing an understanding of the gross behavior of jacket-type platforms. The basic parameters of this model are elastic stiffness, k , force capacity, F_u , and mass, m . The natural period of vibration is $T = 2\pi\sqrt{m/k}$ and the yield displacement, δ_{yield} , is F_u/k .

Analysis Methods

We choose two approaches to exemplify the basic response character of the system and the damage potential of the load: a full dynamic time-step integration procedure and a simplified quasi-static approach. The latter method provides the initial "beyond-static" insight into the structure's extreme-wave, near-failure behavior.

The full dynamic time-step integration procedure is the standard Newmark- β ($\beta = 1/4$) Method with Newton-Raphson iterations. The initial conditions for the analyses were assumed to be zero displacement and zero velocity with the wave surface elevation beginning at the mean water level, i.e., the load begins at zero force. This method includes linear oscillatory effects as well as non-linear force-deformation and damping effects.

The quasi-static approach assumes pre-ultimate behavior to be static. The post-ultimate behavior is analyzed from a simple kinematics-physics perspective: a springless mass acted upon by a force. This approach emphasizes accumulated damage resulting from post-ultimate response.

Discussion of Quasi-Static Approach

In the quasi-static approach, we separate the analysis into two distinct phases: a stiffness-dominated region and a mass-dominated region. This perspective acknowledges the time-varying aspect of the applied load but assumes the inertial and damping forces to be negligible while the system is in the stiffness-dominated pre-ultimate state, i.e., the system responds in a static fashion to the applied load. When the applied load reaches the incipient ultimate level, an additional increment of load changes the state of the system from pre- to post-ultimate. The system has no available static strength reserve and must accelerate to compensate for the static unbalance. This is the mass-dominated phase; for the EPP system, the structure exhibits a zero stiffness, constant-restoring-force static equilibrium path.

The mass-dominated region can be viewed efficaciously as a dynamics problem from simple physics. For an undamped system, the general equation of motion (EOM) is:

$$F_{inertia} + F_{spring} = F_{external} \quad (1)$$

where F_{ij} is the inertial, spring, or external force as a function of time. In the post-ultimate state, the EPP spring force is constant and equal to the ultimate capacity F_u . With Newton's second law of motion, we can see the EOM as representing a mass accelerated by an effective external force equal to the applied force minus the ultimate capacity.

$$F_{inertia} = \frac{d(mx)}{dt} = F_{external} - F_u \quad (2)$$

where \dot{x} is the velocity. The system remains in the post-ultimate (non-positive stiffness) state until the momentum of the system becomes zero and the mass begins to move in the opposite direction. At the point of zero momentum (zero velocity), the system returns to the elastic state and the point of maximum displacement has been reached (assuming that the external load continues to decrease).

The duration of this mass-dominated interval, t_i , can be understood as the time required for the effective-force-impulse to increase the system's momentum and then remove it. The impulse-momentum equation from simple physics is the integrated version of (2).

$$m\dot{x}_{t_a+t_i} - m\dot{x}_{t_a} = \int_{t_a}^{t_a+t_i} (F_{external} - F_u) dt \quad (3)$$

The lower limit of integration t_a is the time at the beginning of the mass-dominated response, i.e., when $F_{external} = F_u$; \dot{x}_{t_a} is the velocity evaluated at time t_a . The upper limit $t_a + t_i$ is the time at which the velocity becomes zero; therefore, the first term on the LHS of (3) is identically zero by definition. If we assume zero initial momentum, the remaining term on the LHS of (3) becomes zero. Since the load environment is a smooth, single pulse, integrating (2) twice gives us the maximum displacement and hence the maximum damage.

$$x_{max} = x_{t_a} + \int_{t_a}^{t_a+t_i} \int_{t_a}^t (F_{external} - F_u) d\tau dt \quad (4)$$

where x_{t_a} is the static displacement evaluated at the onset of the mass-dominated phase, which is simply the yield displacement for the EPP system. For the case where the initial momentum is zero at the onset of post-ultimate behavior, the duration t_i can be seen to be the time it takes for the effective force to have "balanced areas" (see Fig. 1 and Eq. 3). One attractive feature of t_i as a measure of the load's damage potential is that it can be easily computed from the normalized loading history.

An improvement to this simple impulse-momentum analysis of the mass-dominated region is to allow the mass to have initial momentum at the onset of this phase. In order to ensure that we have the proper displacement and velocity continuity between the two analysis phases, let us assume that the velocity of the system at the transition point is simply the "quasi-static velocity." That is, in the stiffness-dominated phase, the system response at any point in time could be approximated by the rate of change of the force divided by the elastic stiffness.

Results from Quasi-Static Analysis

Results for the quasi-static analysis (with and without initial momentum) and the full dynamic analysis for a static overload $F_v = 1.1$ are shown in Fig. 2. The quasi-static results without initial momentum are shown as "Q-S1," with initial momentum as "Q-S2" while the dynamic results are labeled with "DYNA." The system is undamped and subjected to the squared sinusoidal wave-load profile. The independent parameter is taken to be t_d/T , the ratio of load duration to linear structural period. For the water depths, structures, and extreme waves of interest, the corresponding t_d/T range is about 3 to 8, i.e., T_p/T of 6 to 16. The maximum displacement response was normalized by the yield displacement, δ_{yield} ; the result is μ , the "maximum ductility" or simply the "ductility." The analyses were carried out in their non-dimensional form (see Biggs (1964)). The non-dimensional form provides the advantage of being able to vary the linear structural period by changing either the mass or stiffness without affecting the non-dimensional result.

We observe from Fig. 2 that ductility grows rapidly for increasing t_d/T ratio within the range [3,8]. The underlying reasons for this can be found when non-dimensionalizing the governing EOM. After normalizing displacement by the yield displacement and substituting definitions for the structural period T and the stiffness $k = F_u/\delta_{yield}$, the resulting non-dimensional form of (4) is:

$$\mu = 1 + \frac{4\pi^2}{T^2} \int_{t_a}^{t_a+t_i} \int_{t_a}^t \frac{F_{external}(\tau) - F_u}{F_u} d\tau dt \quad (5)$$

where μ is the ductility or simply x/δ_{yield} . If the duration is kept the same and the T is shortened, the ductility should grow like the reciprocal of T^2 . The physical reason for this behavior is associated not with vibratory dynamics but with the nature of the inertial force. For systems with heavy mass (long period), small accelerations will be multiplied by the heavy mass to compensate for the static unbalance. Short period systems (small mass), will require greater accelerations in order to compensate for the same static unbalance. Greater accelerations imply greater overall displacements. For fixed mass and F_u , changing T implies simply changing k and δ_{yield} , hence μ is also changed. However, the displacements incurred beyond yield remain the same, i.e., $x_{max} - x_{t_a}$ is independent of either k or δ_{yield} as can be seen in (4).

As might be expected, the quasi-static approach with initial momentum, denoted here as Q-S2, predicts displacements greater than that from the no initial momentum (Q-S1) approach. In general, we might also expect that the Q-S2 approach would give us better approximations to the full dynamic solution. However in the t_d/T range [3,8], this is not generally true. Rather, the Q-S1 approach performs better. The underlying reasons for this behavior come from the subtleties of the full dynamic solution. Despite their simple mechanics, for the t_d/T range [3,8], the quasi-static approaches are within 25% of the result from the full dynamic approach. This result is generally true for static overloads F_v 's greater than 1.

One of the important understandings obtained from the quasi-static approach is that the damaging portion of the load extends beyond the time when the external load simply exceeds the ultimate capacity. How quickly the external load decreases after reaching its peak value determines how quickly deceleration occurs and affects how much damage (ductility) is accumulated.

Limitations of the Quasi-Static Approach & Results of Full Dynamic Approach

Whereas the quasi-static model reveals the dominant physical behavior (a sliding mass) and captures the major trends in ductility versus load level and duration, the approach ignores two significant aspects that the full dynamic approach includes: the dynamic load factor and the phasing in the displacement response. The quasi-static approach assumes that post-ultimate behavior only occurs for static overload problems, i.e., $F_v > 1$. For those problems of static "underloads," i.e., peak external loads less than the ultimate capacity, the quasi-static approach assumes that the system always responds in the stiffness-dominated phase and therefore responds statically. For a system such as an EPP, this implies linear response completely and therefore no non-linear damage. The net effect of the vibratory aspect of the system response, however small, is to cause potential damage when statically none is predicted. Phasing of the displacement response may cause additional damage. These effects are most severe for lower t_d/T values and lower F_v 's. For higher F_v 's, the static overload tends to swamp out the perturbations caused by the pre-ultimate dynamic response.

For the usual extreme wave environment, the loading appears to be a quasi-static process. But even for F_v 's of about 0.95, the dynamic load effect may create demands greater than capacity,

excess demands which can only be resisted through inertial and damping forces. The entire effect is to cause the system to "yield" for cases where statically no damage would be predicted. This is particularly catastrophic if the system has little or no residual strength beyond deformations associated with the static ultimate strength (post-ultimate residual capacity). A linear DAF analysis shows, for example, that the DAF for the squared sinusoidal load is about 1.06 for a $t_d/T = 4$. For a maximum peak load of $F_u - \epsilon$, i.e., a normalized load slightly less than $F_v = 1$, the predicted maximum displacement if the structure were to remain linear would be 1.06 times the reference yield displacement. Of course, the system is unable to sustain such elastic deformation and for the EPP system the maximum displacement is 1.22 times the yield displacement.

An oscillatory system may also experience linear amplification effects caused by the transitory nature of the load. Such effects, even when small, may cause the load demand to be greater than the system capacity. This more typically occurs in the seismic environment where periods of excitation are much closer to the natural period of the system and the DAF's are large. For cases of static overload, the dynamic effects may cause the system to reach ultimate capacity before or after the time predicted statically. These dynamic perturbations of the static response are responsible for the some of the difference between the full dynamic solution and the quasi-static approach that is observed in Fig. 2.

Effect of Damping

As is generally expected of viscous damping forces, the presence of damping effectively reduces the observed displacement response. For the problems studied, damping was mass-proportional and 5% of critical. The exceptions to this general rule pertain to the "valleys" observed in Fig. 3 which shows the undamped SDOF EPP results. These "valleys" are caused by advantageous phasing of the dynamic displacement response relative to the time-varying nature of the load. Damping tends to cause additional lag in the response and hence disrupts the beneficial effect of having the "right" t_d/T ratio.

EFFECT OF WAVE SHAPE

The selection of a squared sinusoidal wave-load profile is simplistic. However, the only information readily available may be the peak wave force and a gross estimate of the wave period. For a single-pulse type analysis, the wave period T_p supplies what has previously been defined as the load duration $t_d = T_p/2$. Given only these two parameters, there is of course an infinite sample space of functions which could describe the time history variation of the load. To what degree are the gross displacement predictions affected by different reasonable load time history variations? Are there parameters other than t_d and F_v which might better capture the load's damage potential and provide a more effective way of comparing different load histories on the same scale?

Thinking in terms of the Q-S1 approach, an alternative means of presenting the results of Fig. 2 is to use the duration, denoted t_{above} in Fig. 1, that the external load exceeds the ultimate capacity as a load parameter instead of the load duration parameter t_d . Similar to t_d and t_i , an attractive feature of t_{above} is that it is a property of the record and can be easily computed. The parameter t_{above} represents an acceleration phase where the static unbalance is resolved through satisfying dynamic equilibrium and accelerating the system. However, t_{above} does not capture the important deceleration phase which must occur in order to maintain bounded displacements.

As mentioned previously, the duration of inelastic loading t_i includes both the acceleration and deceleration phase. As such it is the time required to "slow" the mass down after the mass has been accelerated by the static unbalance force. Figure 4 presents the results for various static overloads on the undamped SDOF EPP system. It might be hoped that t_i , as defined for the Q-S1 method would be useful in eliminating the need to present different curves for different static overloads and different time-varying properties. As will be seen below (Fig. 6), it is helpful in this respect, but not sufficient. The reasons can be found as before in the subtleties of the full dynamic solution.

A symmetric triangular time-history profile is chosen to compare against the squared sinusoidal profile. The triangular profile is interesting for several reasons: it is a first-order type of estimate given the raw data of T_p and peak amplitude, it provides the same amount of linear impulse as the squared sinusoid given the same t_d and F_v , and it has sharp changes in slope. Results for both the triangular and squared sinusoidal parameterized by t_d are shown in Fig. 5 for the undamped SDOF EPP. For the same t_d/T and F_v the ductilities differ strongly in the [3,8] range; for $F_v = 1.1$, for example, the squared sinusoidal profile gives ductility values 1.5 to almost 3 times larger over this t_d/T range.

Using t_i as an independent parameter rather than t_d should provide a better means of characterizing the load's damage potential. Figure 6 illustrates that, while the results are improved, especially for $t_i/T \geq 0.9$, t_i still does not perfectly capture the effect of load history shape on the load's damage potential. Recall that t_i was defined from a quasi-static perspective and is computed from the normalized loading history. For full dynamic analysis, the actual time of inelastic loading differs from the quasi-static t_i .

However, t_i does not capture the nature of how the load varies in the near-peak region, variations which may induce differences in the predicted damage. If we examine the (quasi-static) time of inelastic duration t_i for each load profile (Fig. 7 and Table), we note that for the same t_d and F_v , t_i differs dramatically. For the triangular load, if the initial conditions are prescribed in such a manner that the transients from the initial conditions become zero and the system responds in phase with the external force, the discontinuity in the first time derivative of the load at the peak will cause oscillatory affects. Such affects may induce yielding. This affect is the most predominant for F_v 's slightly less than 1. The squared sinusoid is relatively smooth in the near-peak region.

Table 1: Values of t_i/t_d for Triangular and Squared Sinusoidal Loads

F_v	Triangular	Squared Sin.
1.05	0.081	0.212
1.10	0.155	0.296
1.15	0.223	0.360
1.20	0.284	0.413
1.30	0.394	0.499

From an analytic standpoint, transients from the zero displacement and zero velocity initial conditions are more severe for the triangular distribution than for the squared sinusoid. This difference arises from the discontinuity in slope of the triangular load at $t = 0$. These transients will affect the phasing of the displacement response as it nears the ultimate condition; this may be a deleterious or beneficial effect. Some care should be taken in choosing the initial conditions so as not to induce unrealistic transient response. Again these effects are most significant for smaller F_v levels.

VARIATIONS OF THE SIMPLIFIED EPP STRUCTURAL SYSTEM

Post-Ultimate Persistence, Negative Stiffness and Residual Strength

Elastic-perfectly-plastic systems exhibit robust post-ultimate behavior and are relatively stable systems. Unfortunately, few real systems behave in this manner. Real jackets exhibit the effects of buckling braces, large displacements (P-delta), and material plasticity amongst many non-linear effects. The impact of systems having post-ultimate strengths less than ultimate capacity and having non-positive-definite stiffness increases predicted displacements beyond EPP results.

We simplify the multitude of post-ultimate issues into three basic system parameters: ultimate strength persistence, post-ultimate negative stiffness, and post-ultimate residual capacity. "Ultimate strength persistence" is defined as the displacement range over which the system is able to maintain ultimate strength (see Fig. 8). To the extent that the system's ultimate strength persists up to or beyond the maximum ductility response, the system behaves identically to the comparable EPP system.

"Post-ultimate negative stiffness" is defined as the rate at which the force capacity falls with increasing deformations. The degree to which the force capacity falls off suggests how similar the system is to the EPP system. For this study, a global post-ultimate stiffness of the same value as the elastic stiffness was assumed. This maintains a fairly rapid drop-off without the numerical problems one may find with a precipitous drop-off (infinite negative slope, i.e., a step-function).

"Post-ultimate residual strength" is the remaining strength of the platform once deformations extend beyond the deformation associated with the static ultimate strength. This parameter reflects the ability of the jacket legs to act as a portal frame and proves to be a critical factor of post-ultimate performance. The residual capacity factor, α , is defined to be the post-ultimate residual strength normalized by the ultimate strength. Figure 9 illustrates the results for 5% damped SDOF Modified EPP systems with varying amounts of residual capacity factors ($\alpha = 0.7, 0.8, 0.9, 1.0$) subjected to a squared sinusoidal load profile with $F_v = 1.0$. For the results of Fig. 9, the ultimate strength persistence is taken to be zero as a worst case scenario, i.e., the system begins its degradation to the residual capacity level immediately after reaching the ultimate level.

We observe from Fig. 9 that ductilities are very sensitive to the residual capacity. For each α and for $F_v = 1.0$, the results reflect the characteristic linear oscillatory DAF camel-back curve discussed earlier; however, each "hump" of the curve is larger for successively smaller α 's. The small DAF's in this case are responsible for "kicking" the system into the post-ultimate region. With each additional 0.1 decrease in α , the results grow in a successively larger amount. For instance, at $t_d/T = 8$, the difference in the results for $\alpha = 0.9$ and $\alpha = 1.0$ (EPP) is $\mu_{difference} \approx 1$ while that for $\alpha = 0.7$ and $\alpha = 0.8$ is $\mu_{difference} \approx 4$. Again, the role of linear oscillatory effects are observed to be significant for F_v 's close to unity. In this case, the system pushed is not only beyond yield but into a post-ultimate region which does retain full ultimate capacity but drops off to a residual level.

Maximum ductilities are even more sensitive to the residual capacity factor for larger static overloads (see Fig. 10 for $F_v = 1.1$). Even for $\alpha = 0.9$, ductilities exceed 4 for many of the t_d/T ratios of interest. For the higher F_v values, the linear oscillatory effects are swamped out by the dominant nature of the static overload.

Pre-Ultimate Non-linear Effects: Strength Reserve

Until now the main issue has been what damage arises from post-ultimate behavior. Our interpretation of parameters such as t_i in reality hinged on the understanding that we were interested only in post-ultimate damage. We consider now effects arising from non-linear pre-ultimate behavior.

The non-linear force-deformation system we wish to consider is depicted in Fig. 11 with the dashed line. The only difference between this system which we shall denote as the Bi-Linear-Perfectly-Plastic (BLPP) and the EPP is the pre-ultimate behavior. The BLPP can also be characterized as having a "strength reserve" which simply means that the system has additional capacity to statically resist loads beyond the first non-linear event. The strength reserve is numerically captured by the load redundancy factor (LRF) which is defined as the ultimate load divided by the load associated with the first non-linear event. A system displacement redundancy factor (SDRF) can be defined in an analogous manner as the displacement associated with first reaching the ultimate restoring force, δ_u , divided by the displacement at which the first non-linear event occurs, δ_{first} . The combination of LRF and SDRF determine the relative slope of the secondary portion of the pre-ultimate force-deformation curve. In order to examine the first-order effect of having a strength reserve, we limit the scope of this study to an LRF = 1.15. We then vary the SDRF and observe ductilities for variations of the original elastic structural period.

We facilitate comparisons with the EPP by defining an "equivalent EPP" model as having the same elastic stiffness and ultimate capacity as the BLPP. The BLPP becomes identical to the EPP when the LRF and SDRF are unity. The reference displacement for the definition of ductility is taken from what we denote as the "global effective reference displacement," i.e., the yield displacement of the *equivalent* EPP model. This displacement δ_{yield}^{eff} is simply the static ultimate capacity divided by the elastic stiffness k . An alternative displacement redundancy factor (DRF) can be defined as the displacement associated with the ultimate restoring capacity divided by the yield displacement of the *EPP_{equivalent}* model. The DRF provides a means of adjusting the *EPP_{equivalent}* results so that meaningful comparison can be made between the BLPP and *EPP_{equivalent}*. We retain the convention of characterizing the peak amplitude of the load by normalizing it by the static ultimate capacity, i.e., F_v .

From the standpoint of static overloads, a system with pre-ultimate non-linear behavior experiences additional deformations vis-a-vis the *equivalent* EPP system. Normally, a strength reserve beyond first non-linear behavior is considered to be a beneficial effect. The perception here is one of seeing the system from an ultimate capacity standpoint and looking back towards the first non-linear behavior versus the opposing view of looking forward to the ultimate capacity from the first non-linear point.

Figure 12 illustrates the observed ductilities for the squared sinusoidal load with $F_v = 1$. The maximum displacements have been normalized by δ_{yield}^{eff} to obtain the observed ductility. The displacement to be used for normalization which that provides the most descriptive power is still under investigation. For increasing t_d/T , we again observe increasingly larger deformations for systems with larger DRF's.

The DRF can be used as means to measure the dynamic impact of the strength reserve vis-a-vis the *equivalent* EPP. From the quasi-static perspective, under loads with $F_v = 1$, the BLPP and *EPP_{equivalent}* respond statically and the maximum displacements will be as given by their respective force-deformation properties. For the *EPP_{equivalent}*, the maximum displacement is

δ_{yield}^{eff} while for the BLPP it is $SDRF \times \delta_{first}$ or simply δ_u . The DRF was defined to be $\delta_u / \delta_{yield}^{eff}$. From a static ultimate load perspective, one way to compare the EPP_{equivalent} is to adjust it by multiplying by the DRF. For instance, for the system with $t_d/T = 8$, $LRF = 1.15$, and $DRF = 1.3$, the ductility is about 1.7. The adjusted EPP_{equivalent} system sustains a ductility of about 1.3 (the EPP result from Fig. 12, i.e., $\mu = 1$, multiplied by the DRF). Not surprisingly, this effect becomes more pronounced as the DRF increases.

WAVE-IN-DECK RESPONSE

When the wave crest exceeds the lowest deck level, a large impulsive shear load is imparted to the portal framing system which connects the deck to the global jacket structural system. We investigate this situation by uncoupling the "deck portal" from the jacket. If we represent the deck portal system with a SDOF model, we can use the previous methods and results which were used to study the extreme-wave / jacket problem for the wave-in-deck problem by adjusting where we enter the figures.

The t_d/T range of interest is now 1 to 6 rather than the 3 to 8 range as before. The wave loading now represents only that portion of the total wave-load imposed on the deck portal. The load duration t_d here corresponds to the time required for the wave crest to first contact the supporting legs in the deck portal, to pass the length of the deck portal, and finally to lose contact with the "leeward" legs. We have calculated average durations, but horizontal the dimension of the structure is critical. The loading duration may be approximately 2 or 3 seconds. The period of vibration for the uncoupled deck portal system may be in the 0.5 to 3 second range.

Figure 2 provides results for an undamped deck portal (EPP) subjected to a squared sinusoidal load-pulse. Whereas the jacket problem was characterized by small linear DAF's, the wave-in-deck region is dynamically sensitive; the linear DAF's for this region are on the order of 1.5. Hence, the results follow a characteristic camel-back curve.

Results for structural configurations other than EPP can be obtained in a manner analogous to the jacket problem by entering the appropriate figure at the t_d/T value of interest. As we have seen, results in this region are more sensitive to load shape; the wave-in-deck force history deserves further study. The general conclusion remains that the wave-in-deck problem is dynamically sensitive in the linear region. Hence static parameters such as F_v and t_i defined for the quasi-static approach are not as powerful predictors of the maximum response. This dynamic environment calls for a dynamic parameter such as F_μ investigated by Bazzurro (1993). This damage measure is based on mass times a spectral acceleration, a dynamic property of the loading history and a the (linear) structure.

CONCLUSION AND RECOMMENDATIONS

Simplified structure and load models have been used to gain insight and physical understanding of the pertinent global structural properties and load characteristics which govern the behavior of jacket-type offshore platforms in the extreme wave and wave-in-deck environment. Quasi-static and full dynamic time-step integration procedures were applied to single-degree-of-freedom models having force-deformation characteristics representing a non-linear static pushover profile of a jacket platform. Specific conclusions developed include:

- The damage potential of the external load was characterized by the peak amplitude of

the load relative to the jacket's static ultimate capacity, F_u , and the duration of inelastic loading as determined by a force-impulse approach, t_i . This latter parameter captures both the acceleration phase caused by the static overload and the deceleration phase required to bound the response and prevent collapse.

- The global jacket response to the extreme wave environment was found to be characterized by a mass-dominated behavior for peak applied loads greater than 10% of the static ultimate capacity. A reasonable first-order prediction of the maximum ductility response was found by beginning the analysis at the incipient ultimate stage.
- When the static overload was less than 10%, the response began to be sensitive to linear oscillatory effects which are generally deleterious but occasionally beneficial in terms of maximum displacement response. These effects are driven by the time-varying nature of the external load and the structural period. A dynamic analysis procedure needs to be adopted for these cases, particularly for peak loads which are slightly less than the ultimate capacity.
- Global system properties such as pre-ultimate non-linearity, post-ultimate stability and post-ultimate residual capacity tend to reflect deleterious system response vis-a-vis the system with elastic-perfectly-plastic type properties. Plots have been developed from which a modification factor of the elastic-perfectly-plastic results can be found to make gross first-order type predictions of accumulated damage to complex systems.
- The wave-in-deck problem was found to be sensitive to linear dynamics whereas the extreme-wave / jacket problem is driven by the static overload nature of the loading.

Recommendations for future work include:

- Develop a measure such as t_i which includes dynamic effects but is a property solely of the loading record, i.e., the analyst need only process the loading record in order to compute the measure. The objective is to provide predictions that are insensitive to the load shape.
- Develop plots for more realistic wave loading profiles, especially for the wave-deck case.
- Develop understanding of wave-in-deck problem via the use of F_u as a load parameter.
- Compare the results of these single-degree-of-freedom models with those from more realistic 2 and 3-Dimensional multiple degree-of-freedom models to confirm trends and to calibrate predictions.

REFERENCES

- American Petroleum Institute (1993a), "Recommended Practice for Planning, Designing, and Constructing Fixed Offshore Platforms," RP 2A, 20th Ed., July 1, 1993.
- Bazzurro, P. (1993). *Seismic Hazard Analysis of Nonlinear Structures with Application to Jacket-Type Offshore Platforms*, Engineer's Thesis, Dept. of Civil Engineering, Stanford University, CA.
- Bea, R.G. and Young, C.N. (1993). "Loading and Capacity Effects on Platform Performance in Extreme Storm Waves and Earthquakes," *Proc. 23rd Offshore Technology Conference (OTC 7140)*, 3-6 May 1993, Houston, Texas.

- Biggs, J.M. (1964). Rigorous Analysis of One-degree Systems. In: *Introduction to Structural Dynamics*, pp. 69-80, McGraw-Hill, New York.
- Billington, C.J., Lloyd, J.R., and Digre, K.A. (to be pub. 1994). "Structural Elements, Systems and Analyses," DRAFT, *Proc. Intl. Work. on Seismic Design of Offshore Structures*, 8-10 December, 1993, New Orleans.
- Eberg, E., Hellan, O., and Amdahl, J. (1993) "Nonlinear Re-Assessment of Jacket Structures Under Extreme Storm Cyclic Loading: Part III - The Development of Structural Models for Cyclic Response," *Proc. 12th Intl. Conf. on Offshore Mechanics and Arctic Engineering (OMAE 1993)*, Vol. 1, pp. 517-528, Glasgow.
- Hellan, O., Tandberg, T., and Hellevig, N.C. (1993) "Nonlinear Re-Assessment of Jacket Structures Under Extreme Storm Cyclic Loading: Part IV - Case Studies on Existing North-Sea Platforms," *Proc. 12th Intl. Conf. on Offshore Mechanics and Arctic Engineering (OMAE 1993)*, Vol. 1, pp. 529-541, Glasgow.
- Stewart, G., Moan, T., Amdahl, J., and Eide, O.I. (1993a) "Nonlinear Re-Assessment of Jacket Structures Under Extreme Storm Cyclic Loading: Part I - Philosophy and Acceptance Criteria," *Proc. 12th Intl. Conf. on Offshore Mechanics and Arctic Engineering (OMAE 1993)*, Vol. 1, pp. 491-502, Glasgow.
- Stewart, G. and Tromans, P.S. (1993b) "Nonlinear Re-Assessment of Jacket Structures Under Extreme Storm Cyclic Loading: Part II - Representative Environmental Load Histories," *Proc. 12th Intl. Conf. on Offshore Mechanics and Arctic Engineering (OMAE 1993)*, Vol. 1, pp. 503-516, Glasgow.
- Stewart, G. (1992). "Non-linear structural dynamics by the pseudo-force influence method. Part II. Application to offshore platform collapse." *Proc. Second Int Offshore and Polar Eng Conf (ISOPE 1992)* San Francisco, CA, USA, 14-19 June 14-19, 1992. pp 264-271.

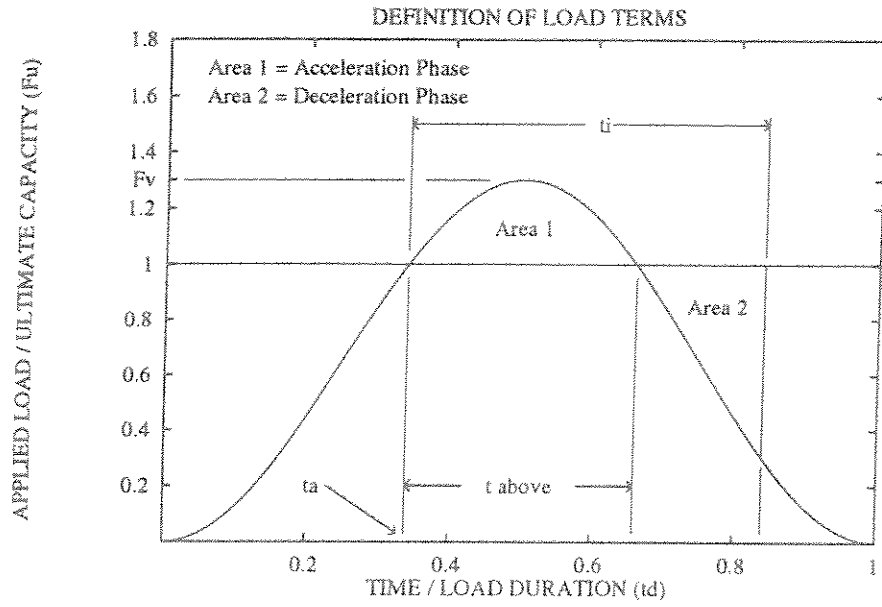


Figure 1: Applied Load Definitions

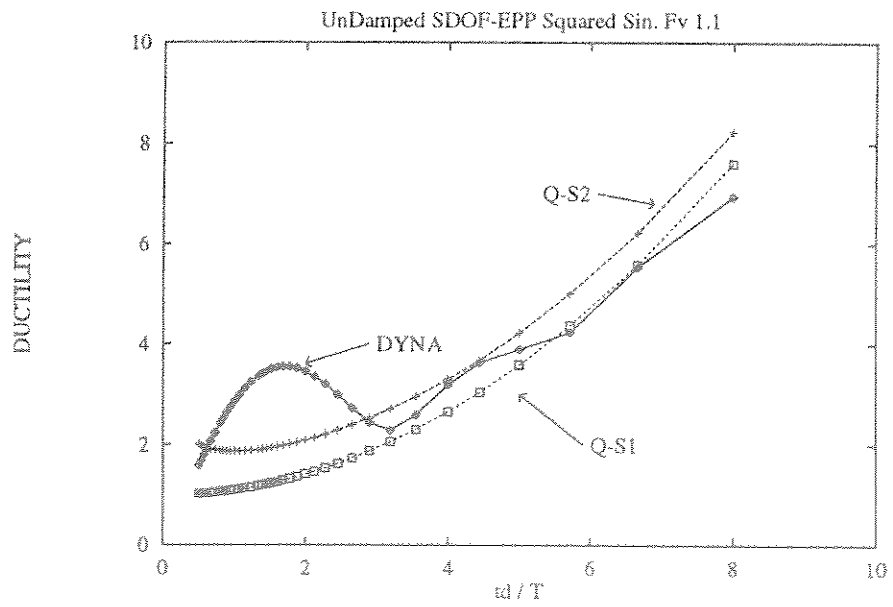


Figure 2: Q-S1, Q-S2, and DNYA Response Predictions. $F_v = 1.1$

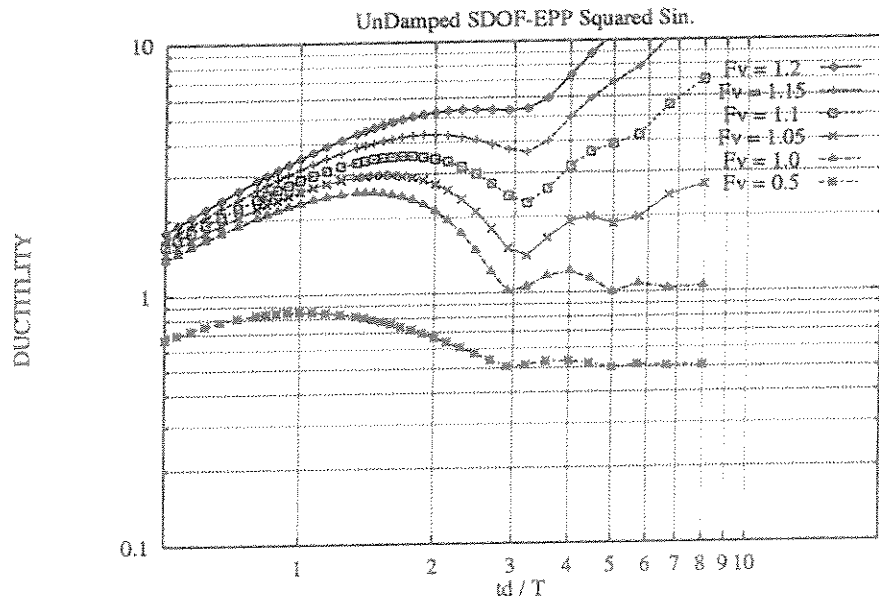


Figure 3: Response of Undamped EPP to Squared Sin. Various F_v 's

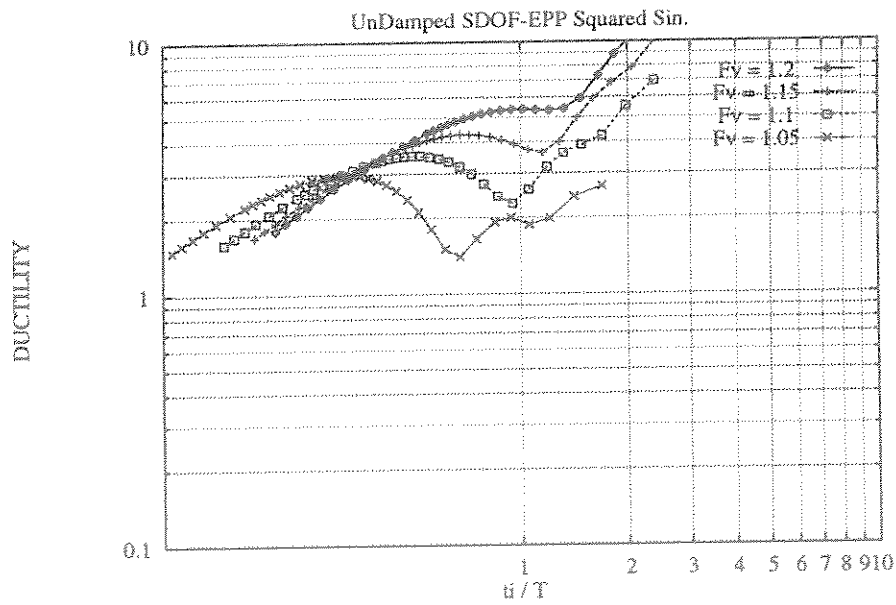


Figure 4: Response of Undamped EPP to Squared Sin. Parameterized by t_i

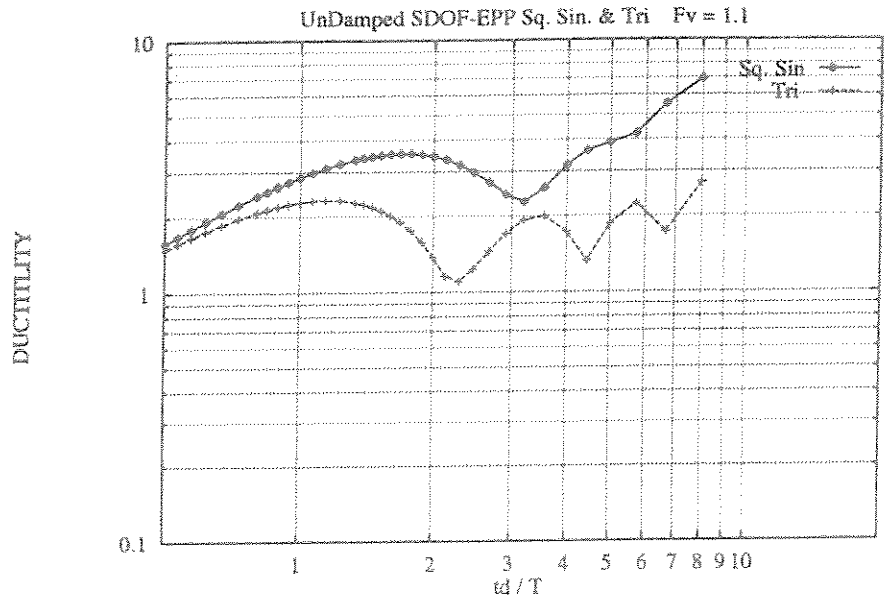


Figure 5: Undamped EPP Squared Sin. & Sym. Tri. Parameterized by t_d . $F_v = 1.1$

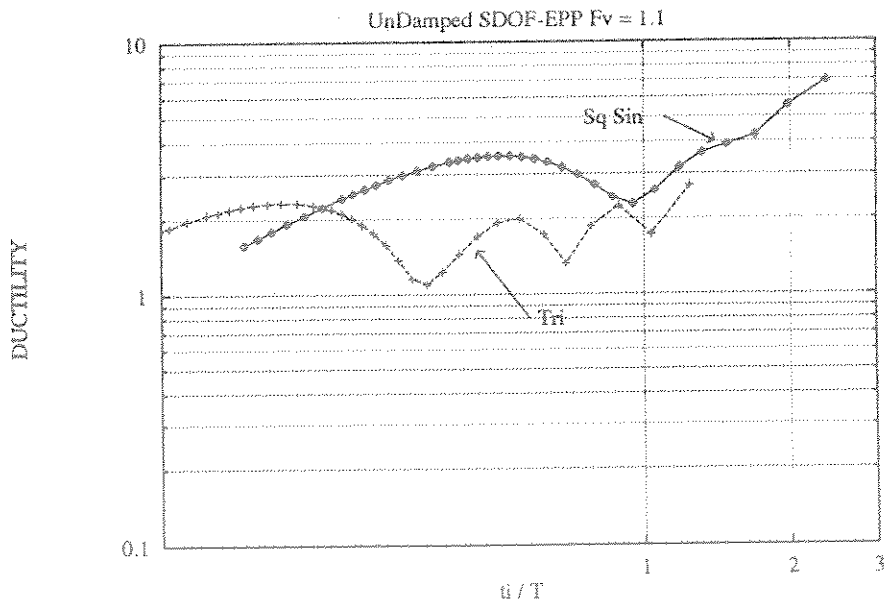


Figure 6: Undamped EPP Squared Sin. & Sym. Tri. Parameterized by t_i . $F_v = 1.1$

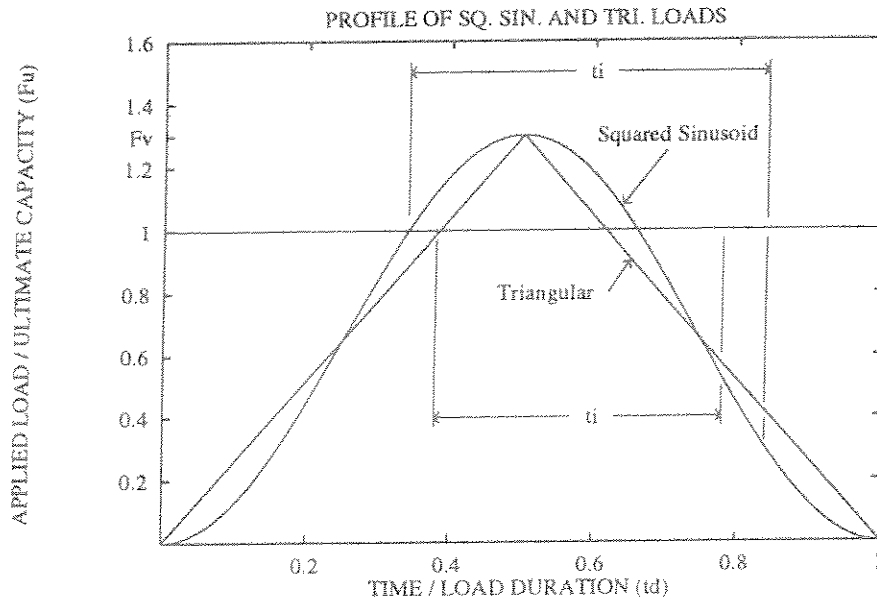


Figure 7: Profile of Squared Sinusoid and Triangular Load

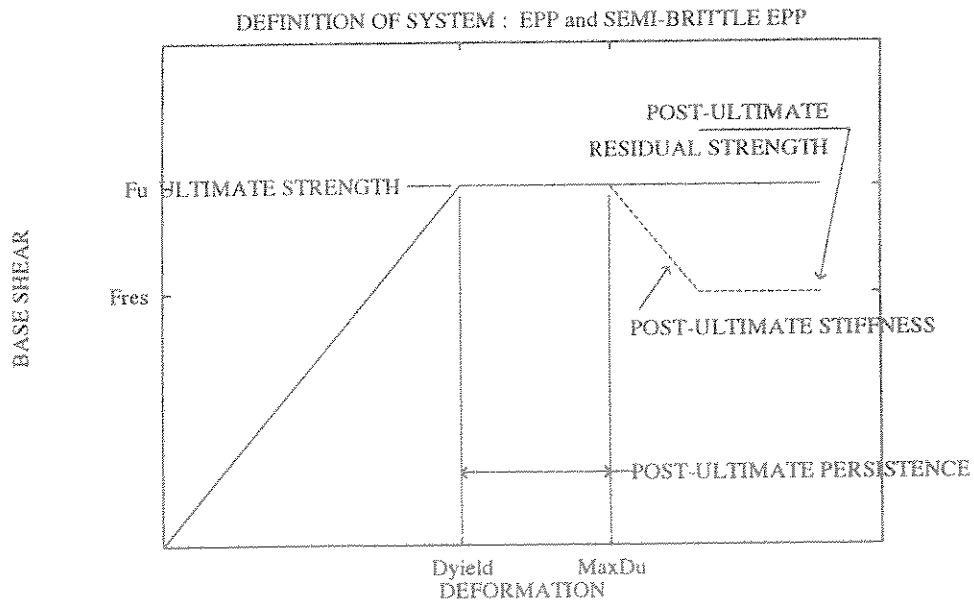


Figure 8: EPP and Semi-Brittle Force-Deformation Characteristics

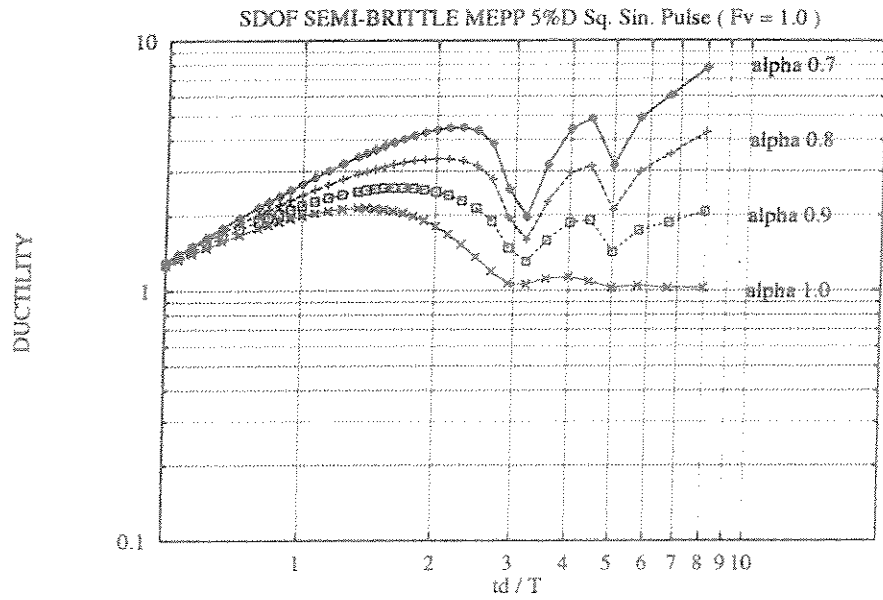


Figure 9: 5% Damped Semi-Brittle MEPP Response to Squared Sin. $F_v = 1$

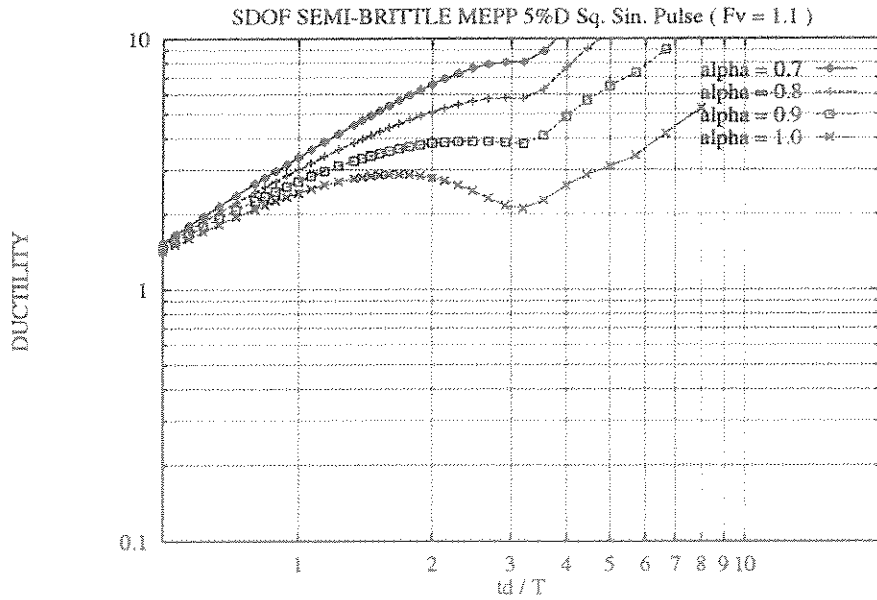


Figure 10: 5% Damped Semi-Brittle MEPP Response to Squared Sin. $F_v = 1.1$

DEFINITION OF SYSTEM : EQUIVALENT EPP and BI-LINEAR EPP

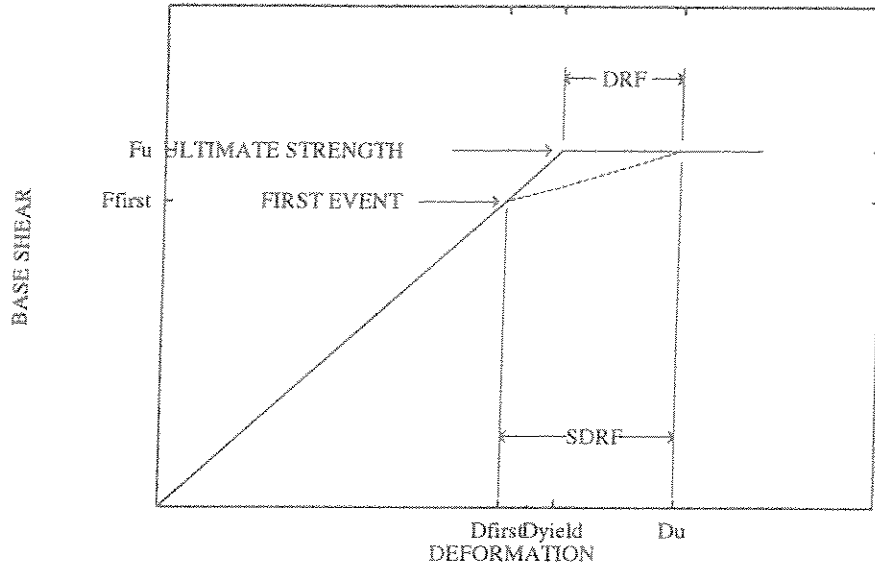


Figure 11: EPP and Bi-Linear Force-Deformation Characteristics

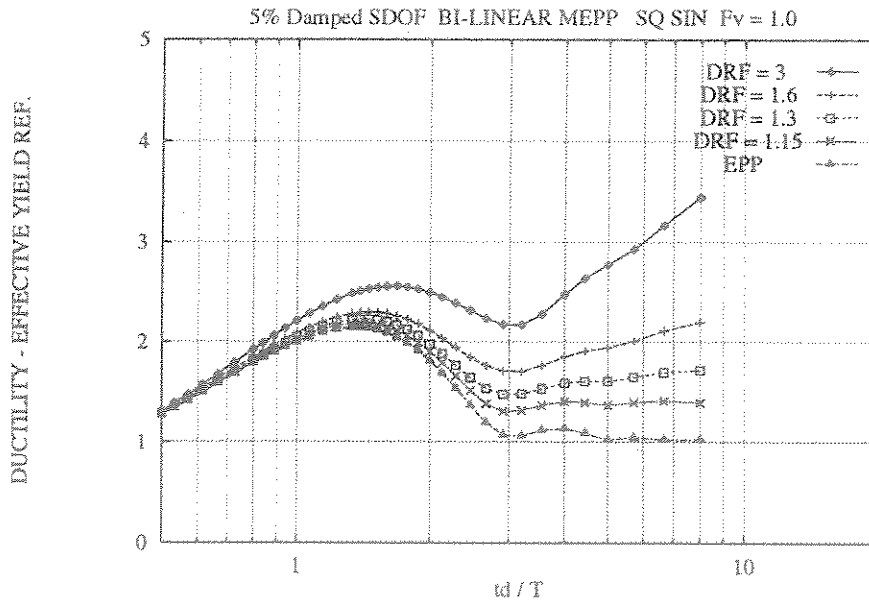


Figure 12: Undamped Bi-Linear-Perfectly-Plastic Response to Squared Sin. $F_v = 1$

APPENDIX

D

EMAMI AZADI, M.R., MOAN, T. AND AMDAHL.: "DYNAMIC EFFECTS
ON THE PERFORMANCE OF STEEL OFFSHORE PLATFORMS IN
EXTREME WAVES" PROC. EUROSTEEL '95, PRAGUE,
CZECHOSLOVAKIA, 1995.

- o0o -

Dynamic effects on the performance of the steel offshore platforms in extreme waves

M. R. Emami Azadi, T. Moan & J. Amdahl
Department of Marine Structures, NTH, Norway

ABSTRACT: The purpose of this study is to investigate dynamic loading effects on the performance of the offshore platforms in extreme wave conditions. The non-linear structural analysis program USFOS has been implemented to study such dynamic effects. The main concept is to model the structure and pile components by two-node beam elements and the plasticity by plastic hinges and the pile-soil interaction as discrete non-linear spring elements along the piles.

The structural model is an 8-leg jacket with 4 pile connections to the ground. This study is conducted in two parts a) By disregarding foundation failure (pile-soil behavior and the associated non-linearities) b) By including pile-soil effects. Characteristic wave and current loading for a specified sea state is generated by using program WAJAC. Non-linear time-domain analysis is performed for the most severe part of the sea loading in a scaled form. Scaling up the characteristic wave load for 100 year return period is progressively continued until the global collapse of the platform. Ductility and overloading ratios are the main performance characteristics of the structure which are studied in the first part. The dynamic response is compared with that of static pushover analysis; and the dynamic overloading (overcapacity) factor as well as ductility ratio are calculated and compared with those derived by others and the results of one-storey plane frame analyses.

In the second part, a simple pile-soil model has been implemented by modelling pile elements as beam elements and soil as non-linear spring elements through the pile depth. The necessary pile-soil data for this part are generated by the API 93 specifications and the modified API models and other existing theories. Both monotonous and cyclic pile-soil load transfer-displacement data for axial, lateral loadings and end bearing are generated by pile-soil programs. Cyclic degradation, strain softening and gapping are considered in the development of these programs. The progressive pile-soil failure from top to bottom and its effect on the overall pile-soil-structural collapse behavior and on the dynamic capacity and ductility ratio of the system are studied.

1 INTRODUCTION

The main aim of this study is to assess the combined effect of wave loadings and the inertial resistance of the structural system for ductile failure modes. For this purpose the 8-leg jacket type platform (as described in the appendix) is considered which is installed at a water depth of 110 m. The loading time history is simulated by a short crested irregular sea with a direction of propagation of zero with the global x-axis on the end-on of the platform. The simulated sea state data $H_s = 27.7$ m and $T_p = 16.0$ sec is described by a Jonswap wave spectrum corresponding to a return period of 100 years. To consider the extreme waves, the wave load

corresponding to 100 years return period is scaled up successively by a factor greater than 1.0 until the ultimate collapse of the structure occurred.

A stationary current with varying direction and a return period of 10 years is also imposed on the structure. The simulation length due to storage capacity limitation was taken as 20 min. Only the most severe portion of these time series (100 sec) and in the dominant forcing direction (x-global) were taken into account and imposed as the dynamic loading on the structure.

To characterize the induced dynamic effects of the system, we will use two parameters: the overloading ratio (β) and the ductility ratio (μ). The ductility ratio is described as the ratio between maximum

sustainable displacement(at the onset of global instability of the structure) to the first global yielding displacement of the structure.The overloading ratio is defined as a ratio between the ultimate dynamic load and the ultimate static resistance load of the structure (dynamic over capacity ratio).

A pushover-static analysis is first performed by imposing the generated extreme wave history on the structure incrementally.The ultimate collapse and the post-collapse behavior of the platform are simulated.Subsequently a dynamic pushover analysis is conducted to simulate the wave loading effects and structural characteristics on the performance of the Jacket.To verify the results a series of non-linear dynamic analyses are performed on single and double braced plane frame models and the results are compared with those of given in[3,14,15].The results might illustrate further different platform behaviors in severe sea storms.

The dynamic behavior of jacket type platforms might be influenced significantly by their foundation stiffness properties specifically soil non-linearities[6].

2 THEORETICAL BACKGROUND

2.1 Dynamic model

The pile-soil interaction has been modelled as beam elements for piles and a number of non-linear springs connecting the pile with soil,based on the existing and modified API code [2,4,7,8,13,18].The pile layout for the platform is skirt pile system.An equivalent centred single pile system is considered,this will enable us to get rid of Mindlin interactive effects from one pile to soil and then to another pile at the same group or another closely stationed pile group.Pile-soil-pile interaction in one pile is considered in most of the so-called standard curves recommended by API or generated by the pile-soil analysis programs[4,7,8].

The dynamic non-linear time-domain structural analysis program USFOS [1,5,9,16] is implemented. The main feature of the analysis is to model the Jacket as a space frame structure by using only two-node beam-column elements.The advantage is to reduce number of nodes by implementing a more direct integration approach for incremental loading of the structure.For this aim, a variational form of the total work potential is established for the structural system.Geometric nonlinearities have been accounted for by implementing a total Lagrangian formulation on element level.The global geometrical effects have

been taken into account by updating nodal coordinates.

The effects of the material non-linearities is modelled in USFOS by introduction of hinge mechanisms.A kinematic hardening is assumed for the yield surfaces in USFOS analysis.The structural damping is modelled by a stiffness and mass proportional damping system.A predictor-corrector scheme is adopted to solve governing differential equations.

2.2 Time domain dynamic analysis

A brief theory background and the solution strategy adopted in USFOS for time domain dynamic analysis is described in the following subsection[1].

2.3 Equation of motion

Dynamic equilibrium may be written as:

$$F^i(t) + F^d(t) + F^r(t) = R(t) \quad (1)$$

Where $F^i(t) = M\ddot{x}$ vector of inertia forces

$F^d(t) = C\dot{x}$ vector of viscous damping forces

$F^r(t) = Kx$ vector of structural restoring forces

$R(t) =$ vector of external forces

2.4 Mass matrix

The inertia of the discretized system is represented by the consistent mass matrix :

$$M = \int_{i=1}^{n+1} a_i^T \int_{V_i} \rho_i N^T N dV a_i \quad (2)$$

where ρ is the density and N the element interpolation polynomials. a_i is the transformation vector from element system to assembled system.A consistent mass matrix for a 4 DOF beam with third order polynomial shape functions is used.Concentrated masses may be specified at nodes.Added mass for submerged elements will be included.

2.5 Damping

Based on the distributed material damping property C ,the well-known equivalent viscous damping model

is given by:

$$F^d = C \cdot \dot{x} \quad (3)$$

Where the damping matrix is given by:

$$C = \int_{v_1}^{n \times 1} a_i^T C_i N^T N dV a_i \quad (4)$$

For computational (normal mode approach) reasons the damping matrix C is usually expressed in terms of mass and stiffness matrices M and K matrices in the form of Caughey series. The expansion reduces to a Rayleigh damping form when the series is truncated after two first terms and after adding a viscous term will have the following form:

$$C = C_0 + \alpha_1 M + \alpha_2 K \quad (5)$$

The α_j Rayleigh damping factors are calculated from modal damping data available for the structure.

2.6 Solution procedures

The α -method of time integration has been used in USFOS [1] instead of conventional Newmark- β method. The only difference is the presence of some additional terms in the damping, stiffness and external forcing expressions. The damping C is considered to consist of a viscous term and mass and stiffness proportional damping terms as indicated in Eq.(5). In this way governing dynamic equation may be written as:

$$K^* \Delta r_{n+1} = \Delta R^*_{n+1} \quad (6)$$

Where K^* the effective stiffness matrix may be expressed as:

$$K^* = a_K K + a_C C + a_M M \quad (7)$$

where a_K, a_C, a_M are functions of integration parameters and Δt time increment. Similar to Newmarks- β method, the total displacements, velocities and accelerations at step $n+1$ can be computed as:

$$r_{n+1} = r_n + \Delta r_{n+1} \quad (8)$$

$$\dot{r}_{n+1} = \frac{\gamma}{2\beta} \Delta r_{n+1} + (1 - \frac{\gamma}{\beta}) \dot{r}_n - \Delta t (\frac{\gamma}{2\beta} - 1) \ddot{r}_n \quad (9)$$

$$\ddot{r}_{n+1} = \frac{1}{\Delta t^2 \beta} \Delta r_{n+1} - \frac{1}{\Delta t \beta} \dot{r}_n + (1 - \frac{1}{2\beta}) \ddot{r}_n \quad (10)$$

The predictor-corrector approach is adopted as the solution procedure. Eqs.(9) and (10) are split into two parts:

$$\dot{r}_{n+1}^P = \dot{r}_n + \Delta t (1 - \gamma) \ddot{r}_n \quad (11)$$

$$\dot{r}_{n+1} = \dot{r}_{n+1}^P + \Delta t \gamma \ddot{r}_{n+1} \quad (12)$$

$$r_{n+1}^P = r_n + \Delta t \dot{r}_n + \frac{\Delta t^2}{2} (1 - 2\beta) \ddot{r}_n \quad (13)$$

$$r_{n+1} = r_{n+1}^P + \Delta t^2 \beta \ddot{r}_{n+1} \quad (14)$$

Where β and γ are integration parameters [1]. The predictor equations which are denoted by a superscript p in the latter equations are evaluated on the basis of the values at step n. It is assumed that \ddot{r}_{n+1} is zero in the predictor equations.

Now iterations can be performed by the use of Eq.(14) based on the total acceleration \ddot{r}_{n+1} as:

$$r_{n+1}^{i+1} = r_{n+1}^i + \Delta_{n+1}^{i+1} \quad (15)$$

$$\dot{r}_{n+1}^{i+1} = (\dot{r}_{n+1}^{i+1} - \dot{r}_{n+1}^P) / \Delta t^2 \beta \quad (16)$$

$$\ddot{r}_{n+1}^{i+1} = \dot{r}_{n+1}^P + \dot{r}_{n+1}^{i+1} \Delta t \gamma \quad (17)$$

where superscript i denotes iteration steps and Δ^{i+1} denotes iterative displacements at the iteration step $i+1$. Using the predictor-corrector approach could reduce any possible large drift from the yield surface. Both effective load vector and effective stiffness matrix are nonlinear functions of Δt . And so various displacement components vary non-proportionally within the time step Δt .

3 Wave and current loading

As described briefly in section 2.1 for a sea state described by Jonswap wave spectrum with significant wave period $T_s = 16.0$ sec and the

significant wave height $H_s = 27.3m$, the loading time history is simulated by a short crested irregular sea with a direction of propagation of zero with the global x-axis on the end-on of the platform corresponding to a return period of 100 years[17].

The corresponding wave load is then scaled up successively by a factor greater than 1.0 until total collapse of the structure occurred. The latter will correspond to a recurrence period far greater than 100 years. This is discussed in [15].

A stationary current with a varying direction and a return period of 10 years is also imposed on the structure.

The simulation length due to storage capacity limitation was 1200 sec. Only the most severe 100 secs portion of these time series (see Fig.1) was imposed as dynamic loading on the structure in the global x-direction. This is the dominant force direction.

4 Dynamic limit state of collapse:

4.1 Analysis of simple plane frame

To have a good perception of dynamic effects and to establish any relationship between structural ductility and dynamic overloading ratios first a series of non-linear time-domain dynamic analyses were performed on single and double one storey braced plane frames with natural period of $T_n=0.5sec$ [6]. The natural period for these plane frames was the same for the 8-leg Jacket. Varying the natural period of the plane frames will result in different performance characteristic relationships[6]. The analysis results for the single and double plane frame with $T_n=0.5 sec$ and $T_n=1.0 sec$ with Damping ratios $D=2\%$ and 5% are shown respectively on Figs. 2 and 3. The fitted curve on Fig. 2 indicates the following relationship between the overloading ratio F_v and the ductility factor μ :

$$F_v = \sqrt{\mu} \quad (18)$$

The latter might predict dynamic overcapacity ratio for the Jacket-platform with $T_n=0.5sec$.

4.2 Analysis of Jacket-Platform:

The simulated sea load history in Fig.1 is used as dynamic loading history and scaled up successively until reaching the limit state of total collapse which

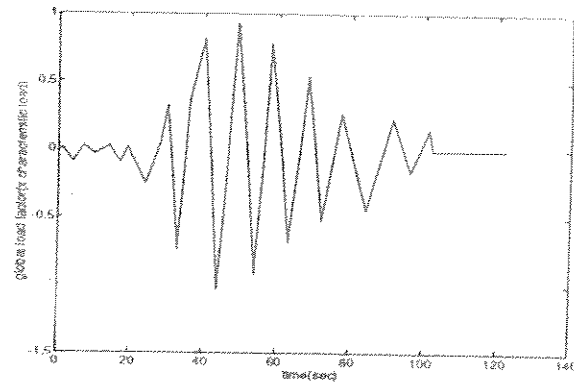


Figure 1: Simulated sea load history for its most severe part for duration of 100 sec

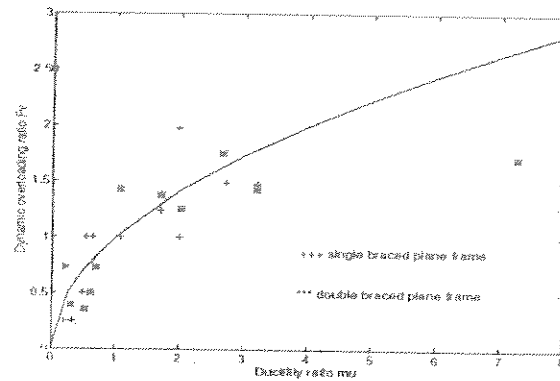


Figure 2: Ductility versus overloading ratio for single and double braced frames and a 12-leg platform

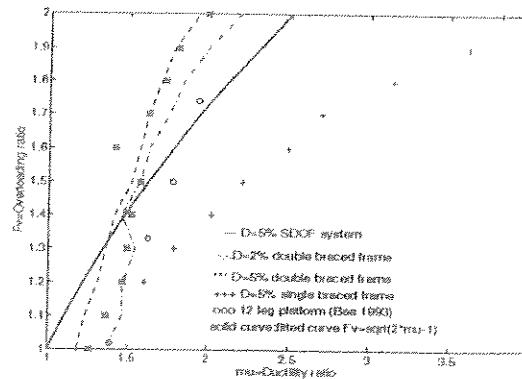


Figure 3: Comparison of ductility overloading ratio relationships for SDOF system, single and double braced frames and a 12-leg Jacket Platform

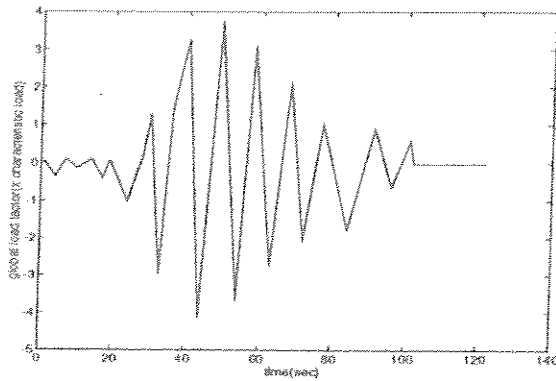


Figure 4: Scaled up sea load history

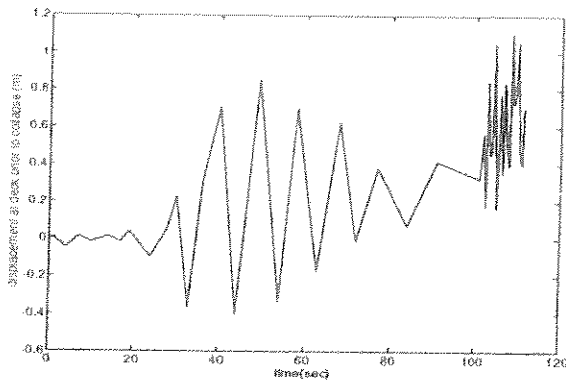


Figure 5: Displacement history for pushover-dynamic analysis

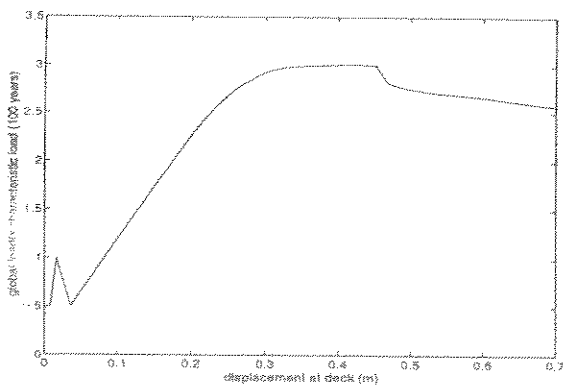


Figure 6: Static load-displacement curve

is characterized by very large (inoperable) overall deformation of the platform with very high degree of utilization in the structural components. Scaling is conducted uniformly for the whole loading history with a factor greater than 1.0. The load history

corresponding to the dynamic limit state of collapse is given in Fig.3. The maximum load factor is 4.104 which means that the platform could pass safely at its ultimate capacity through this very severe sea loading.

The ultimate static capacity of the platform was evaluated from static pushover analysis is obtained to be 3.013 times the characteristic load, confer Fig.6. The dynamic overcapacity ratio in this case is found to be:

$$F_v = \frac{RD_u}{RS_u} = 1.362 \quad (19)$$

and the ductility ratio is:

$$\mu = \frac{0.6021}{0.3245} = 1.855 \quad (20)$$

So

$$F_v = \sqrt{\mu} = 1.362 \quad (21)$$

From Fig.6, it is evident that the studied platform is a ductile structure with a high residual strength. Study of similar ductile platform and their corresponding ductility spectra [3], justifies the high overloading ratio found here.

This behavior is probably due to the high inertial resistance of the structure combined with the dynamic loading effects. Bea [3] and Stewart [14] found that the dynamic overloading ratio for ductile platforms is about 1.20. And for semi-ductile platforms it is between 1.07-1.00. It is also shown that the combined dynamic loading and structural performance characteristics results in a overcapacity ratio between 1.20-1.70 for ductile structures. (For ductility ratios between 1.50-5.00 for a structural period of 1.0 sec [3,6]).

5 Structural response

The static load-displacement and the dynamic response at the deck top are plotted in Figs.6 and 7 respectively. Stiffness degradation of the structure due to dynamic loading effects and overall structural performance regarding its ductility can be seen from the latter figures.

The ductility ratio is about 2.54 for this platform for a structural damping ratio of 2%. Comparing this result with the ductility spectra given in [6], these studies suggest the following relationship:

$$F_v = \sqrt{2\mu - 1} \quad (22)$$

where μ and F_v denote respectively dynamic overcapacity ratio and ductility ratio. Fig.3 shows the results of a SDOF system, single and double braced plane frame analyses and compares them with those obtained by Bea[3] for a 12-leg drilling and production platform with natural period of $T_n=1$ sec and damping ratio of $D=5\%$ subjected to earthquake loading. The latter relationship as plotted in Fig.2 gives far lower ductility demand for the studied 8-leg jacket with $T_n=0.5$ sec and $D=2\%$. While for the same structure with damping ratio $D=5\%$, the latter relationship overestimates the overloading ratio by about 20%.

Fig.3 also indicates that the SDOF and plane frame results give somewhat lower ductility demands for the same overloading values compared with those of the jackets platforms.

6 Fracture check

To demonstrate the potential influence of the element (structural member) fracture on the overall performance of the structure, another analysis was carried out with a fracture criterion included.

The fracture check is based upon the so-called "load 3" CTOD criterion [10]. A simplified model is adopted for calculating the strains in the plastic hinges [16]. The crack tip opening displacement "CTOD" is computed on the basis of the nominal strain, the corresponding stress (which may be raised due to hardening) and an assumed crack length [15]. The CTOD values are assumed to be in the range of 0.3-0.5mm which are often found to be critical [10]. The defect size was assumed to be in the range of 3-5mm which are detectable by standard inspection methods. The fracture model assumes that fracture will take place before reaching the ultimate strain to comply with this the following condition should be fulfilled:

$$CTOD_{crit} < \pi \epsilon_u \frac{\sigma_u}{\sigma_y} \cdot a \quad (23)$$

where ϵ_u =ultimate strain; σ_u =ultimate stress; σ_y =yield stress, a =defect size and $crit$ =critical CTOD.

The results are given in Figs.8 to 11. The ultimate dynamic capacity of the structure is then reduced to $RD_u=1.885$ i.e. the dynamic overloading ratio for the fractured structure; the ratio between the intact and the fractured dynamic overcapacity ratios is obtained as follows:

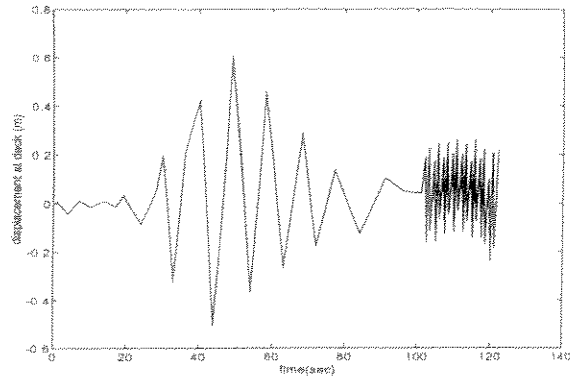


Figure 7: Displacement history prior to the ultimate collapse of the fractured structure

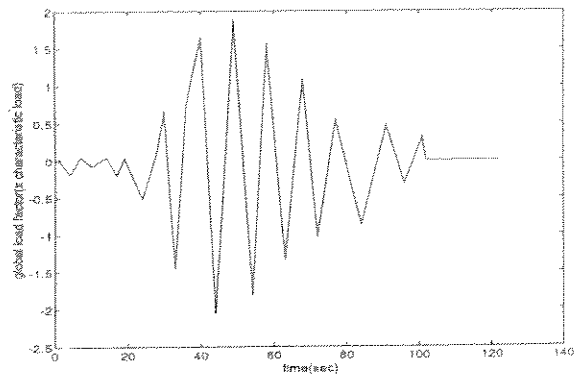


Figure 8: Global load history prior to the ultimate collapse of the fractured structure

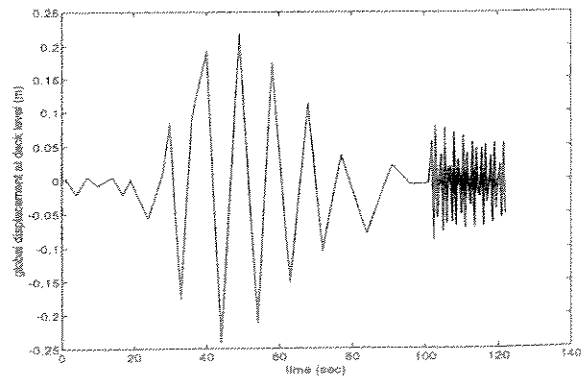


Figure 9: Global displacement history prior to ultimate collapse

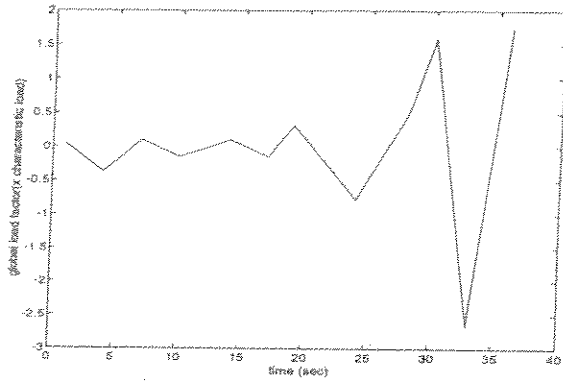


Figure 10: Sea load history

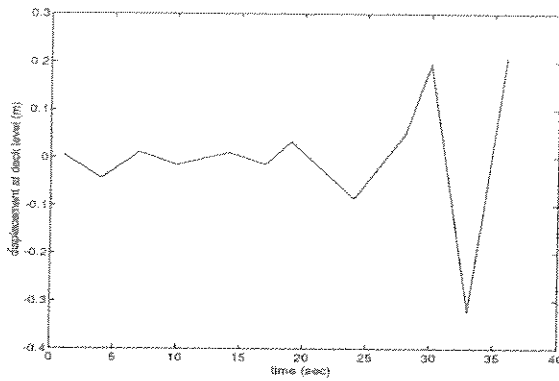


Figure 11: Displacement response

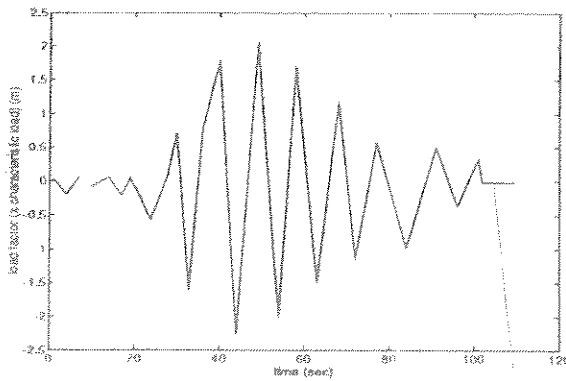


Figure 12: Sea load history

$$(F_v)_{\text{fractured model}} = \frac{RD_u}{RS_u} = \frac{1.885}{3.013} \approx 0.626 \quad (24)$$

This shows a drastic decrease in the dynamic capacity when fracture criterion is included. This is due to the fracture limit set for the loading capacity

Table 1. Platform description

Type	Steel - Jacket
Water depth	110 m
No. of Legs	8
No of Supports	4
Long bracing	Diagonal & X
Transverse bracing	K & X

Table 2. Soil profiles

DEPTH (m)	SOIL TYPE	UNIT WEIGHT (kN/m³)	POISSON'S RATIO	MODULUS OF ELASTICITY (kN/m²)	COHE. (kN/m²)	ANGLE OF INTERNAL FRICTION (°)	ADHESION (kN/m²)	SOIL STRENGTH (kN/m²)												
0																				
1																				
2																				
3																				
4																				
5																				
6																				
7																				
8																				
9																				
10																				
11																				
12																				
13																				
14																				
15																				
16																				
17																				
18																				
19																				
20																				
21																				
22																				
23																				
24																				
25																				
26																				
27																				
28																				
29																				
30																				
31																				
32																				
33																				
34																				
35																				

as well as the stiffness of elements. When the fracture criterion is violated the latter values are set to zero and redistribution of forces takes place [16]. The ductility ratio for the fractured model is about one ($\mu_{\text{fractured model}} = 1.0$).

The latter indicates that in the fractured case the proposed relationship above for evaluation of the dynamic overloading ratio will highly overestimate it. The following relationship is suggested in [6] when the fracture is included :

$$(F_v)_{\text{model}}^{\text{frac}} = \sqrt{\frac{11}{2}} \quad (25)$$

7 Foundation failure effects

In the example presented, foundation is modelled as linear springs to the ground. Therefore no foundation

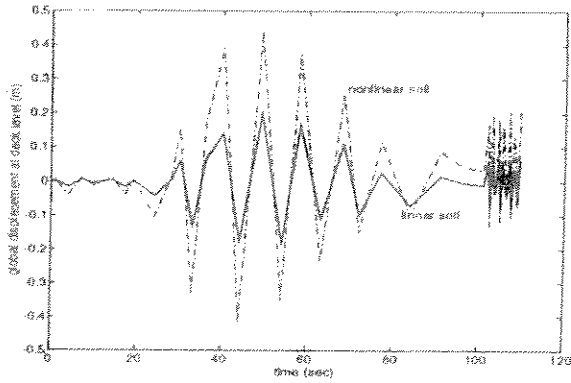


Figure 13: Displacement response for both linear and nonlinear soil conditions

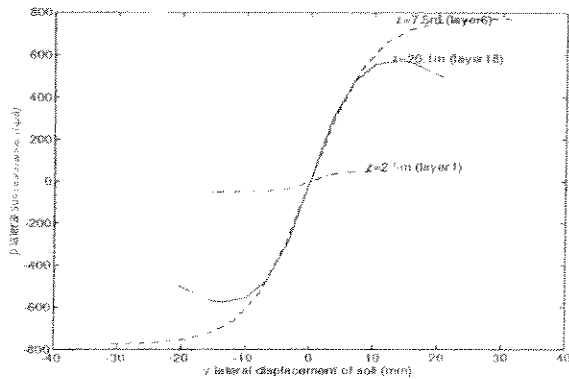


Figure 14: p-y load transfer-displacement curves for three different soil layers

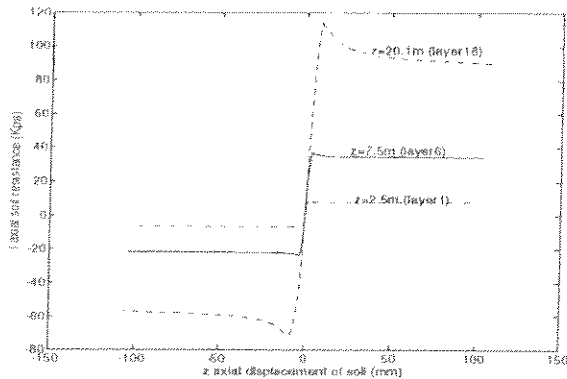


Figure 15: t-z load transfer-displacement curves for three different soil layers

yielding has been reported. At this stage possible foundation failure is considered. The foundation will be modelled as non-linear lumped springs with their load transfer -displacement characteristics specified as p-y, t-z and q-z curves respectively for both lateral, axial loadings and the end bearing of piles.

Figs.14,15 and 16 show the pile-soil load-transfer displacement curves for both axial and lateral loadings and the end bearing. Fig.17 shows the structural failure mode due to progressive yield in the soil layers from top to bottom accompanied by formation of hinges in the piles. The results of pile-soil-structure analysis shows the important effect of pile-soil non-linearities in the overall static capacity and dynamic response of the platform. The analysis results predicted that in the given soil conditions (see Table.2), the ultimate static capacity $RS_u=2.21$ times the characteristic wave load. The ultimate dynamic capacity of structure is reduced to $RD_u=2.33$ and the ductility demand is $\mu=2.28$ which is 23% higher than that in the linear foundation case ($\mu=1.86$). This is predictable because of the larger displacement of the overall system due to pile-soil failure. The displacement response of the platform is plotted in Fig.13. And the corresponding load history plot is given in Fig.12. Due to soil damping effects after passage of the most severe parts of the waves the structure recovers rapidly and the response dies out quicker than in the previous case. For comparison, both simulations are shown in the same figure. $F_v=1.05$ which shows the following approximate relationship:

$$F_v = \sqrt{\frac{D}{Z}} \quad (26)$$

A number of jacket-type platforms with specified natural period and ductility levels should be studied to verify the suggested relationships here and those given in [3,14,15,6]. Nevertheless, the obtained relationships are in reasonable agreement with the results found by other studies [3,14,15,6].

7 Safety assessment

For safety assessment, the ultimate strength check may be formulated as [8]:

$$\frac{R_u}{\gamma_m} \geq \gamma_D D + \gamma_B \cdot E \quad (27)$$

where R_u is the system's ultimate strength based on the characteristic material properties, D and E the functional loads (including gravity and buoyancy



Figure 16



Figure 17

Table 1

λ
st
fa
Nl
rec
Fv
fa
Nl
rec

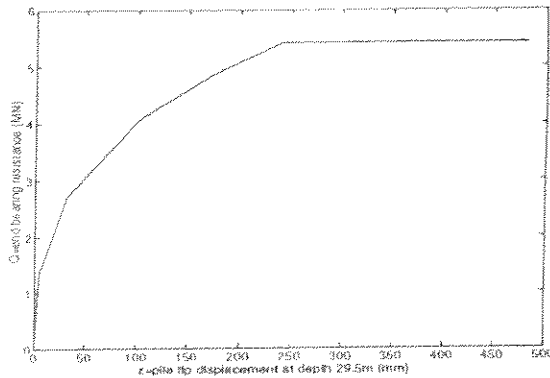


Figure 16: End bearing curve

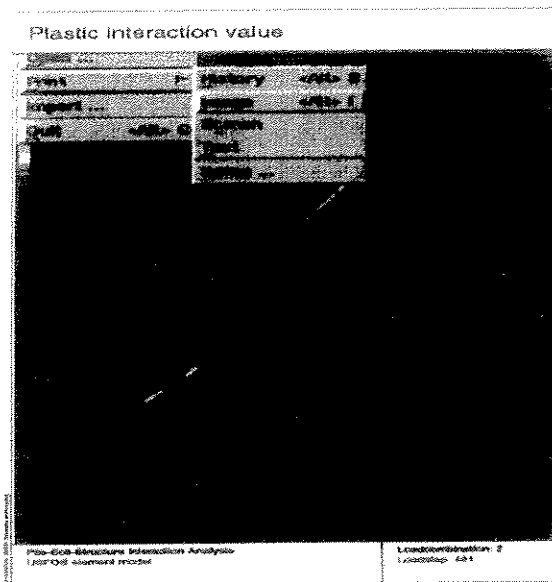


Figure 17: Progressive foundation failure mode

Table 3: Safety assessment

λ	static pushover	dynamic pushover
structural failure	3.01	4.10
NPD requirements	1.50	1.50
Foundation failure	2.20	2.33
NPD requirements	1.70	1.70

loads) and environmental loads, respectively. γ_m is a material coefficient, γ_D and γ_E are load factors. The recommended partial factors γ_m , γ_D and γ_E and the characteristic environmental loads depend on the design code. In the present study NPD regulations have been adopted. To satisfy the NPD regulations [15] the characteristic environmental loads correspond to those with a 100 year return period and with a load factor of 1.3. The factor γ_D is taken as unity and the characteristic yield strength for all components are taken as minimum specified values in the code. The material factor γ_m varies for different components (structure, pile, soil etc), but for the structural part it is considered as 1.15. The above equation would be rewritten as :

$$R_{ult} \geq \eta D + \lambda E \quad (28)$$

where $\eta = \gamma_D \cdot \gamma_E$ and $\lambda = \gamma_E \cdot \gamma_m$. This implies that for compliance with the safety requirements of NPD $\lambda \geq 1.15 \times 1.3 = 1.5$ for all wave attack directions. For other codes /regions λ might differ from this value. From the results of static and dynamic analyses shown in Figs.6 and 7, it is seen that in both cases the acceptance criteria are satisfied with good safety margins (See Table.3).

8 Conclusion

The nonlinear structural behavior of a jacket under transient dynamic loading was studied. In order to gain insight into the performance of ductile platforms in the case of hurricanes and earthquakes.

Disregarding foundation failure a dynamic overcapacity ratio of 1.36 is obtained. The ductility ratio for the jacket was obtained to be 1.86.

A structural fracture mode does influence the global behavior by making it semi-brittle and also reducing the overloading ratio. The "level 3" fracture criterion adopted in our analysis is sensitive to CTOD and the crack size. So a reasonable range 0.3-0.5 mm for CTOD and 3-5mm for the defect size are considered critical for the adopted criterion.

When the potential fracture is taken into account, a significant change in the structural performance emerges. The dynamic overcapacity ratio decreases to 0.625 which is only 46% of unfractured model and the ductility ratio is reduced to about 1.0. This is due to the fracture limit set for the loading capacity, stiffness and straining level of elements. Therefore the plastic tensile strain can not develop infinitely, if the criterion violated. And so there will be loss in the loading capacity of elements which subsequently will

result in brittle behavior and lower overloading capacity of the structure.

Two approximate but satisfactory relationships based on simple models studied in [6] are proposed for the natural period of about 0.50 sec and damping ratios from 2% to 5%.

The proposed relationships are comparable with those given by Bea [3] for a structural periods 1 and 2 sec and damping ratio 5%.

In the last part, the effects of foundation failure were studied. A progressive foundation failure mode from the upper soil layers downwards was encountered. A rather severe bending collapse mode occurs at the upper soil layers. Consequently this results in a major sway mode and by progressive pile-soil failure, it switches to an overturning collapse mode at very large displacements.

The results show a significant increase in the system's ductility ratio which attains 2.28. The complete yield of soil occurs particularly at the upper soil layers where soil reaches its peak capacity. This also resulted in lowering the dynamic overcapacity ratio to about 1.05 which is about 77% of the model for which the soil is considered as linear with initial pile-soil interaction stiffness values.

REFERENCES

- [1] Amdahl, J., and Eberg, E. (1992), USFOS Phase 2: Dynamic Collapse Analysis Program, SINTEF Structure and Concrete, Trondheim, Norway
- [2] API (1993) Recommended Practice 2A-LRFD (RP 2A-LRFD), First Edition, July 1, 1993
- [3] Bea, R.G and Young, C.N (1993) ,Loading and Capacity Effects on Platform Performance in Extreme Storm Waves and Earthquakes. OTC Paper No. 7140
- [4] Clausen, C.J.F. (1992), SPLICE Computer Program for Pile-Soil-Structure Interaction Analysis, NGI and Aker Engineering, Oslo, Norway
- [5] Eberg, E., Hellan, Ø. and Amdahl, J. (1993), Nonlinear Re- Assessment of Jacket Structures Under Extreme Storm Cyclic Loading Part III, SINTEF Structures and Concrete and NTH, Norway
- [6] Emami Azadi, M.R., Pile-Soil-Structure Interaction Analysis in extreme waves and in Earthquake , Chps. 2 and 3, Ph.D. ,(to be published)
- [7] Emami Azadi, M.R. (1994), GENSODM program , Modified Version of Gensod Program Based on Modified API 93 Pile-Soil Models (to be published)
- [8] Emami Azadi, M.R. (1994), GPSD Fortran program for generating pile-soil data (to be published)
- [9] Moan, T., Amdahl, J., Engseth, A.G and Granli, T. (1985) Collapse behavior of trusswork steel platforms. Int. Conf. On Behavior of Offshore Structures (BOSS 85) , Delft, Holland
- [10] Næss , A.A. (1985) Fatigue handbook, Offshore steel structures , Tapir , NTH , Norway
- [11] Poulos, H.G. (1988). Influence of Cyclic loading on axial pile response. Proc. r , Int. Conf. on Numerical Methods in Offshore Piling 1988, Austin, Texas. USA
- [12] Poulos, H.G. (1989) Pile behavior-Theory and application (Lecture) Geotechnique. 34(2).
- [13] Pelletier, J.H., Murff, J.D. and Young, A.C. (1993) Assessment of the current API Design for axially loaded piles, Shell Development Co.
- [14] Stewart, G. (1993) Non-Linear Structural Dynamics By The Pseudo-Force Influence Method . Part II: Application to offshore Platform Collapse. Proc. Int. Offshore and Polar Engineering (ISOPE), USA
- [15] Stewart, G., Moan, T. and Eide, O. (1993). Nonlinear Re-Assessment of Jacket Structures Under Extreme Storm Cyclic Loading, Part I: Philosophy and Acceptance Criteria.
- [16] Søreide, T.H., Amdahl, J., Eberg, E., Holmås, T. and Hellan, Ø. (1993). USFOS -A Computer program for progressive collapse analysis of steel offshore structures, Theory manual, SINTEF, Norway
- [17] WAJAC (1992). Wave and Current Loads on Fixed Framed Structures, DnV, Norway
- [18] Wu, D., Broms, B.B. and Chao V. (1993). Re-examination of laterally loaded piles in clays using improved p-y curves, ISOPE '93, Vol. 1, pp. 522-527

APPENDIX

E

EMAMI AZADI, M.R. AND MOAN, T.: "DUCTILITY DEMAND OF SIMPLIFIED PILE-SOIL-JACKET SYSTEMS UNDER EXTREME SEA WAVES AND EARTHQUAKES" PROC. EURO DYN '96, TRONDHEIM, NORWAY, 1996.

- o0o -

Ductility demand of simplified pile-soil-jacket system under extreme sea waves and earthquakes

M. R. Emami Azadi & T. Moan

Department of Marine Structures, NTH, Norway

ABSTRACT: This paper offers some insight into the dynamic loading effects on the performance of jacket platforms under extreme (sea) waves and earthquakes. To facilitate this study, a ductility measure is established as representative of potential structural damage. Two simplified structural systems are used to represent the platform. First a single-degree-of-freedom (SDOF) system is used to study the dynamic nonlinear behaviour of the structure. In the second part of this study a simplified model consisting of a multi-stack of disks is used to represent the dynamic pile-soil behaviour. The equivalent dynamic system is based on the stiffnesses at the pile head. A series of ductility analyses are performed to show the effects of various structural and loading parameters on the overall performance of the idealized system. The resulting ductility spectra indicate that the ductility demand (μ) is highly dependent on the dynamic overloading ratio (F), the natural period of the platform, damping ratio, the elasto-plastic behaviour of the structure and soil and also on the dynamic loading characteristics.

1. INTRODUCTION

The present work attempts to answer the following questions:

- 1) Why do the jacket platforms with different structural characteristics behave differently under extreme sea waves and earthquakes?
- 2) How does a jacket platform behave under various loading time histories with the same intensity (overload ratio)?
- 3) Whether a jacket platform designed for a static loading will sustain (pass safely through) a dynamic loading with the same intensity (a static overload ratio of 1.0)?
- 4) What is the effect of pile-soil interaction on the overall performance of the structure?

Several previous studies (Bea et al. 1993), (Eberg et al. 1993), (Emami et al. 1995), (Fajfar et al. 1993), (Schmucher et al. 1994) and (Stewart et al. 1993) have addressed some of these issues in a limited manner by considering some of the effects. These studies have either neglected the dynamic pile-soil interaction or have used a Winkler spring approach (e.g. see (Bea et al. 1993) and (Emami et al. 1995)). This study focuses on these issues and tries to provide some insight into nonlinear dynamic behaviour of jacket platforms by means of ductility

demand analysis.

The ductility ratio (μ) is defined as the ratio between the maximum sustainable displacement (regarding the stability of the structure) and the first global yield displacement of the platform at the deck level. The overload (overcapacity) ratio is defined as the ratio between the ultimate dynamic load and the ultimate static resistance of the structure.

The near failure nonlinear dynamic behaviour of structures will be influenced by changes in the characteristics such as its natural period, damping ratio, elasto-plastic behaviour, post-peak reserve strength ratio, soil shear modulus. Furthermore dynamic loading effects such as overloading effect, dynamic amplification effect, randomness-periodicity effect, duration of the most severe part of the load history also are involved combined with the structural effects. Due to limited scope of this study not all the preceding effects will be considered.

To address these issues two simplified equivalent dynamic systems are used to represent the platform. First the simplest single-degree-of-freedom (SDOF) system is used to idealize the overall dynamic behaviour of the structure.

Subsequently the dynamic interaction between the

soil foundation is included by means of a simplified multi-stack of disks model (Wolf et.al, 1994).

Both linear and nonlinear soil conditions are considered. The idea is to use an equivalent spring and dashpot system with their spring and damping characteristics computed from the disk model at the pile head.

Structural nonlinearities are represented by using the well known Bouc's hysteretic model.

The wave load time history is generated by using WAJAC computer program (Dnv, 1992) based on Jonswap energy spectra. The simulated wave histories are scaled up successively and only the most severe part of them are imposed .

Five medium to long period earthquake records are used for seismic ductility demand analysis.

Ductility spectra are established here which could provide the basis for predicting the global dynamic behaviour of the platform systems.

2 SIMPLIFIED STRUCTURAL MODEL

2.1 SDOF system

A very simple single-degree-of-freedom (SDOF) system is initially used to only indicate the overall dynamic behaviour of the jacket platform. The jacket model and the equivalent SDOF systems are shown in Fig.1.

The structural model assigned to this SDOF system is a well known Bouc type hysteretic model which is explained more in (Bouc et al., 1967, Park et al., 1986, Sues et al.,1988 and Bessason, 1992). By varying the parameters of Bouc's model in special cases, elastic-perfectly-plastic and bi-linear models might also be represented.

The SDOF system is defined by its mass (m) and the equivalent natural period of the structure defined as $T_n=2\pi\sqrt{m/k}$ where k is the initial stiffness of the system.

The dynamic equation of motion of SDOF system is expressed as:

$$m\ddot{u} + c\dot{u} + k\mu = f(t) \tag{1}$$

- where u = displacement of the mass
- \dot{u} = velocity of the mass.
- \ddot{u} = acceleration of the mass
- k_t = the tangential stiffness of spring as shown in Fig.1
- c = viscous damping
- $f(t)$ = the loading time history which is equal to

$-m\ddot{u}_g$ in the case of a seismic input.
 \ddot{u}_g = the ground motion acceleration.

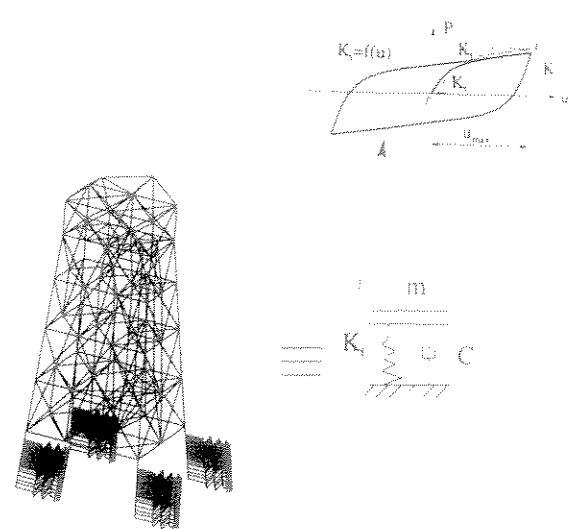


Fig.1. Equivalent SDOF system

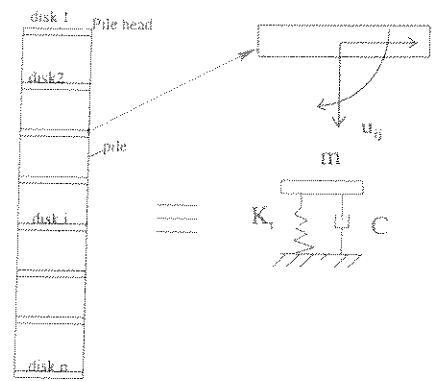


Fig.2. Disk model of pile-soil system and an equivalent system.

2.2 A simplified system based on disk modelling of pile-soil

In this section we describe a simplified equivalent dynamic model based on a physical disk model (Wolf et al., 1994) for the pile-soil foundation of the jacket platform.

As shown in Fig.2, the pile-soil system is modelled as a multi-stack of disks representing the pile-soil interaction elements. It is assumed that these disks are connected to each other via pile beam elements

with their stiffnesses and masses are included. It is also assumed that the soil mass trapped between the various disks as shown in Fig.2 will be mathematically subtracted from the dynamic system (Wolf et al., 1994) as follows:

$$P_0 = A^T S / A u_0 - M \ddot{u}_0 \quad (2)$$

where P is the modified pile-soil interaction force amplitude, A is called the kinematic-constraint matrix which connects the displacement amplitudes at the disk positions into that of the interface point (pile head), S^T is called the dynamic flexibility matrix and is obtained by using Green's function approach (Meek et al., 1993), u_0 is the displacement vector at the pile head, \ddot{u}_0 is the acceleration at the pile head and M is the trapped soil mass inside the pile.

It is also assumed that the shear modulus of soil (G) will be a function of soil's shear strain (γ), which might be derived based on (Svano et al., 1993) as follows:

$$G^T = G(\gamma, h, k, \sigma_m, \alpha, \beta) = G_0 (1 - \alpha, z(r))^\beta \quad (3)$$

where in the above equation G^T is the tangential shear modulus of soil, h and k are curve fitting parameters given by (Svano et al., 1993), σ_m is the effective mean stress of soil, α is the dynamic attraction parameter of the soil, G_0 is the shear modulus of the soil at the pile-soil interface, α and β factors are found empirically by Svano et al., (1993) from triaxial test results. $z(r)$ may be taken as a non-dimensionalized shear stress function varying exponentially with the radial distance r from the pile-soil interface as shown in Figs.3 and 4. Eq.3 is derived in terms of γ in the Appendix.

To obtain the equivalent dynamic tangential stiffness parameters at the pile head, the Green's function approach (Meek et al., 1993) is used combined with Eq.3. Moreover, the following assumptions regarding strain and stress conditions are made: (i) plane strain condition around the pile (ii) the strain components will not vary with the soil depth (see for e.g. Konagai and Nogami et al., 1989) (iii) that shear stresses induced in the soil due to application of the axial forces at the pile head or ground motion might vary over an imaginary disk with a radius of n times the pile's radius (see Fig.4), (iv) the normal stresses induced in the soil at the pile-soil interface may vary over an imaginary disk with a radius of n times the pile's radius (see Fig.4), the normal stresses due to lateral force around the pile will be carried by the shear stresses around the imaginary disk assumed to exist at the interface, illustrated in Fig.4.

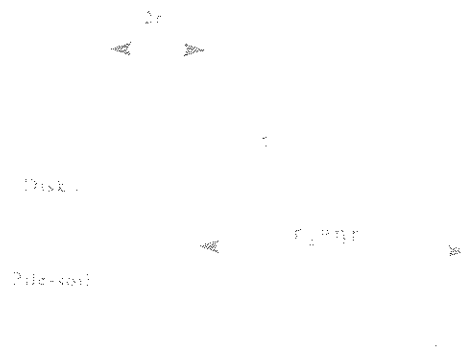


Fig.3 Approximate shear stress distribution around the pile-soil disk for axial loading case



Fig.4 Approximation of the normal and shear stress distributions around the pile-soil disk for axial loading case

Similar assumptions may be made about the rocking and torsional motions of the pile-soil disk.

By making the assumptions mentioned above, the displacements at the pile-soil disk points (u_{disk}) may be found as a function of the shear strain (γ) at the pile-soil interface by integrating the shear stress over the radius of the imaginary disk. Towards that aim, it may be required to obtain γ the shear strain at an arbitrary distance r from the pile-soil interface as follows:

$$\gamma = \int_0^r \frac{dz}{G^T}$$

where G^T is given by Eq.3. To simplify the simplifying assumption made earlier, the imaginary soil disk around the pile is assumed to approach zero at the far end of pile's radius, i.e. n times radius of pile is assumed to be zero. This may be assumed as:

$$\tau(r) = \frac{2r}{\gamma} \exp\left(-\frac{r}{\gamma}\right)$$

where τ_i and τ_r are respectively, the actual and the failure shear stresses at the pile-soil interface, r and r_i are radial distances as shown in Fig.3 and 4. From Eq.5, the radius factor of the imaginary soil disk (η) may be determined. For engineering purposes, a factor of 10 to 15 would be sufficient. By inserting $\tau(r)$ from Eq.5 into Eq.4 and integration the following expression is obtained :

$$\gamma = \frac{\tau_f}{G_i \alpha (1-\beta)} [1 - (1 - \alpha \frac{\tau_i}{\tau_f} \psi(r))^{1-\beta}] \quad (6)$$

The axial displacement at the pile-soil disk points may be obtained from the following :

$$u_{disk}^a = \int_{r_i}^{r_{id}} \gamma(r) dr = \frac{\tau_f}{G_i \alpha (1-\beta)} \int_{r_i}^{r_{id}} [1 - (1 - \alpha \frac{\tau_i}{\tau_f} \psi(r))^{1-\beta}] dr \quad (7)$$

where superscript a refers to axial displacement and r_{id} is the radius of the imaginary disk around the pile as shown in Figs.3 and 4. The integration of Eq.7 may then be performed either numerically or analytically. The analytical solution may be achieved for positive integer values of (β) exponent in Eq.7, while numerical integration would be preferred to obtain the results for any possible real value of (β). The practical range of (β) is found empirically by Svanø et. al., (1993) to be between 1 and 4.

For lateral loading of pile-soil disk as shown in Fig.4, the reacting normal stresses (σ) may be related to the shear stresses (τ) via an equilibrium relationship around the pile-soil (Janbu et al., 1985):

$$S_u = \frac{k_w p_f}{N_{ru} d} \quad (8)$$

where S_u is the undrained shear strength of soil, d the pile diameter. N_{ru} is a number corresponding to a shear failure situation around the pile (see Fig.5), k_w is the so-called gap factor. Assuming that for p less than the lateral pressure at failure p_f , τ will be less than the shear strength of soil S_u , then τ_i may be written as follows:

$$\tau_i = \frac{k_w \sigma_i}{N_{ru} d} \quad (9)$$

where σ_i and τ_i are respectively, the normal and shear stresses at the pile-soil interface as shown on Fig.4. For an undrained soil condition, the soil volume may be assumed to be constant. Thus for a soil element at the pile-soil interface, the following relationship may be written :

$$\gamma = \epsilon_r - \epsilon_\theta \quad (10)$$

where ϵ_r and ϵ_θ are respectively the radial and circumferential strain components as shown in Fig.5.

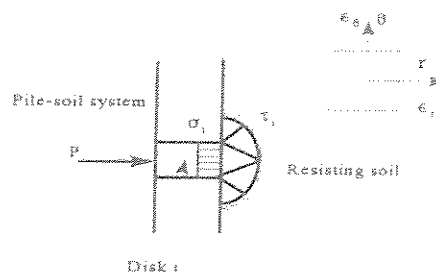


Fig.5 Shear resistance of soil around the pile and deformation of a soil element at pile-soil interface

In this case $|\epsilon_r| = |\epsilon_\theta|$, thus Eq.10 will be reduced to:

$$\epsilon_r = \frac{\gamma}{2} \quad (11)$$

where γ is given by Eq.4. Therefore the lateral displacement of disk u_{disk} may be computed as follows:

$$u_{disk}^r = \int_{r_i}^{r_{id}} \epsilon_r dr = \int_{r_i}^{r_{id}} \frac{\gamma}{2} dr = F(\tau_i) \quad (12)$$

where superscript r refers to lateral (or radial) displacement. By combining Eqs.7 or 12 and A6 or A9, G^T may be obtained as a function of u_{disk} :

$$G^T = \phi(\tau_i) = \phi(F^{-1}(u_{disk}^{i,n})) \quad (13)$$

where superscripts i and n denote the disk and the integration step numbers, respectively.

By using the Green's function method (Meek et al, 1993), the equivalent dynamic stiffness coefficients

for
calc
are
u_i,
β_yⁿ

where
from
rece
and
step
term
(199
doub
v un
nonl
expr
Co
give
the c
As s
degr
dyna
stanc

3. W

3.1 A

A nu
by u
base
using
The
time
corre
16.0
Only
histo
port
one
100s
until
respe

3.2 F

Seve
grou
stud

for the pile-soil system at the pile head may be calculated. The complex Green's function elements g_{ij} are calculated in terms of G^T which is a function of u_{disk} as given by Eq.13. So we will have:

$$g_{ij}^n = g_{ij}^n(t, a_{ij}, u_{disk}^{i,n}) + g_{ij}^n(t, a_{ij}, u_{disk}^{i,n-1}) \quad (14)$$

where a and a' represent respectively, the distances from the source disk j and its mirror image to receiver disk i as show in Fig.6. In Eq.14, indices i, j and n represent the receiver, source and integration step numbers, respectively. The Green's function terms involved in Eq.14 can be found in Meek et al. (1993). All terms in the Green's functions for a double cone model such as the seismic wave velocity v and the static stiffness K can be computed as a nonlinear function of G^T thus resulting in u_{disk} as expressed above.

Consequently the dynamic stiffness matrix K as given in Eq.1 will be a nonlinear function of u_{disk} or the displacement at the pile-soil-jacket interface u_{psj} . As shown in Fig.2, both translational and rotational degrees of freedom are considered the equivalent dynamic system is finally solved by means of a standard predictor-corrector method.

3. WAVE AND EARTHQUAKE LOADINGS

3.1 Wave loading

A number of wave load time histories are simulated by using computer program WAJAC (DnV, 1992) based on well known Morison's equations and by using Jonswap wave energy spectrum.

The significant wave heights (H_s) for the simulated time histories are between 12.75 m and 15 m the corresponding mean periods between 12.5 sec and 16.0 sec.

Only the most severe portion of the generated time histories are scaled up. The length of the selected portions ranges from 50 to 100 secs. Fig.7 shows one simulated wave load history from time 50 sec to 100sec. The scaling has been successively continued until reaching the maximum overload ratio with respect to the ultimate static capacity of the system.

3.2 Earthquake loading

Several severe earthquakes are used as seismic ground acceleration time histories throughout this study. The seismic records correspond to standard

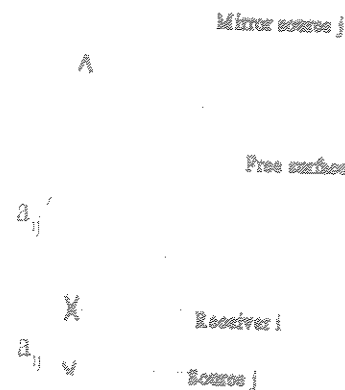


Fig.6 Representing the pile-soil system by the source, receiver and mirror image disks (Wolf's model)

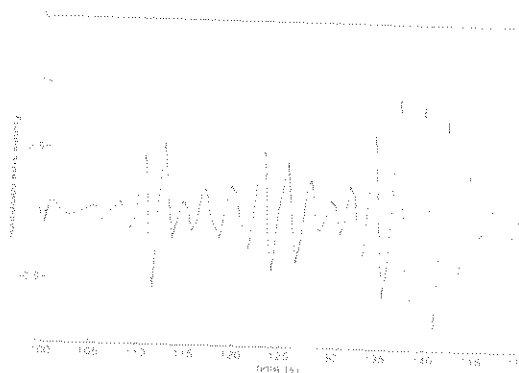


Fig.7 A sample of simulated wave load time history ($H_s=15$ m and $T_s=15.8$ sec)

medium to long period earthquakes. They have been scaled according to their periods and categories by using a standard caltech procedure (Caltech, 1995). Only the most severe portion of the earthquake records in Table.1 have been imposed on the structures with a length ranging from 10 to 20 secs.

Table 1. A brief description of the earthquake records which are used during this study

Earthquake	Peak Acc. (m/s ²)	Duration (s)
Elcentro	2.1	33.5
Parkfield	1.0	50.0
Santacruz	1.2	65.0
Taft	1.5	54.4
Woodfords	0.8	25.0

4. DUCTILITY ANALYSIS RESULTS

Ductility spectra for different wave and earthquake conditions are given in Figs.8-18. The reference values for G , f_y and α_1 parameters are chosen to be 42 MPa, 350 MPa and 0.1 respectively.

It is shown in the Figures 8 to 18 that the ductility demand (μ) of system generally decreases by increasing the natural period of the platform.

There are some peaks and valleys (humps) associated with the most of the spectra, which are especially in the range of $T_n \approx 2.0-3.0$ sec. They might be due to resonance effects related to multiples of the primary force harmonics (Morison et al., 1992). However the general trend as shown by the fitted curves in Figs.8 to 18 is the increase of (μ) by decreasing T_n towards 0.5 sec.

As shown in the presented ductility spectra, the relative maximum displacement (ductility demand) of the platform is highly dependent on the overload ratio (F_0) for the range of $T_n \approx 2.0-3.0$ sec.

As seen in Figs.13 and 14 increasing the yield strength (f_y) or the width parameter of the system (α_1) in the hysteretic Bouc's model results in shifting the ductility curves (μ vs. F_0) towards smaller T_n values. The latter might be interpreted as change of the effective (natural) period of the structure due to change in its stiffness. This seems to be a beneficial effect in the sense that the required ductility ratio is reduced. However the peak ductility demand is not altered very much in Figs.13 and 14.

The influence of other important parameters such as viscous damping is shown in Fig.10. It is observed that generally increasing the damping ratio reduces the ductility demand. The influence of damping for shorter periods is much greater than that for larger periods. The higher damping as seen damps out the peaks in the spectra.

It is observed from Figs.8 through 18 that the ductility demands for extreme wave loadings are higher than those for seismic loadings for the same overload ratios. This difference might be due to the much longer duration of extreme waves than that of the earthquakes. The loading duration effect may cause the system to reach its ultimate capacity sooner than it might have been anticipated in a static loading.

In the case of extreme sea waves, the odd and even multiples of the primary force components in the Morison's equation would give rise to some dynamic effects. Meanwhile for large overload ratios $F_0 > 1.0-1.1$, the dynamic amplification effects might be dominated by the (static) overload related to the structural characteristics.

The influence of soil's shear modulus G on the ductility demand is presented on Fig.12. It is observed that the peaks are reduced by increasing the soil's shear modulus particularly in the range of $T_n < 2.0-3.0$ sec. These effects are comparable with those seen in Figs.13 and 14.

The variation of the ductility demand for different earthquakes and waves can be seen on Figs.8 to 9 and on Figs.15 through 18, respectively. The highest peaks for a given overload ratio varies significantly for different earthquake or wave loading time histories. For the earthquake records studied here, the coefficient of variation of the ductility demand (μ) is obtained in the range of 20% to 40% for varying overload ratio. While for the simulated wave load histories, the COV of the ductility demand (μ) is higher in the range of 30% to 65%.

The variation in the ductility demand (COV of μ) may be due to different duration, frequency contents, random phasing and acceleration amplitudes associated with various records. The study by (Bea et al. 1993) on various synthetic earthquakes showed that the ductility demands for such earthquakes on average would be less than those for the recorded earthquakes. While he found that for simulated sea waves with high degree of (phasing) randomness, the ductility demand (μ) on average is higher than that for a recorded one with the same overload ratio (F_0). In the light of these results, it is expected that the spectra presented here to provide somewhat conservative estimate of the ductility demand on average.

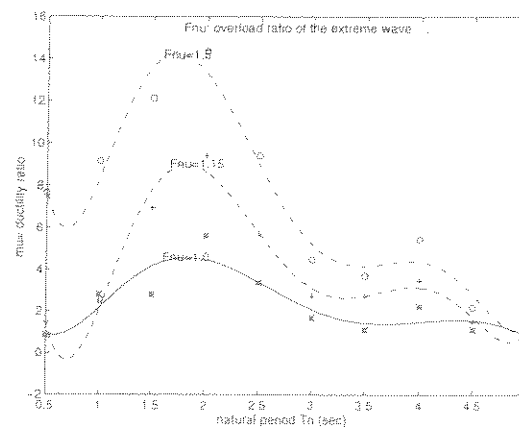


Fig.8 Ductility spectra for a simulated extreme wave ($H_s=15$ m, $T_z=15.8$ s)

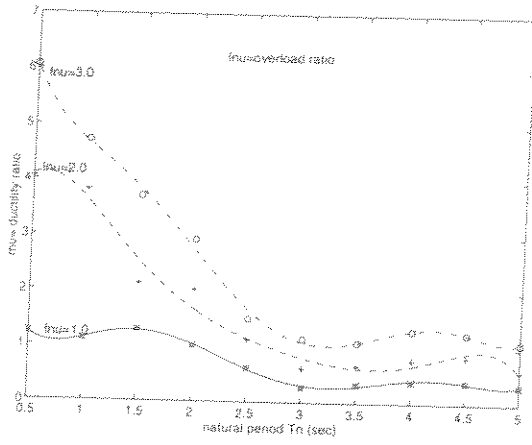


Fig.9 Extreme wave ductility spectra for a simulated wave ($H_1=12.75$ m, $T_z=12.5$ s)

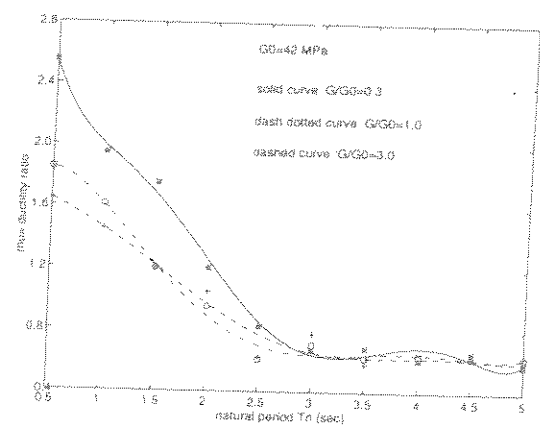


Fig.12 Seismic ductility spectra for variation of soil's shear modulus G (El Centro, 1940)

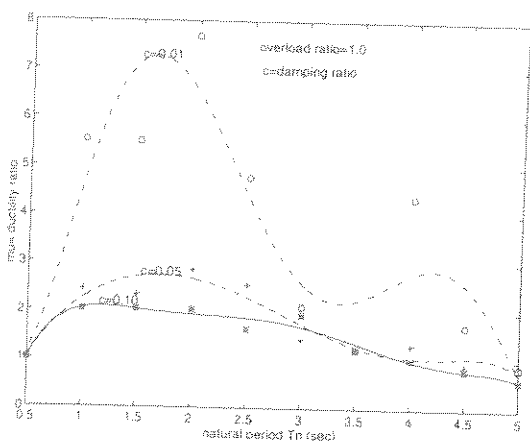


Fig.10 Extreme wave ductility spectra for variation of viscous damping ratio ($H_1=15$ m, $T_z=15.8$ s)

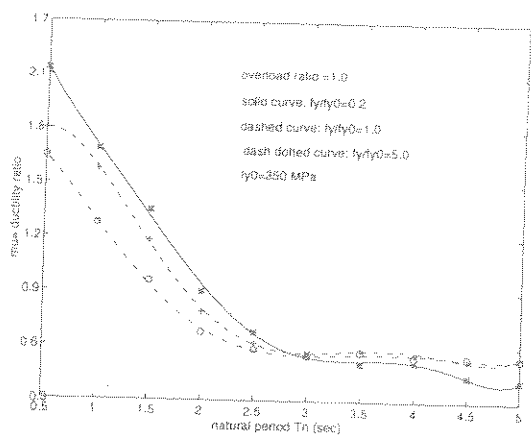


Fig.13 Seismic ductility spectra for variation of yield strength f_y of the structure (El Centro, 1940)

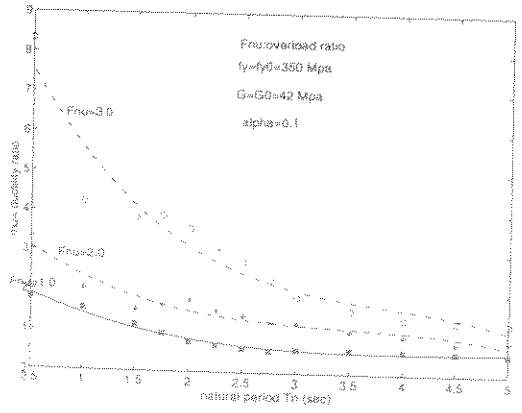


Fig.11 Ductility spectra for a severe earthquake (El Centro, 1940)

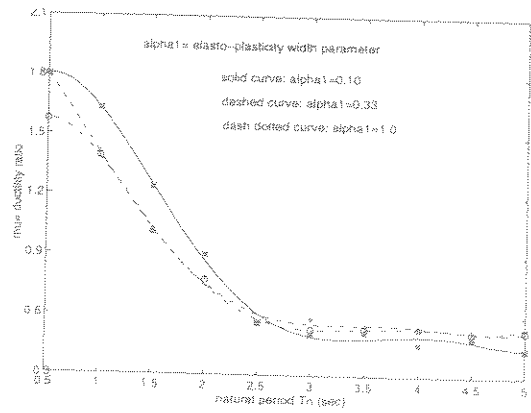


Fig.14 Seismic ductility spectra for variation of hysteretic loop's width parameter (El Centro, 1940)

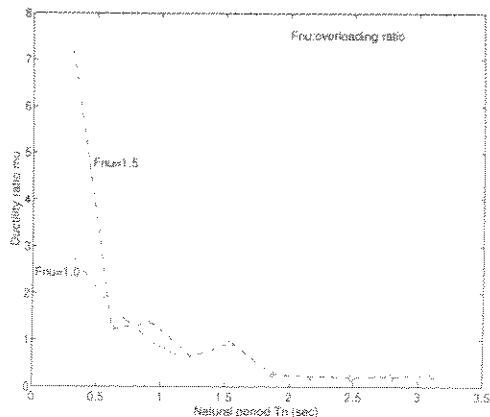


Fig.15 Seismic ductility spectra (Santa Cruz, 1989)

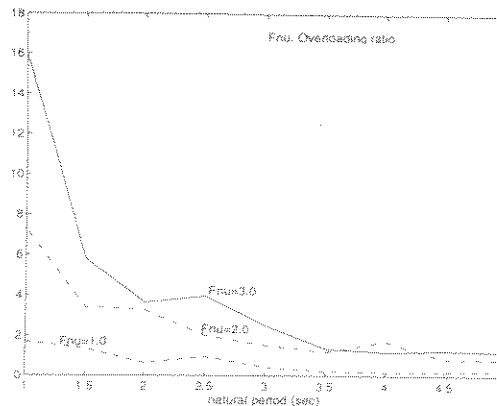


Fig.18 Seismic ductility spectra (Taft, 1952)

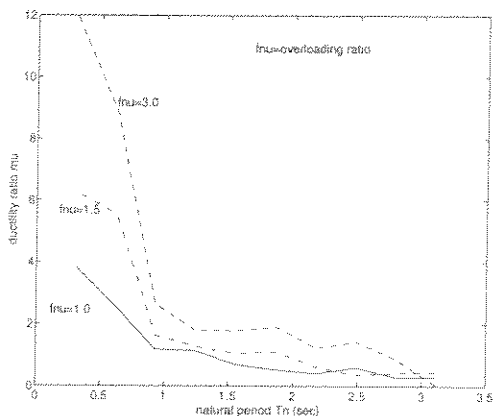


Fig.16 Seismic ductility spectra (Woodfords, 1995)

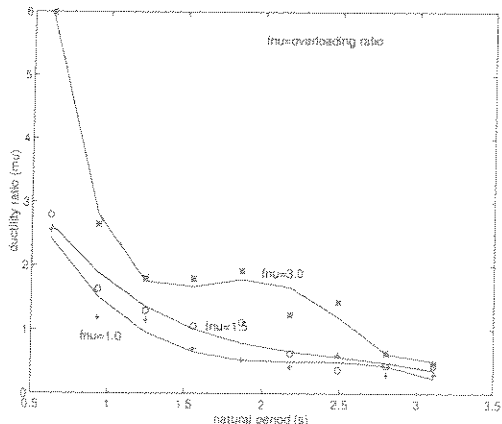


Fig.17 Seismic ductility spectra (Parkfield, 1994)

5. CONCLUSIONS

In the current study, it is shown that a ductility measure can be used to study global dynamic behaviour of the offshore jacket platforms by means of simplified equivalent models.

The study showed that the potential damage to the offshore jacket platforms under extreme waves and earthquakes might vary significantly depending on their structural and soil characteristics. The ductility variations are much higher for shorter periods and so the demands. The effective natural period concept might be a useful tool to describe some of observed discrepancies.

Damping has a significant effect on reducing the ductility demand and removing the local peaks and valleys in the ductility spectra.

The seismic ductility demand of the equivalent systems are less than the ductility demands for the extreme sea waves with the same overload ratio due to much smaller duration of seismic waves compared with the that of extreme sea waves.

The ductility demand for different earthquakes or wave loading histories may vary for the same overloading ratio.

6 REFERENCES

- API RP2A 1994 ,20th Edition ,Draft Section 17.0, American Petroleum Institute, Dallas.
- Bea ,R.G. and Young ,C.N. 1993. Loading and Capacity Effects on Platform Performance in Extreme Storm Waves and Earthquakes, *Proc. of Offshore Tech. Conf.*, OTC No 7140,

- Houston, Texas.
- Bessason, B. 1992. Seismically Isolated Bridges, Ph.D Thesis, Dept. of Marine Struct., NTH, Trondheim.
- Caltech Seismic Lab. 1995. Seismic data and correction procedures, California.
- Det norske Veritas 1992. Wajac Computer Program for Generating Wave Forces on the Jacket, Høvik
- Eberg, E., Hellan, Ø. and Amdahl, J. 1993. Non-linear Re-Assessment of Jacket Structures Under Extreme Storm Cyclic Loading, Part III, *Proc. of the 12th Int. Conf. on Offshore Mech. and Arctic Eng.*, OMAE, New York: ASME, Vol.1, pp. 517-528.
- Emami Azadi, M.R. and Moan, T. and Amdahl, J. 1995. Dynamic Effects on The Performance of Steel Offshore Jacket Platforms Under Extreme Waves, *Proc. of 1st European Conf. on Steel Struct.*, Rotterdam: Balkema, pp. 411-420.
- Fajfar, P., Vidic, T. and Fischinger, M. 1993. Influence of Damping Model on Seismic Response of Nonlinear SDOF Systems, *Proc. of 2nd European Conf. on Struct. Dynamics*, Rotterdam, Balkema, Volume 1, pp. 77-84.
- Janbu, N. 1985 Soils In Offshore Engineering, *25th Rankine Lecture, Geotechnique*, Vol 35, No3
- Nogami, T. and Konagai, K. 1989. Time Domain Flexural Response of Dynamically Loaded Single Piles, *J. Eng. Mech.*, ASCE, Vol.114 No.9, pp. 1512-1524.
- Meek, J.W. and Wolf, J.P. 1993. Approximate Green's Function for Surface Foundations, *J. of Geotech. Eng.*, ASCE, Vol.119, pp.1499-1514
- Morison, D.G. 1992. Dynamic Design of Deep Water Bottom Founded Towers, *Proc. of Civil Eng. in the Oceans V, R. T.*, ASCE, Texas.
- Schmucher, D.G and Cornell, C.A. 1994. Dynamic Behaviour of Semi-Ductile Jackets under Extreme Wave and Wave-In-Deck Forces, Civil Eng. Dept., Stanford Univ.
- Stewart, G., Moan, T. and Eide, O. 1993. Non-linear Re-Assessment of Jacket Structures Under Extreme Storm Cyclic Loading, Part I: Philosophy and Acceptance Criteria. *Proc. of 12th Int. Conf. on Offshore Mech. and Arctic Eng.*, OMAE, New York: ASME, Vol.1, pp.503-516.
- Stewart, G. 1993. Non-linear Structural dynamics by The Pseudo-Force Influence Method: Part II Application to Offshore Platform Collapse, *Proc. of the 2nd Int. Offshore and Polar Eng. Conf.*, San Francisco, pp. 264-271
- Svanø, G., Madshus, C. and Langø, H. 1993. On the Validity of Nonlinear Spring Idealization of Soil Structure Interaction, *Proc. of 2nd European Conf. on Struct. Dynamics*, Rotterdam: Balkema, Vol.1, pp. 403-410
- Wolf, J.P. 1994. *Foundation Vibration Analysis Using Simple Physical Models*, Engelwood Cliffs: PTR, Prentice-Hall.
- Wolf, J.P., 1992 Simple Physical Models for Foundation Vibration Towards a Strength of Materials Approach, *The 10th World Conf. on Earthquake Eng.*, Madrid.
- Wolf, J.P., Meek, J.W. and Song, Ch. 1992. Cone Models for Pile Foundations, *Geotech. Special Publication*, ASCE, No. 34, pp. 94-113.

7 APPENDIX

The relationship between the tangent shear modulus of soil G^T and its shear strain γ may be derived from Svanø's cyclic shear mobilization model (Svanø et al, 1993) as follows:

$$g = g_{\max} \left(\frac{1}{1+h \cdot s} - \lambda \cdot s \right) \quad (A1)$$

where g is the normalised shear modulus g as:

$$g = \frac{G_s}{\sigma'_m + a_d} \quad (A2)$$

where G_s is the shear modulus of soil, σ'_m the mean effective stress and a_d the dynamic attraction of soil. In Eq.A1 g_{\max} is the maximum normalised shear modulus of soil which then is easily followed from Eq.A2 by only replacing G_s with G_{\max} . h, λ are curve fitting parameters obtained empirically and s is the normalised shear stress at the pile-soil interface which can be written as:

$$s = \frac{\tau}{\sigma'_m + a_d} \quad (A3)$$

where τ is the cyclic shear stress at the pile-soil interface and the other parameters are defined above. The relationship between τ and γ near the pile shaft may be written as:

$$\tau = G_s \cdot \gamma \quad (A4)$$

The tangent shear modulus of soil can be found as:

$$G^T = \frac{\partial \tau}{\partial \gamma} \quad (A5)$$

By combining Eqs.A1 to A5, yields :

$$G^T = \frac{g_{\max} (\sigma'_m + a_d) (1 - \lambda s - \lambda h s^2)}{(1 + 2hs)} \quad (A6)$$

By combining Eqs.A1 to A5, the following relationship between s and γ is obtained :

$$s = \frac{-1 + \sqrt{1 + \frac{4bh}{c}}}{2h} \quad (A7)$$

where $b = g_{\max} \gamma$ and $c = (b\lambda + 1)$. By combining Eqs.A6 and A7, G^T is obtained as :

$$G^T = \frac{G_s (1 - \lambda \frac{b}{c})}{\sqrt{1 + 4 \frac{bh}{c}}} \quad (A8)$$

where $G_s = g_{\max} (\sigma'_m + a_d)$ and b and c are given above. By inserting b and c and G_s into Eq.A8, the following expression for the tangent of the pile-soil's skeleton curve emerges :

$$G^T = \frac{g_{\max} (\sigma'_m + a_d) (1 - \frac{\lambda \gamma g_{\max}}{\lambda \gamma g_{\max} + 1})}{\sqrt{1 + 4 \frac{h \gamma g_{\max}}{\lambda \gamma g_{\max} + 1}}} \quad (A9)$$

From Eq.A9, for $\gamma=0$, the initial shear modulus will be equal to G_s given in Eq.A2, while for $\gamma \rightarrow \infty$ the ultimate tangent shear modulus of soil will approach zero.

APPENDIX

F

MOAN, T., HELLAN, Ø. AND EMAMI AZADI, M.R.: "NON-LINEAR DYNAMIC VERSUS STATIC ANALYSIS OF JACKET SYSTEMS FOR ULTIMATE LIMITS STATE CHECK" PROC. ADVANCES IN MARINE STRUCTURES (DERA), DUNFERMLINE, SCOTLAND, 1997.

- o0o -

1. The first part of the document discusses the importance of maintaining accurate records of all transactions and activities. It emphasizes the need for transparency and accountability in financial reporting.

Non-linear Dynamic versus Static Analysis of Jacket Systems for Ultimate Limit State Check

T.Moan
Dept. of Marine Structures
NTNU N 7034 Trondheim
Norway

Ø .Hellan
Division of Structural Engineering
SINTEF N 7034 Trondheim
Norway

M.R. Emami Azadi
Dept. of Marine Structures
NTNU N 7034 Trondheim
Norway

ABSTRACT

This work deals with a comparison between the traditional (static) pushover method and a non-linear dynamic approach as applied for integrity assessment of the ultimate limit state check of the jacket systems.

A brief account of structural, foundation, load and system modelling is presented emphasizing their combined effects with the analysis methods on the assessment of the ultimate collapse behaviour of the platform.

The concept of dynamic overloading ratio relative to static capacity is used, and its relation to the ductility of the jacket-pile-soil interaction under extreme environmental loading is examined.

The influence of foundation failure on the ultimate dynamic resistance of the platform is investigated through different pile-soil models.

The impact of alternative load modelling on the dynamic response of the platform under extreme wave condition is investigated.

The results of this study are compared with those of previous studies based on simplified as well as MDOF jacket-pile-soil models.

Key words: ultimate strength, system, static, dynamic, jacket

INTRODUCTION

Ultimate limit state checks of structures have traditionally been carried out by linear global analyses to calculate member forces and only include inelastic and second order effects in the determination of the ultimate capacity of the individual components. The strength of materials formulations used in codes for component limit states have been extensively validated against test results. This methodology hence, focuses on the first failure of a structural

component and not the overall collapse of the structure, which obviously is of main concern in view of the failure consequences. The advent of computer technology and the finite element method have made it possible to develop analysis tools that include second order geometrical and plasticity effects and to account for possible re-distribution of the forces and subsequent component failures until system's collapse.

Initially such methods were developed for calculating the residual strength of systems with damage (progressive limit state checks of NPD). More recently, such methods are also applied for re-assessment of aging structures to determine the consequences of fatigue induced fracture of members in connection with inspection planning.

The purpose of this paper is to present a design format applicable for ULS system checks as well as briefly the recent theoretical developments and their validations. Since the main efforts so far have been devoted to ultimate strength under monotonically increasing loading (pushover analysis), the focus herein will be on extension to dynamic behaviour, associated with system failure.

DESIGN FORMAT

The ULS check for components may be written as (ENV,ISO):

$$R(f_{di}, a_{di}, \dots) \geq S(\sum Q_{di}) \quad (1)$$

where f_{di} and a_{di} and Q_{di} are the design values of material (strength) parameters, geometrical parameters and load (dead, permanent, functional and environmental loads), respectively, which are expressed as:

$$\begin{aligned} f_{di} &= \frac{f_{ci}}{\gamma_{mi}} \\ a_{di} &= a_i \pm \Delta a_i \\ Q_i &= \gamma_{Qi} \cdot Q_{ci} \end{aligned} \quad (2)$$

in which characteristic values are indicated by a subindex c. γ_{mi} and γ_{Qi} are material and resistance factors and Δa_i geometrical margins.

It is noted that both the modulus of elasticity and yield strength are material parameters for compression members. γ_{mi} is typically applied on the resulting ultimate stress.

To suit the format of nonlinear pushover analysis, it is convenient to refer R and S to a global load effect like base shear. The notation $S(\sum Q_{di})$ may then be simplified by omitting the S. Different material factors γ_{mi} may then be used for members, joints and piles. Some codes specify γ_{mi} 's which depend upon the member slenderness. Hence,

$$\begin{aligned} &R_{ult}(\{\frac{f_{ci}}{\gamma_{mi}}, a_{di}\}_M, \{\frac{f_{ci}}{\gamma_{mi}}, a_{di}\}_J, \{\frac{f_{ci}}{\gamma_{mi}}, a_{di}\}_{P-S}) \\ &= R_{ult}(\{\frac{f_{ci}}{\gamma_{mi}}, a_{di}\}_M, \{\frac{f_{ci}}{\gamma_{mi}}, a_{di}\}_J, \{\frac{f_{ci}}{\gamma_{mi}}, a_{di}\}_{P-S}) / \gamma_{mREF} \geq \sum_i \gamma_{Qi} \cdot Q_{ci} \end{aligned} \quad (3)$$

in which γ_{mREF} represents the material factor, indices M, J and P-S refer to member, joint and the pile-soil components, respectively.

It is natural to choose the material factor for the most critical type of component as reference factor, γ_{mREF} . Material factors γ_{mi} should be introduced for yield stress. To have an appropriate material factor for slender structures a similar γ_{mi} needs to be applied for the

modulus of elasticity which affects the buckling stress even if this factor is excessive for linear elastic behaviour.

In the non-linear structural analysis, dead, permanent and live loads are incremented (accumulated) up to their respective load $\gamma_{mREF}\gamma_{Qi}Q_i$. Finally, environmental loads are incremented until collapse. To comply with the safety requirements of the selected code, the system strength R_{ult} should exceed the factored environmental load $\gamma_{mREF}\cdot\gamma_{Qj}Q_j$.

THEORETICAL BACKGROUND

General

Significant efforts have been devoted to develop methods for nonlinear analysis of fixed offshore structures. Methods for static analysis have been established by Ueda et al, (1974), Marshall, (1977), Rashed, (1980), Moan et al, (1985), S et al, (1994) and Crisfield, (1991).

A brief review of the dynamic, structural, pile-soil and system modelling is presented in the following subsections.

Dynamic model

The main features of the dynamic model is structural mass and a non-linear (tangent) stiffness system, a proportional structural damping, an (inherent) non-linear hysteretic damping of soil and an equivalent viscous damping accounting for other sources of damping.

The system's dynamic equilibrium may be expressed as follows:

$$F_i(t) + F_r(t) + F_d(t) = F_e(t) \quad (4)$$

where $F_i(t)$ is the vector of inertial resistance of the system, $F_r(t)$ is the vector of structural and foundation's force restoring contribution, $F_d(t)$ is the vector of damping forces in the system, $F_e(t)$ is the vector of excitation forces (e.g. wave and current loading)

It is evident from eqn.4 that the ultimate dynamic capacity of a system can be greater than its maximum static resistance due to the contribution of the inertial $F_i(t)$ and the damping forces $F_d(t)$. A dynamic overload ratio r_ν can be defined as follows:

$$r_\nu = F_{e,max}/F_{r,max} \quad (5)$$

in which $F_{e,max}$ is the maximum dynamic excitation force and $F_{r,max}$ is the ultimate restoring force (or static capacity) of the system which may be determined from a pushover analysis. The static strength of the system is conveniently expressed by the ratio, RSU as $F_{r,max}/F_{100}$, in which F_{100} corresponds to the 100-year wave load. Similarly the dynamic ultimate strength factor may be defined as: $F_{e,max}/F_{100}$.

The associated ductility ratio μ of a non-linear system may be defined as follows:

$$\mu = u_{max}/u_{fy} \quad (6)$$

in which u_{max} is the maximum (sustainable) displacement of the system and u_{fy} is the displacement corresponding to the first global yield of the system (Fig.1b)

From the non-linear dynamic point of view, a system's overload factor would depend on upon two counteracting effects, a beneficial inertia resistance and dynamic amplification.

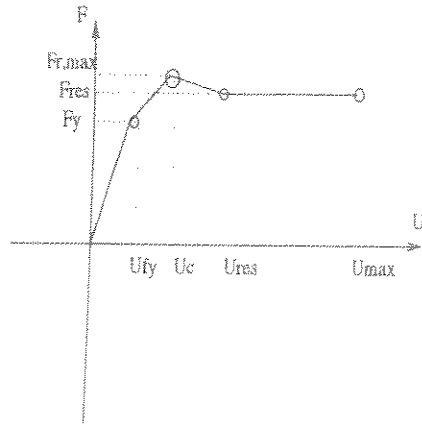


Fig. 1a. An illustration of system's ductility parameter by static load-deformation characteristics

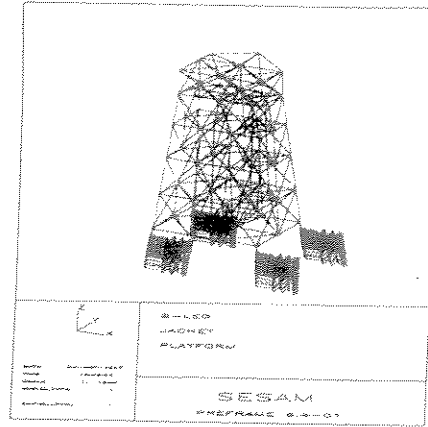


Fig. 1b. An 8-leg jacket North-sea platform

For a non-degrading elastic-perfectly-plastic system which possesses sufficiently large ductility (i.e $\mu \gg 1.0$) then the system can accelerate to resist the overload factors up to infinity. On the other hand, if the period of the excitation force matches the natural period of the system, the response will be dynamically amplified. amplification in the system's response. For a brittle system, which has $\mu = 1$, the dynamic amplification effect may reduce the overload factor r_v . The effects of post-peak degradation may also be considered to reduce further r_v (see e.g Schmucker et al, 1996, Emami et al, 1997). These issues are discussed further subsequently.

Structural modelling

Models which have been used to idealize structural members include phenomenological models (e.g Marshall,1977) and various finite element type models (Ueda et al, 1976, Moan et al, 1985 and S et al, 1994). While both beam and shell type finite element discretizations of elasto-plastic continua offer the greatest versatility, they also pose severe challenges for the user.

More cost-effective solutions are obtained by using special displacement functions (e.g. Livesley "stability" functions) and concentrating the material non-linearities in yield hinges as applied in the current method (Hellan, 1995). Yield hinge models are developed at different refinement, from yield hinges with zero extension along the elements to models that account for the extension of the yield hinge. Yield hinges may be introduced at the position of maximum stresses, or at specific, pre-defined locations along the member. Elastic-perfectly plastic hinge models treat the cross section as elastic until it reaches full plastification. Other models introduce yield hinges at first fibre yield and include a gradual plastification of the cross section, strain hardening and the Bauschinger effect.

The difference between yield hinge formulations have been investigated by Hellan et al, (1994), and show significant differences. Elastic-perfectly plastic models over-predict the column buckling capacity of ideally straight tubulars. For yield-hinge models incorporating first fibre yield, gradual plastification and strain hardening, the buckling capacity depends on the plasticity parameters given to model the transition from elastic to plastic behaviour.

In general, these formulations may be slightly conservative for stocky columns, and slightly un-conservative for slender columns.

For both these formulations, exact fit to any given column curve can be obtained by introducing initial imperfection in the element formulation. This is discussed in more detail in (Hellan et al, 1994).

Several methods are in use to model joint behaviour in non-linear pushover analyses. One method is to model the joint behaviour by a linear (joint flexibility) or non-linear (joints capacity) spring between the brace end and the center of the chord. Spring properties can then be determined from test data, FE analyses or parametric formulae. Alternatively, the springs can be replaced by a beam-column element with the ultimate capacities determined from the capacity equations for the joint. The joint behaviour may be modelled by a plastic potential, with interaction between the axial force, in-plane bending and out-of-plane bending. Formulations have also been published that accounts for brace-to-brace interaction by adding 'beam' elements between the brace ends.

Foundation model

Various models for embedded foundation such as pile-soil have been developed in the past two decades. Most of the existing pile-soil models are empirical or semi-empirical which have been established based on the acquisition of data from a limited number of large diameter pile tests from early 1970's until now. Although these empirical models have provided practical tools for the designer of the offshore pile-soil foundation, they are associated with some uncertainties (see Horsnell et al, 1996 and Nadim et al, 1996).

The model used here is based on Mohr-Coulombian soil behaviour and hence expresses the soil's shear strength in terms of the effective stress components in the soil (see e.g. Janbu et al, 1985, Nordal et al, 1989 and *Svanø* et al, 1993).

In the present study, the pile-soil behaviour is represented by a stack of uncoupled flexible disks. Figure.2a illustrate the concept in a schematic way. The disks in the model are connected via two node (flexible) beam elements of the pile. The initial linear double cone model of Wolf et al, (1994) was combined with this flexible disk model and extended for non-linear dynamic analysis of pile-soil-jacket system (see Emami et al, 1996, 1997).

It is assumed that the pile-soil interaction for each segment of pile-soil takes place within a finite disk surrounding the pile shaft (Emami et al, 1996). The following simplifying assumptions are made about the pile-soil model:

Each disk is considered to carry axial and lateral loading in the form of shear stresses into the infinity within its plane (see Figs.2a and b). Plane strain condition is assumed for each disk (see for e.g. Nogami and Konagai et al, (1989) The stress and strain is assumed to decay exponentially with the radial distance from the pile-soil interface. The soil condition for clay is assumed as undrained which may be applied only for short term loading.

The combined dynamic loading rate and cyclic excess pore-pressure generation effects(see Janbu et al, 1975, Finn et al, 1982) are assumed to counteract and hence their effects may be neglected.

The peak skin friction of soil may be obtained based on effective stress relationships by means of Mohr-Coulomb Criteria. Dilatancy and Contraction behaviour of soils are considered(see Janbu et al, 1985)

Based on these assumptions a tangent stiffness of soil is established(Emami et al, 1996 and 1997) to account for the soil's non-linearities and the load transfer-deformation characteristic

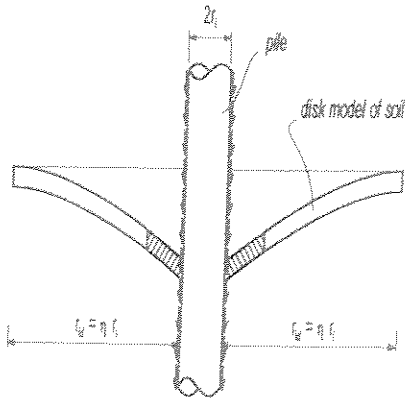


Fig.2a. Disk idealization under axial loading

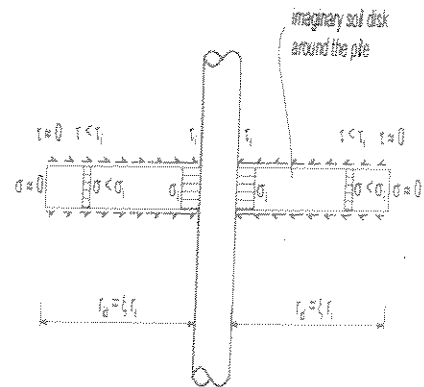


Fig.2b. Disk idealization under lateral loading

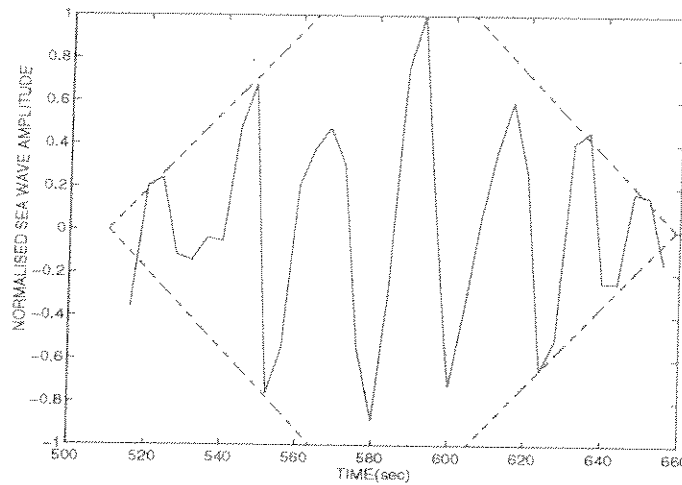


Fig.3.A sample simulated sea state with a fitted envelope

of disk model are calculated. The computed load-deformation curves have been incorporated into USFOS by assigning them to the general one-node non-linear spring elements. Further details and verification of the model are given in Emami, (1997).

Extreme wave loading

The dynamic response of platform is simulated by using a sea load history obtained as follows. Random sea-states are simulated based on the Jonswap energy spectrum with a significant wave height of H_s and the corresponding period T_z for the relevant directions.

The simulation length is taken as 1200sec from which the most severe portion of the wave load history of duration of about 100-150 sec is then selected (see Fig.3). Typically the largest peaks of wave occur only in one or two cycles.

An in-line current has been superimposed on the wave with a velocity profile which has been extended (Wheeler stretching) to the wave surface. The water particle velocities gener-

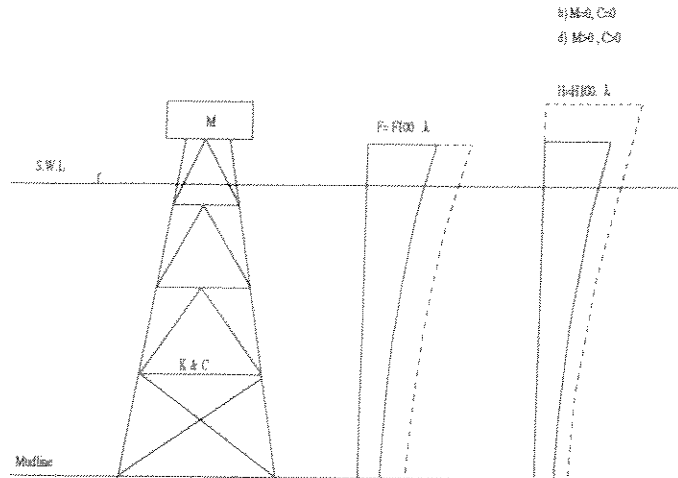


Fig.4. The extreme wave load modelling methods static(pushover) with a) increasing the intensity and constant wave height b) quasi-static approach with scaling the wave height c) dynamic approach with scaling the wave height

ated by waves are computed according to the Stoke's theory, and then added to the current velocities. The resultant particle kinematics are used in the Morrison's equation to calculate the wave forces on each wet member of structure. The relative motion of the fluid with respect to the encountered member is considered. Mass and drag coefficients are considered as 0.77 and 2.0, respectively.

A sequence of extreme waves was re-generated to determine a suitable loading history for the dynamic analysis. The length of the most severe portion of the storm is taken as between 100-150secs (Fig.3). The envelope consists of a linear(build-up) portion of about three wave length(three cycles), a constant part of two wave length(cycles) and a decreasing portion of about three wave lengths. These extreme wave considerations are consistent with the extreme wave theory of Tromans et al, (1991) and the storm model of Stewart et al, (1993). The determination of ultimate strength under dynamic wave loads involves repeated calculation of the dynamic response to identify the load level that causes the system collapse.

Three different load models are considered here to calculate the ultimate capacity of the jacket system:

- 1) The load vector corresponding to a return period of 100 years (design load) used as a reference load and incremented proportionally until ultimate collapse of the system(fixed load vector height implies fixed sea elevation) see Fig.4a
- 2) The wave height is increased successively until ultimate static collapse of the platform (varying load vector height or wet zone on the structure) without inertial effects (see Fig.4b)
- 3) Cyclic approach based on incrementing the wave height as (2)
- 4) Cyclic approach as (3) with dynamic reaction forces included

The first approach corresponds to the conventional way of performing pushover analysis. By assuming that the sea surface elevation is constant when the wave load is incremented, implies that no sea load is considered to act on the upper most part of the structure. This may result in underestimation of the total wave force on the structure. The impact of this simplification may be particularly pronounced for the jacket structures with a small air gap

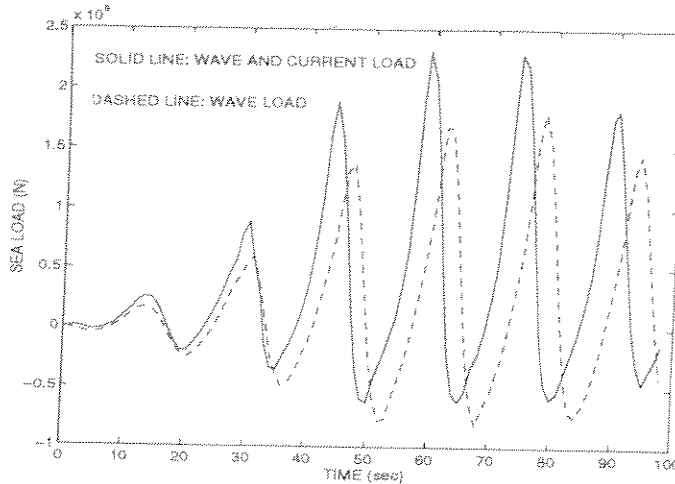


Fig.5. Comparing the sea load histories (with and without the in-line current)

(see e.g. Bea et al, 1993 and Emami, 1997).

In the second approach, the wave height is incremented but no cyclic action of the wave is considered. The wet zone and the distribution of the induced load on each element in this zone varies with each increment. Hence, the variation of the total base shear of the structure is non-proportional in this approach. Apparently this method offers a more realistic description of the sea load on the structure compared to the first approach.

The third method captures the cyclic action of the wave loading (reverse of the loading and possible damage accumulation or cyclic degradation). The fourth method considers the effects of varying sea surface elevation as (ii), cyclic action of storm as (iii) and the dynamic resistance of the structure. Hence, the latter approach can capture the dynamic overload effects as described above and will be discussed further subsequently. Fig.5 shows a typical extreme sea load history indicating the effect of the in-line current on the asymmetry of the loading.

Solution method

The dynamic equation of motion eqn.4 is solved in the time-domain by using an integration technique such as predictor-corrector based on α HHT method (Hilber et al, 1976). The method is based on the Newmark's beta method, the difference is in introducing some extra terms in the effective stiffness and damping parameters. A bi-section method is used to scale back the stress state to the yield surface (Eberg and Amdahl, 1992).

CASE STUDY

System model

The finite element model of the jacket structure used in the case study is shown in Fig.1. The structure consists of two longitudinal and four transversal frames. Longitudinal frames have K-braces in the upper bays and X-braces in the first bay's corner. The transversal frames

Table 1: The end-on response of the jacket-pile-soil system (plugged)

	static(pushover)		cyclic	
	load incr.	wave height incr.	quasi-static	dynamic
First member failure load	1.99	1.94	1.96	2.38
Ultimate collapse load	3.15	2.89	2.55	2.86
Residual strength	2.92	2.56	-	-

have K-braces in all bays. The supporting deck has been modelled as a truss and the top deck facilities have been modelled by a pyramid frame.

The foundation of the jacket system in this study is modelled as equivalent single piles penetrating to a depth 28m below the mud-line. Due to the relatively short lengths of the designed skirt piles in this case, they have been grouted at the bottom where the piles have penetrated into a sand layer. Hence, the pile-tip is considered to be plugged to ensure end-bearing. Since the lateral resistance may be mobilized at the upper part of the soil, the designed pile condition is not modified and will be used in the first part of this study. The pile-soil interaction is modelled as non-linear disks as described above.

Static behaviour

The ductility ratio, μ , the ultimate (static) resistance factor, RSU of the platform is initially determined through pushover analyses in the main longitudinal (end-on) and the transversal frame (broad-side) directions of the platform.

The static response of the system under end-on loading is shown in Fig.6 for linear, non-linear plugged and un-plugged systems. The near collapse behaviour of the linear support system is seen to exhibit a rapid degradation while for the non-linear pile-soil systems, larger residual strength ratios have been obtained associated with higher ductility values. The pre-collapse response of the plugged pile-soil and the linear supported jacket systems are stiffer compared to the un-plugged system. The softening of the response for the latter case may be attributed to the rapid yield occurring in the soil along the pile shaft with a relatively smaller contribution from the tip resistance. The proximity of the pre-collapse response of the linear and the plugged case is due to far larger end-bearing contribution which is an order of magnitude higher than that of total skin friction along the pile.

The global load factors corresponding to the first member failure and the ultimate capacity of the system are given in Table 1. It is seen that the ultimate strength factor of 3.19 has been obtained in conventional static pushover analysis is about 20 percent larger than that for the cyclic. This discrepancy is partly due to the effect of increased wet zone over the jacket which is not accounted for in the conventional pushover method. Secondly, it might be due to the accumulated plastic degradation as shown in Fig.8. The degradation effects may be physical as well as numerical (Hellan et al, 1991 and Eberg et al, 1993) due to small drift off from the actual yield surface during each cycle. It is also seen in Fig.6e that by including the wind induced load the obtained ultimate capacity from static pushover method is closer to the corresponding value obtained from quasi-static method.

The following simple relationship is obtained between the base shear and the corresponding wave height and the period based on a number of deterministic wave simulations by the

WAJAC program(DNV, 1992):

$$BS_w = a_1 \left(\frac{T}{T_{100}} \right)^{b_1} H^{a_2} + a_3 \left(\frac{T}{T_{100}} \right)^{b_2} (H - H_d)^{a_4} \quad (7)$$

in which BS_w = the total base shear in MN, H = the scaled wave height in m, H_d = the deck height w.r.t the S.W.L in m, T = the period associated with a scaled wave height H in secs, T_{100} = the period corresponding to the 100 year wave height in m, a_i and b_i are the coefficients of the curve fitting (regression coefficients).

For the studied platform, the exponent term a_2 was obtained to be 1.71 for the end-on loading and about 1.65 for the broad-side loading. The exponent values characterize a mixed drag-inertia regime for the jacket platform. The mean value of the exponent coefficient b_1 is obtained to be 0.6 for end-on loading and about 0.39 for broad-side loading. The regression coefficient a_1 obtained as 0.38 and 0.49 for West-bound(end-on) and North-bound (broad-side) waves, respectively. The second term on R-H-S of eq.7 was omitted due to the presence of large air gap.

Comparison of wave height incrementation and wave load incrementation methods

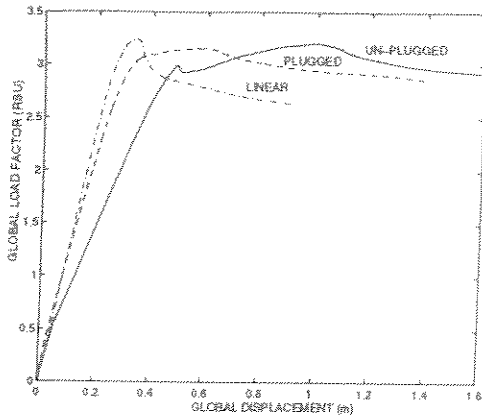
In a conventional static pushover approach, the environmental loadings such as induced by wave and current are imposed incrementally on the structure until the ultimate collapse occurs. This method does not take into account the variation of the sea surface elevation during each increment of loading.

The variation of the sea surface elevation changes the wet zone on the platform and hence the resultant total base shear and the overturning moment. Additional forces may be imparted on the structure, if the extreme wave's crest reaches the cellar or main deck areas. With respect to these effects, a new pushover approach is established based on incrementing the wave height. The procedure involves several incrementation of the wave height and if a wave on deck is encountered then the additional deck forces are calculated according to the draft sec.17 of API 1994. Figs.6c and 6d compare the results of new and the conventional static pushover analyses for end-on and broad-side loading of the studied platform. As seen, the near collapse response of the platform according to the new method is softer to some extent. The maximum discrepancy occurring near the ultimate collapse is about 9 percent. This is mainly due to the additional forces imparted on the upper part of the structure including part of the cellar deck (about 1.1 m at collapse) and changes in the distribution of the forces over the structural elements. It is seen that the structural behaviour of the jacket platform concerning the ductility has not been changed in a significant manner.

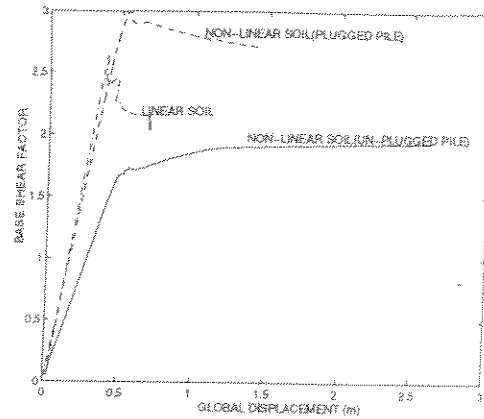
Dynamic overstrength factor

Accounting for the dynamic resistance forces of the structure has resulted in an overload factor of $RDU = 2.86$ which is about 12 percent higher than the cyclic (quasi-static) approach. This overload factor is due to activation of the inertial resistance of the system allowed by the available ductility of $\mu = 4.06$ beyond the static collapse. The reserve strength beyond the first component failure of system obtained from all three methods are substantial ranging from 20 to 60 percent.

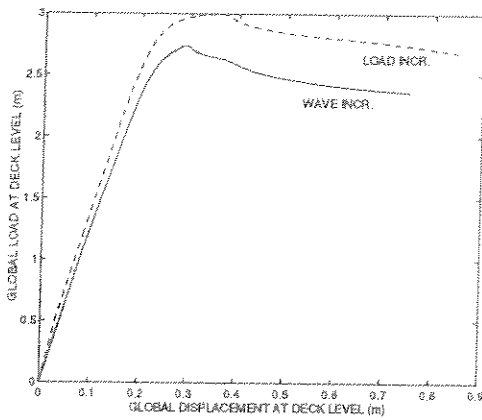
The ultimate dynamic collapse value obtained here is therefore is closer to that of the static pushover method. This means in a more realistic dynamic analysis approach, the



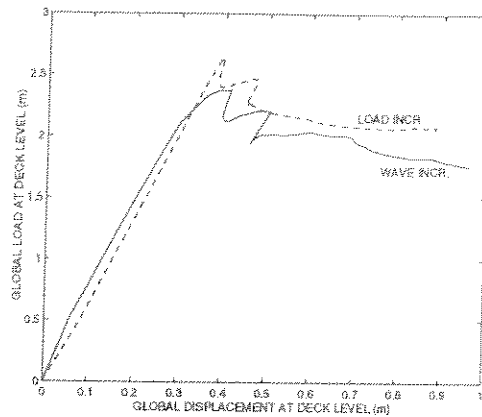
(a)



(b)



(c)



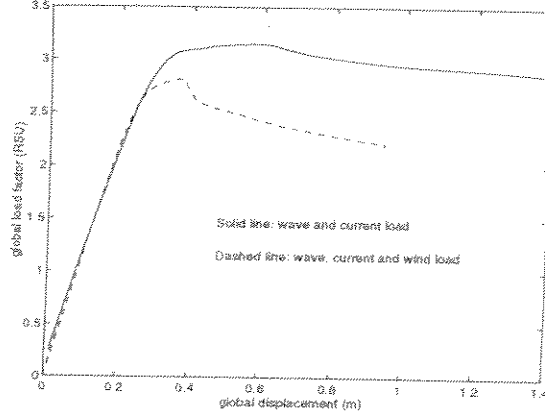
(d)

degrading effect of the increased wet zone on the structure has been counteracted by the increasing dynamic overload ratio over unity due to sufficient ductility available in the system. However, for more slender structures, for which dynamic amplification effects could be more important, applying a dynamic analysis approach without even considering variation of the sea surface (wet zone) would result in lower ultimate capacity compared to that of static pushover method (see e.g. Amdahl et al, 1994)

Simplified dynamic models

These results may be compared with the predicted values of ultimate dynamic capacity of the system (or the overload factor) based on the previous studies of the equivalent simplified system such as SDOF, 3DOF and one storey plane frame analyses (Bea et al, 1993, Stewart et al, 1993, Schmucker et al, 1994, Emami et al, 1995 and Schmucker et al, 1996).

Table 2 compares the overload ratios obtained from various simplified predictive models with those obtained from MDOF analysis of the platform. The overload and ductility ratios obtained from the quasi-static analysis are 1.12 and 4.06, respectively. This ductility ratio may be called the apparent ductility ratio which is measured against the first global yield



(e)

Fig.6. The static response of the jacket with non-linear pile-soil vs linear support system under a) end-on loading b) broad-side loading c) wave height incrementation method vs. conventional wave load incrementation method for end-on loading d) modified vs. conventional for broad-side loading e) wind load effects e.g. under end-on loading

rather than first member yield in the load-deflection response as shown in Fig.6. The observed dynamic overstrength of about 12 percent in this case is due to the sufficient ductility which has allowed the inertial resistance of the platform to be activated. Since the post-peak degradation of the static resistance as shown in Fig.6a is not severe for the end-on loading of the platform, hence, the effective ductility ratio will be closer to the apparent ductility ratio. But for a brittle case such as shown in Fig.6b using an apparent ductility ratio μ in a ND-EPP based relationship obviously will lead to overestimation of r_v . An effective ductility ratio may be introduced in such cases (see Emami, 1997)

The following simple relationship between overload and ductility ratios has been obtained from analyses of SDOF systems by Emami et al, (1995):

$$r_v = \sqrt{\alpha_{mu}\mu} \quad (8)$$

where $\alpha_{mu} = 1$ for linear and 0.5 for the non-linear foundation system. Substituting for the μ in eqn.8 will result in a ratio of about 1.42 vs. obtained 1.12. However, the given relationship has not accounted for the changes in the sea surface elevation.

Based on eqn.4 a simple relationship is obtained by Emami, (1997) as follows:

$$r_v = \alpha_{res} f_{ND,EPP} \left(\frac{\mu}{DAF} \right) \quad (9)$$

in which $\alpha_{res} = \frac{F_{r,res}}{F_{r,max}}$, indices res and max refer to the residual and maximum values of the restoring force and $f_{ND,EPP}$ is an overload function obtained for ND-EPP system such as eqn.8.

The dynamic overload ratio has also been suggested by Stewart et al, (1993) to be in the range of 1.1 to 1.2 for ductility ratios of 1.5 to 5.0. The obtained overload ratio 1.12 from the MDOF analysis for the varying sea surface elevation is within the suggested range.

It is seen that the approach of Schmucker et al, (1996) based on linear SDOF systems has underestimated r_v . This is because the natural period of the system T is assumed to be

Table 2: The predicted versus computed overload ratios of jacket-plugged pile-soil system under end-on and broad-side loadings

Predictive method	Overload ratio (end-on)	Overload ratio (broad-side)
MDOF analysis	1.12	0.96
Bea et al, 1993	2.67	1.13
Stewart et al, 1993	1.10-1.20	1.00
Schmucker et al, 1996	1.04	0.91
eqn.8	1.42	1.07
eqn.9	1.27	0.97

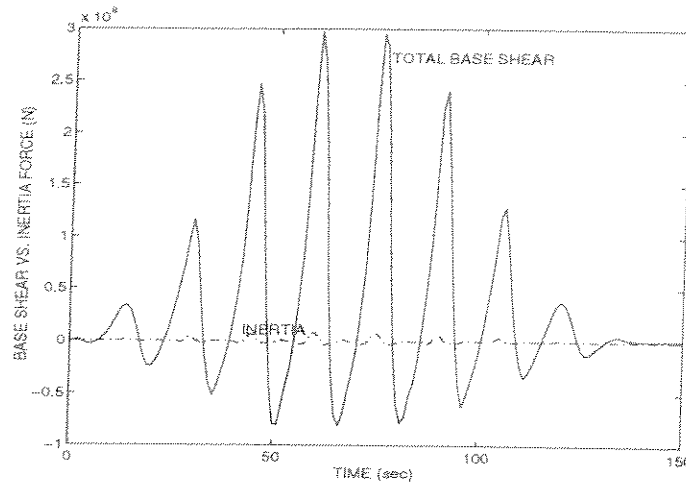


Fig.7. The base shear and inertial resistance histories of the (plugged) jacket-pile-soil system (end-on loading)

constant (linear dynamics) in the latter approach while in a non-linear system the effective natural period of the system varies as a function of its tangent stiffness K^T . (see Emami, 1997)

Due to the large computational efforts required in global non-linear dynamic collapse analyses, simplified methods to estimate the overload factor are very useful. The results given in Table 2 show that fairly accurate initial estimates have been obtained based on the (overall)simplified relationships. However, further improvement of the accuracy is needed to better reflect the nature of r_v . Such improvements may include the consideration of sea surface variation, stiffness degradation etc.

The base shear and displacement response histories of the platform obtained by dynamic collapse analysis under end-on loading are given in Figs.7 to 9a.

As seen from the displacement response history in Fig.8, the ultimate collapse of the platform occurs at time about $t = 76.5$ secs, which corresponds to the largest peak of the wave loading (Fig.7). The vertical and horizontal response histories at the pile head is also plotted in Fig.8 which do not indicate any pile-soil pull-out or lateral collapse. As seen, a permanent plastic deformation has developed incrementally prior to the ultimate collapse which is also shown at the beginning of the dynamic response corresponding to the ultimate

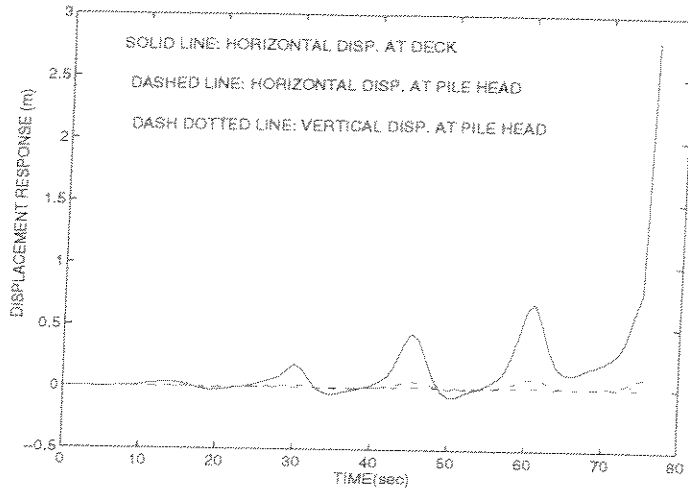


Fig.8. The dynamic displacement response of the (plugged) jacket-pile-soil system under end-on (West-bound) loading at deck and mudline

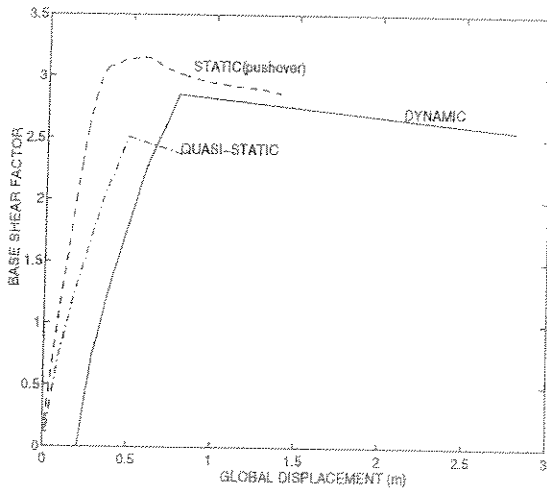


Fig.9a. The global load-displacement response of the (plugged) jacket-pile-soil system static vs. cyclic (quasi-static) and dynamic under end-on loading

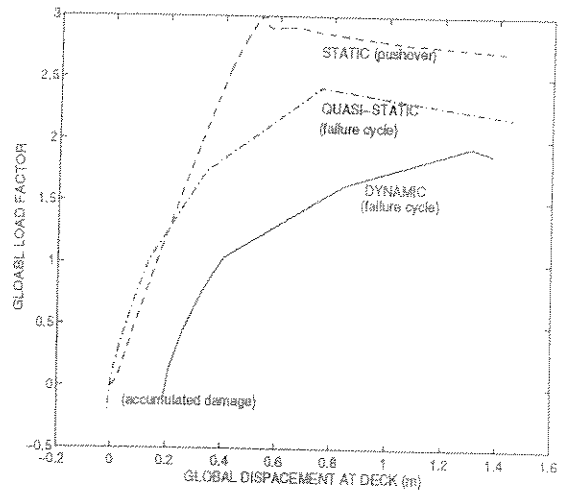


Fig.9b. The global load-displacement response of the (plugged) jacket-pile-soil system static vs. cyclic (quasi-static) and dynamic under broad-side loading

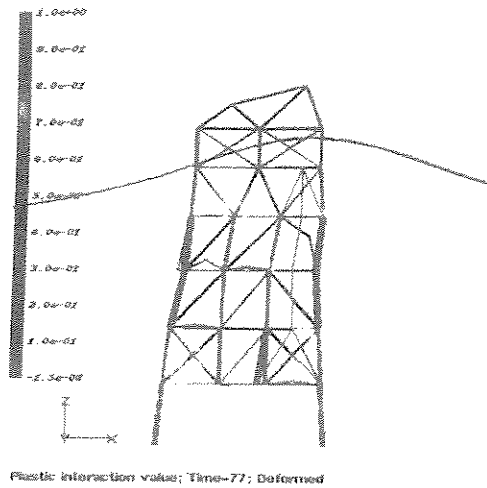


Fig.10a. The deformed and plastic interaction model of platform under end-on loading for plugged pile-soil system

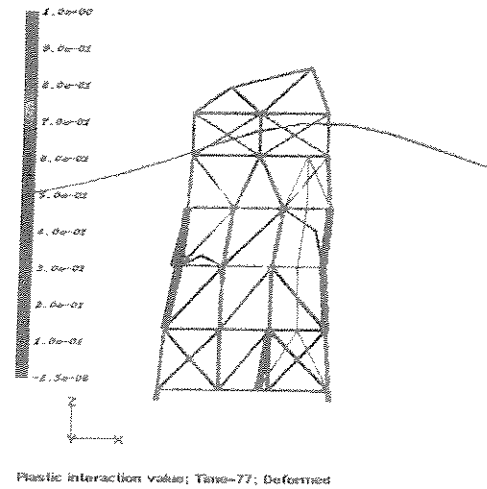


Fig.10b. The deformed and plastic interaction model of platform under end-on loading for linear pile-soil system

failure cycle (solid line in Fig.9a).

The corresponding displacement response history of the platform at the deck level is asymmetric with larger displacements occurring in the positive global X-axis (wave direction) which may be partly due to the loading asymmetry and partly due to the mentioned permanent (plastic) deformations developed in the jacket.

Fig.9a compares the static base-shear -deflection response of the platform (plugged pile) with those from the failure cycles corresponding to cyclic and dynamic analyses. It is shown that the latter curves have lower peaks due to the wave load modelling effects. And the dynamic response is somewhat stiffer than those of static and cyclic (quasi-static) ones mainly due to the inertial effects.

Fig.10a shows the collapse mode of the plugged pile-soil-jacket system, indicating that the most of the plastically utilised members are located in this area. Also the horizontal members in the bottom bay connected to the main legs at the corners have buckled. A plastic hinge formation is seen in the left pile in Fig.10a at about upper one third of pile depth. This signifies that a lateral plastic interaction has taken place between the soil-pile at this point. This may be initiated mainly by the base shear transferred to the pile-soil system at the interface level. No axial failure mode (such as pull-out or plunge) is observed for the end-on loading of platform.

Fig.10b shows the collapse mode of the jacket with a linear support system. The most plastically utilized (failed) members are situated at the second and the third bays from bottom, and at the bottom bay all four horizontal bracing members have failed in compression.

Figs.10a and b, show different structural failure modes depending upon the applied foundation model, namely linear and non-linear plugged.

As shown in Fig.6b, the response for broad-side loading of the jacket with foundation modelled as linear springs at the sea-bed is quite brittle and the maximum RSU factor is about 2.64 compared to the 2.99 factor obtained with a plugged non-linear pile-soil model.

Table 3: The broad-side response of the jacket-pile-soil system (plugged)

	Static		Cyclic	
	Load Incr.	Wave Incr.	quasi-static	dynamic
First member failure load	2.049	1.79	1.889	1.756
ultimate collapse load	2.994	2.23	2.012	2.094
residual strength	2.711	2.04	2.42	2.32

Table 4: The ultimate capacity and overload ratio of Jacket-pile-soil system (plugged vs. un-plugged)

loading direction	tip condition	RSU	RQS* ^a	RDU	r_v
End-on	plugged	3.15	2.55	2.86	1.12
End-on	un-plugged	2.99	2.29	2.42	1.06
Broad-side	plugged	2.99	2.42	2.32	0.96
Broad-side	un-plugged	1.94	1.44	1.58	1.10

*RQS is referred above to the ultimate collapse factor obtained from a quasi-static analysis

This is mainly due to the ductility provided by the foundation which has changed the ultimate collapse mode from a brittle to a semi-ductile one which endorses the idea of having a static jacket-pile-soil interaction in this case. The effect of un-plugging on the ultimate collapse behaviour of the platform is even more pronounced, as seen in Fig.6b, the *RSU* factor is then reduced to 1.94. The corresponding initial and near collapse response are much softer than for the linear and non-linear pile-soil models.

Table 3 shows the global load factors corresponding to the first member failure (brace buckling), the ultimate collapse and the residual strength of the jacket -plugged pile-soil system under broad-side loading. The reserve strength of the system beyond its initial member failure is less than that for the end-on loading (Table 1). The ratio of residual to ultimate capacity of the system is lower than that for the end-on loading which indicates a post-peak degrading system under broad-side loading.

Table 4 compares the results of MDOF dynamic analyses of jacket with plugged and un-plugged piles under end-on and broad-side loadings.

It shows that the overload ratio is smaller for the broad-side loading of the plugged jacket-pile-soil system than others. This difference may be due to the more ductile behaviour of the un-plugged pile system compared to the plugged condition in which the failure mostly occurs in the jacket structure. However, for the end-on loading (west-bound wave) a good dynamic reserve strength has been provided due to sufficient ductility.

The ratio between the quasi-static and the static(pushover) capacity ranges from 0.74 to 0.81 which indicate the influence of the load modelling and analysis method. The ratio between the dynamic and the static (pushover) capacities of the system varies between 0.78 to 0.91 which also confirms the latter conclusion. From a safety point of view this issue has an important implication for ULS check of the jacket platform under broad-side loading. It can be seen in Table 4 that for a more realistic wave loading approach the ultimate static capacity of the system is 0.74 of that capacity predicted by a conventional static (pushover)analysis. The corresponding total load factor which is 1.44 is above the design level but less than

the typical minimum safety requirement. However, by taking into account the inertial and damping effects the ultimate capacity *RDU* has increased by about 10 percent. It is worth of notice that for the un-plugged pile model the inner shaft skin friction has also been taken into account according to API RP2A 1994.

It is observed that for an un-plugged pile case the overall collapse mode (overturning) of the platform is governed by the pile-soil failure in tension. The larger discrepancy in the un-plugged case may be attributed to the effect of increased overturning moment by varying the sea surface.

Dynamic behaviour

The predicted overload ratios for broad-side loading of the platform are given in Table 1. The obtained overload ratio from dynamic analysis in this case is about 0.96 which is slightly higher than the value 0.94 obtained previously for a linear spring case. An overload factor slightly lower than unity, indicates that small dynamic amplification effect may be present in the system due to superharmonic effects (Moe and Moan et al, 1984). However physical and numerical degradation effects as mentioned above may have also contributed partly to this reduction. The wave incrementation step size has also effect. For instance, by using a smaller step of 5cm instead of 25cm near the ultimate collapse, the obtained overload factor varied by up to 2 percent.

The apparent (maximum) ductility ratio obtained from the static (pushover) analysis is about 3.81. Due to the post-peak degradation of the re-storing force, an effective ductility ratio of 1.14 corresponding to the quasi-static analysis (dash-dotted curve) in Fig.6b is considered more relevant.

The predictive model (eqn.8), which takes into account DAF, post-peak degradation effects, provides the best match for the overload value in this case. The approach of Schmucker et al, (1996) has also considered DAF effect and given a lower bound prediction of r_v as 0.91.

The other simplified models give ratios greater than unity without accounting for DAF effect. r_v value is found to be equal to unity for $\mu = 1$ representing a brittle behaviour of system.

Though the behaviour of this jacket-pile-soil system is mainly dominated by ductility, nevertheless some linear dynamic amplification (DAF) effects may have been present due to the odd and even multiples of the primary force components computed from the drag term of Morison's equation and surface elevation (Moe and Moan, 1984).

These effects may be more pronounced for a real sea-state or a random sea state with a range of frequency content. In the current simulation, however, the DAF effect may be considered as secondary to the main r_v and μ ones. The predicted values of r_v according to simplified methods are in the range of 0.91-1.13.

CONCLUDING REMARKS

The response of the jacket-pile-soil system near ultimate collapse has been studied by means of static(pushover) and nonlinear dynamic analyses methods.

It is shown that the conventional (static) pushover approach may slightly overestimate the ultimate capacity of the jacket platform compared to an advanced method based on incrementing the wave height. The maximum discrepancy related to these two static pushover methods in terms of the ultimate capacity for the studied platform was found to be about

9 percent. However, for the cyclic(quasi-static) approach generally lower ultimate capacity values were obtained due to possible accumulated plastic damage in both structure and soil, drift off from the yield surface during each cycle and wave incrementation step size(numerical inaccuracies).

The inertial resistance of the structure is shown to be important in providing an additional reserve strength for structures with sufficient ductility.

The foundation model is found to have significant influence on the global collapse mode as well as the ultimate collapse strength of the system. Hence, it is concluded that realistic (nonlinear) pile-soil models should be used in the analysis.

It may be concluded that the effect of ductility can be significant in providing an overload factor of large than unity. Overload factors of 1.12 and 0.96 were obtained for the end-on and broad-side loadings of the platform with design (plugged) pile condition, respectively.

A static pushover analysis approach combined with a simplified method to calculate the dynamic overload factor e.g. based on a ductility measure and other parameters. Moreover, an appropriate method for scaling the wave height to simulate a realistic extreme situation involving a varying sea surface is applied. Further work is necessary to improve the currently available simplified methods.

REFERENCES

- Amdahl, J., Johansen A. and *Svanø* G.(1994) Ultimate Capacity of Jack-Ups Considering Foundation Behavior, Proceedings of OMAE Conference 1994, USA.
- API RP2A (1994) ,20th Edition ,Draft Section 17.0 ,May 1994 ,USA.
- Bea ,R.G. and Young ,C.N. (1993).Loading and Capacity Effects on Platform Performance In Extreme Storm Waves and Earthquakes, Proceeding of OTC 1993, Houston, Texas, USA.
- Crisfield, M.A. (1991) Non-linear Finite Element Analysis of Solids and Structures, Vol.1, John Wiley Sons, UK.
- Det norske Veritas (1992) -Wajac Computer Program for Generating Wave Forces on the Jacket, Hovik, Norway.
- Eberg, E. , Hellan, Ø. and Amdahl, J.(1993) Non-linear Re-Assessment of Jacket Structures Under Extreme Storm Cyclic Loading , Part II, The Development of Structural Models for Cyclic Response," Proc., 12th Int. Conf. On Offshore Mech. Arctic Eng. Symp., ASME, Vol.1, p 517-523.
- Eberg E. and Amdahl J. (1992) Phase 2 Time Domain Integration in USFOS, Div. of Structural Engineering, SINTEF, Trondheim, Norway.
- Emami Azadi, M.R. and Moan ,T. and Amdahl ,J. (1995), Dynamic Effects on The Performance of Steel Offshore Jacket Platforms Under Extreme Waves, Proceedings of EuroSteel'95, Athens, Greece.
- Emami Azadi, M.R and Moan, T. (1996), Ductility Demand of Simplified Pile-Soil-Jacket System Under Extreme Sea waves and Earthquakes, Proc. of Eurodyn'96, vol.2, pp.1029-1038 Florence, Italy.
- Emami Azadi, M.R. and Nordal, S. and Moan, T. (1997), The predictive abilities of various t-z and p-y models, due to be submitted to J. of Geotechnical Engineering, American Society of Civil Engineers, USA.
- Emami Azadi, M.R.(1997), Pile-Soil-Jacket Interaction Analysis, Dr.ing thesis, to be published, Dept. of Marine Structures, NTNU, Norway.

- Hellan, Ø., Skallerud B., Amdahl, J. and Moan, T. (1991), "Re-assessment of Offshore Steel Structures: Shakedown and Cyclic Non-linear FEM Analysis," Proc. of 1st Int. Offshore Polar Conf., Publ. by Int. Soc. of Offshore and Polar Engineers (ISOPE), p 34-42.
- Hellan, Ø. (1994) Re-assessment of Marine Structures, Parameter Studies, SINTEF Report STF70 F94031, SINTEF, Structures and Concrete, Trondheim, Norway.
- Hellan, Ø. (1995) Non-linear Pushover and Cyclic Analyses In Ultimate Limit State Design and Re-Assessments Of Tubular Steel Offshore Structures, Dr.ing thesis, NTH, Trondheim, Norway.
- Hilber, H.M, Hughes, T.J.R. and Taylor R.L (1976) Improved numerical dissipation algorithms in structural dynamics. Rep.no. 76-29, Earthquake Eng. Res. Center, Univ. of California, LA, USA.
- Horsnell M.R. and F.E. Toolan (1996), Risk of Foundation Failure of Offshore Jacket Piles, The 28th Offshore Technology Conf.(OTC), p381-392, USA.
- ISO (1995) Analysis Modelling ISO Adhoc Group, Draft Section X, Den Haag, The Netherlands.
- Marshall, P.W., Gates, W.E. and Anagnostopoulos, S. (1977) Inelastic Dynamic Analysis of Tubular Offshore Structures, Proc. Offshore Structures, Proc. of Offshore Technology Conf. (OTC), Paper No. 2908, Houston, USA.
- Moan, T., Amdahl, J., Engseth, A.G and Granli, T. (1985) Collapse behaviour of Trusswork Steel Platforms, BOSS'85, Delft, Holland.
- Moe, O. and Moan, T. (1984) Environmental Load Effect Analysis of Guyed Towers, Proc. of the Third International Offshore Mechanics and Arctic Engineering Symposium, Vol.1, 68-79, ASME, USA.
- Nadim, F. and Dahlberg, R. (1996) Numerical Modelling of Cyclic Pile Capacity in Clay, Proc. of Offshore Technology Conf. (OTC), Vol.1, 347-356, USA.
- Nogami, T. and Konagai, K. (1989), Time Domain Flexural Response of Dynamically Loaded Single Piles, ASCE, USA.
- Norwegian Petroleum Directorate (1992), Regulations for Load bearing Structures for Petroleum Industry, Oslo, Norway.
- Rashed, S.M.H (1980) Behaviour to Ultimate Strength of Tubular Offshore Structures by the Idealized Structural Unit Method, Report SK/R51, Division of Marine Structures, NTH, Norway.
- Schmucker, D.G and Cornell, C.A. (1994), Dynamic behaviour of Semi-Ductile Jackets Under Extreme Wave and Wave-In-Deck Forces, Civil Eng. Dept., Stanford Univ., USA.
- Schmucker, D.G (1996), Near Failure behaviour of Jacket-Type Offshore Platforms in The Extreme Wave Environment, Ph.D thesis, report no. RMS-21, June, 1996, Stanford Univ., USA.
- S, T.H, Amdahl, J (1994) USFOS- A Computer Program for Ultimate Strength Analysis of Framed Offshore Structures, Theory manual, Report STF71 A86049, SINTEF Structural Engineering, Trondheim.
- Stewart, G., Moan, T. and Eide, O. (1993) Non-linear Re-Assessment of Jacket Structures Under Extreme Storm Cyclic Loading, Part I : Philosophy and Acceptance Criteria, Proc. of Int. Offshore and Polar Engineering (ISOPE), USA.
- Svanø, G. (1993), Long Term Processes In Geomaterials, SINTEF Geotech. Division, Norway.
- Tromans, P.S., Anaturk A.R. and Hagemeijer P. (1991), A New Model for the Kinematics of Large Ocean Waves- Application as a Design Wave, The Proc. of the First Int. Offshore

and Polar Engineering Conf. (ISOPE), UK.

Ueda, Y. and Rashed, S.M.H (1974) An Ultimate Transverse Strength Analysis of Ship Structures, J. of Society of Naval Architecture of Japan, Vol.136.

Wolf, J.P. (1994), Foundation Vibration Analysis Using Simple Physical Models, PTR, Prentice-Hall USA.